DØNote XXXX
Version 3.6

DØ Search for HZ$\rightarrow\mu^+\mu^- b\bar{b}$ using p17 Data with NN Event Selection

Andrew Haas

Columbia University / Nevis Labs – USA

July 27, 2007

Abstract

The production of the Standard Model (SM) Higgs boson (H) in association with a Z boson is searched for, where the Z decays to $\mu^+\mu^-$ and the H to $b\bar{b}$. The full Run IIa p17 data set is used, with an integrated luminosity of about 1.1 fb^{-1}. The certified p17 Neural-Network (NN) b-tagger is used to separate the data into two orthogonal selected sets: single-tight and not double-loose b-tagged (1T), and double-loose b-tagged (2L). Neural-net's are trained to distinguish between signal and background events and used to optimize the expected signal significance in the 1T and 2L channels separately, for each of six candidate Higgs masses (as well as for ZZ and $t\bar{t}$ signals, for fun and as a cross-check, respectively). No Higgs signal is observed, and limits are set on the ZH cross-section $\times$ BR(H$\rightarrow b\bar{b}$) as a function of the Higgs mass, from 105 to 155 GeV.

1 Introduction and Theory

The SM requires at least one Higgs boson in order to consistently give masses to the W and Z bosons as well as to the quarks and charged leptons. Extensions of the SM, such as Supersymmetry, demand at least 3 neutral Higgs bosons, at least one of which must be less than about 200 GeV in general models, and less than 135 GeV in the Minimal Supersymmetric SM [1]. Recent global electro-weak fits prefer a light Higgs, <166 GeV at 95% C.L., and LEP has excluded the SM Higgs with a mass below 114.4 GeV [2].

Given this very strong experimental evidence and theoretical preference for a Higgs boson in the mass range of 114 to about 200 GeV, both the CDF and D0 experiments have embarked on an ambitious program to maximize their chances of observing the Higgs boson - and thus making a rough measurement of its mass, the last unmeasured parameter of the SM. At the Tevatron, the two most important production mechanisms are through gluon-fusion with a virtual top quark loop ($gg \rightarrow H$), and associated-production with a W or Z ($q\bar{q} \rightarrow WH$ or ZH) [3]. The dominant decay of the Higgs below about 135 GeV is to $b\bar{b}$, with about a 90% BR. Above this mass, the dominant decay is to a pair of (oppositely charged) W's. Searches for low-mass Higgs (<135 GeV) are forced to use associated production, due to the overwhelming $b\bar{b}$ background present to gluon-fusion followed by the Higgs decay to $b\bar{b}$. Searches for a heavier Higgs can also take advantage of the gluon-fusion production followed by the Higgs decay to W's.

This analysis searches in the ZH associated production channel where the Higgs decays to $b\bar{b}$ and the Z decays to muons. A very similar analysis has also been done for the electron channel. Another analysis searches for the more prevalent, but background-rich, ZH associated production where the Z decays to neutrinos. The associated Higgs production cross-sections are known at NNLO in the QCD expansion and at NLO in the electro-weak expansion. The residual theoretical uncertainty is rather small, less than 5% [3].

The full Run IIa data set is used (including "cable-swap" data), corresponding to an integrated luminosity (using the new luminosity constants) of about 1.1 fb^{-1}. The signal signature is two high p_T muons from the Z decay, and two b-jets from the Higgs decay. After requiring a reconstructed Z boson, b-tagging is used to select the signal from the dominant Z + (light) jets background. The data is divided into two orthogonal channels, those events with a single tight b-tag and not two loose b-tags, and those events with two loose b-tags. The major remaining backgrounds (in each channel) are Z + b-jets, Z + light jets (where a light jet has been misidentified as a b-jet), $t\bar{t}$, QCD (where jets fake a Z boson), and di-boson (WZ, ZZ) production. QCD is measured in data, whereas other backgrounds are estimated from MC simulation.

A NN is trained, using simulated events (except for QCD which is taken from non-isolated muon data), to distinguish between background and signal events, in the 1T and 2L channels separately, for each of six candidate Higgs masses (105-155 GeV, in 10 GeV steps). The NN output distributions are used to search for evidence of a signal [17]. No excesses are observed, and limits are set on the ZH production cross-section $\times$ BR($H \rightarrow b\bar{b}$) as a function of the Higgs mass, from 105 to 155 GeV. NN's are also trained (in the 1T and 2L channels) against ZZ as a signal, whose production $\times$ BR($\rightarrow b\bar{b}$) is

about 5 times larger than ZH (at 115 GeV). No excess is observed, and an upper limit is set on the ZZ production cross-section. Also, as a cross-check, NN's are trained again $t\bar{t}$ as a signal, and the presence of $t\bar{t}$ is verified in both the 1T and 2L channels.

2 Data

Re-fixed p17 data in CAF format from the 2MUhighpt skim, which requires at least 2 Loose muons with central p_T>10 GeV, was processed using CAFe. The SAM data set definitions were:

- CSG_CAF_2MUhighpt_PASS3_p17.09.06
- CSG_CAF_2MUhighpt_PASS3_p17.09.06b
- CSG_CAF_2MUhighpt_PASS3_p17.09.03

No trigger requirements were made, in order to retain the highest possible efficiency for signal. The data was filtered by the CafeDataQualityProcessor [4] using definition 2007-01-08.CALO.CFT.MUON.SMT.dqdef, which removes bad runs and luminosity blocks as defined by the SMT, CFT, Calorimeter, and Muon groups. The integrated luminosity of the data sample *after the data quality selection* was measured using the standard luminosity tools (dq_util/util/lumitool.py) [4], and found to be 1060 pb^{-1}, using the *new* luminosity constants. It is expected that the new constants have increased the measured integrated luminosity by about 15%.

3 MC Samples

The various MC samples that were used can be seen in Table 1. Release p17.09.01 was used for generating the samples, except for ZH signals of mass 105, 115, 125, and 135 GeV (req-id 28575-28578), which were generated with p17.06.02. The main difference was slightly different track momentum resolution due to a bug in the Lorentz drift angle in p17.06.02. No difference in b-tagging efficiency is present for these samples since TRF's are used, and the muon resolution is corrected specially for these samples using the smearing constants derived for p17.06 MC. The SAM definitions were of the form CSG_CAF_MCv3-reqid, meaning that the CAF trees were produced with p18.05.00 with smearing. All samples were generated with Pythia, except for the Z+jets background which used ALPGEN interfaced with Pythia. A Pythia-only Z+jets sample was also used as a cross-check for the simulated (Z+Drell-Yan)$\rightarrow\mu\mu$ invariant mass shape. Finally, the samples were run through the full GEANT 3 detector simulation, digitization, and reconstruction.

The ZH signal cross-sections, as well as those for $t\bar{t}$, WZ, and ZZ are taken from MCFM, using the CAPS settings [5]. These cross-sections are NLO, and use CTEQ5M PDF's. For the ALPGEN+Pythia samples, a matching procedure (MLM) was used so as to not double count the radiation of additional jets between ALPGEN and Pythia [6]. The matching algorithm calculates a sample weight for each parton multiplicity,

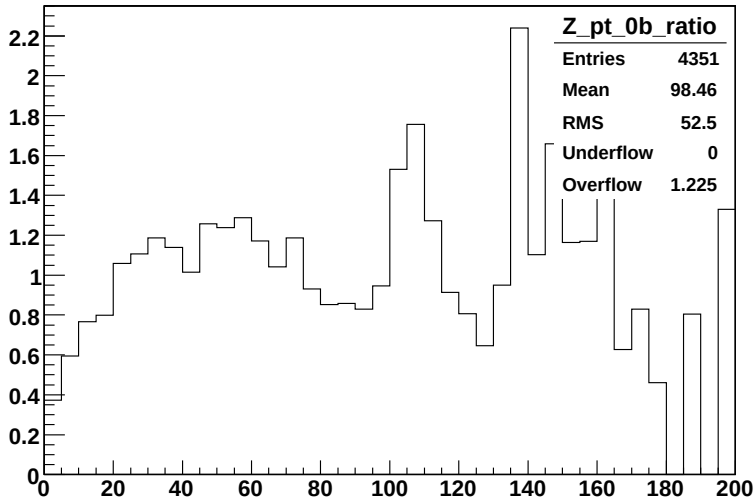

Figure 1: The ratio of data/MC Z+>=2 jet event rates as a function of the Z p_T. This ratio is used to weight each event in the Z + (light) jets MC samples.

which is stored in the CAF trees, and this weight was measured (using getXsection.py) and applied to each sample. To correct for a bug in ALPGEN production, the 3lp_incl. cross-sections were divided by a factor of 1.5. And to correct for another ALPGEN bug, the mZ=60-130 0lp events were weighted by exp(4.07-0.05113*Mz) with 60<Mz<79.6 GeV, and the 1lp events by 2.247-0.0166*Mz with 60<Mz<75.1 GeV.

NLO k-factors of 1.3 and 1.5 were applied to the Z+light and Z+$b\bar{b}$ samples, respectively, to account for the NLO cross-sections of these process (as calculated with MCFM) as compared to the LO cross-sections from ALPGEN. This scale factor is considered to be a rough approximation, good to ±50%, while a much more thorough correction or solution is currently being evaluated [7]. The Z + charm jet production is included by ALPGEN in the Z + light jets samples, so a similar 1.5 NLO k-factor should be applied to the charm events, but has not been for technical reasons. However, since charm jets will anyways make up less than 20% of the total background, and the uncertainty on the k-factor is already large, this omission adds negligible additional background systematic uncertainty.

The Z p_T distribution is poorly modeled by both the Pythia and ALPGEN MC generators, for events with Z p_T<∼100 GeV. It is corrected for by measuring the distribution of Z p_T in Z+>=2 jet data and weighting each event in the Z + (light) jets MC with Z p_T<∼100 GeV such that the total distribution in MC then matches that in data. Figure 1 shows the ratio of event rates vs. Z p_T in data / ALPGEN MC.

All Z + light jets MC is scaled to match the Z peak in data, after requiring a good reconstructed Z and at least two jets (see detailed event selection criteria below). Given the measured integrated luminosity of 1.06 fb^{-1}, the Z peak in Z + >=2 jet data is found to have a cross-section which is 90±5% of that expected from simulation at NNLO (depending on 1T vs. 2L and Pythia vs. ALPGEN for Z+jets background).

This scale factor (0.90) is understood to be the (trigger × data/MC) scale factor for Z + 2 jets and is applied to all other MC samples as well.

4 Event Selection

The following criteria are used to select events. The cuts and were not optimized in any systematic way. Instead, the philosophy was to keep selections as loose as possible, with the expectation that the neural net event selection will make optimal use of the information.

- Events are required to have at least two Loose quality muons with Loose track matches, and p_T>10 GeV, defined by the standard MuonSelector in CAFe [9]. The muon p_T in data is corrected using the beam spot info for each run, if the muon track has no associated SMT hits.

  A good Z candidate is required, reconstructed from some pair of selected muons. The reconstructed Z mass must be >70 and <110 GeV. The standard Z selection from wz_cafreco [10] is used, which includes a pseudo-acoplanarity of >0.05 (anti-cosmic) and requires that the muons be of opposite sign.

  The two muons which form the Z are together required to have *product scaled isolation* <0.01. The product scaled isolation is the product of the scaled isolation variables for each of the two muons which form the Z. Scaled isolation is defined as (track p_T+ cal. p_T) / muon p_T. The track p_T is the sum of all other tracks in a cone of ΔR<0.5 around the muon track (and not including the muon track). The cal. p_T is the sum of all calorimeter energy in a hollow cone around the muon from 0.1<ΔR<0.4 [9].

- At least 2 'good' JCCB (0.5 cone) [11] jets are required in each event, with *corrected* p_T>15 GeV and $|\eta|$<2.5. Jet energies are corrected using the standard JES with no muon corrections [12]. In MC, jets are also smeared and removed (to account for data/MC efficiency differences), with the standard JetSSR processor [13] using the p17 parameters (with no shifting). MET is recomputed using the JES corrected jets (and after smearing and removal for MC) and correcting for the escaping p_T of all muons.

- Jets are b-tagged using the certified NN b-tagging algorithm [14]. The tagging is applied *after* the JetSSR processor in MC so that the jet p_T>15 GeV cut required for taggability is applied to the smeared jet p_T. Standard taggability was applied using the Top group's EMTaggability parametrization, from the pre-selected W+jets data in the electron channel. The L4 and VERYTIGHT operating points were used to separate the data into two orthogonal samples: the events with (exactly) 1 VERYTIGHT tag and not 2 (or more) L4 tags (called '1T'), and events with 2 (or more) L4 tags (called '2L'). In MC, the tag-rate-functions (TRF's) for data corresponding to the L4 and VERYTIGHT operating points were applied to each jet and used to calculate the probabilities that the event would fall into the 1T and 2L categories.

Sample	Cross section x BR	SAM req-id's	N. Events
ZH($\to\mu^+\mu^- b\bar{b}$), m_H=105 GeV	3.87 fb	28575	50000
ZH($\to\mu^+\mu^- b\bar{b}$), m_H=115 GeV	2.66 fb	28576	50000
ZH($\to\mu^+\mu^- b\bar{b}$), m_H=125 GeV	1.67 fb	28577	50000
ZH($\to\mu^+\mu^- b\bar{b}$), m_H=135 GeV	0.91 fb	28578	52250
ZH($\to\mu^+\mu^- b\bar{b}$), m_H=145 GeV	0.41 fb	32426	49750
ZH($\to\mu^+\mu^- b\bar{b}$), m_H=155 GeV	0.17 fb	32427	50000
Z($\to\mu^+\mu^-$)+0lp excl. (mZ=15-60 GeV)	335 * 1.3 pb	32900, 32901, 32902	650250
Z($\to\mu^+\mu^-$)+1lp excl. (mZ=15-60 GeV)	38.5 * 1.3 pb	32903, 32904, 32905	512500
Z($\to\mu^+\mu^-$)+2lp excl. (mZ=15-60 GeV)	10.1 * 1.3 pb	32906, 32907	205000
Z($\to\mu^+\mu^-$)+3lp incl. (mZ=15-60 GeV)	4.2/1.5 * 1.3 pb	32908, 32909	100500
Z($\to\mu^+\mu^-$)+0lp excl. (mZ=60-130 GeV)	139 * 1.3 pb	28762, 28884, 38410, 38409, 38408, 38364, 37409, 37408, 37407, 37004, 37003, 29279, 29278, 29273, 29272	1469750
Z($\to\mu^+\mu^-$)+1lp excl. (mZ=60-130 GeV)	41.6 * 1.3 pb	28763, 28885, 38362, 37416, 37005	874116
Z($\to\mu^+\mu^-$)+2lp excl. (mZ=60-130 GeV)	10.3 * 1.3 pb	28764, 38368, 37006	413500
Z($\to\mu^+\mu^-$)+3lp incl. (mZ=60-130 GeV)	5.3/1.5 * 1.3 pb	28767, 38372, 37007	317000
Z($\to\mu^+\mu^-$)+0lp excl. (mZ=130-250 GeV)	0.90 * 1.3 pb	32621	108000
Z($\to\mu^+\mu^-$)+1lp excl. (mZ=130-250 GeV)	0.36 * 1.3 pb	32623	100250
Z($\to\mu^+\mu^-$)+2lp excl. (mZ=130-250 GeV)	0.097 * 1.3 pb	32624	100750
Z($\to\mu^+\mu^-$)+3lp incl. (mZ=130-250 GeV)	0.053/1.5 * 1.3 pb	32648	99750
Z($\to\mu^+\mu^-$)+0lp excl. (mZ>=250 GeV)	0.072 * 1.3 pb	33738	106250
Z($\to\mu^+\mu^-$)+1lp excl. (mZ>=250 GeV)	0.036 * 1.3 pb	33739	105750
Z($\to\mu^+\mu^-$)+2lp excl. (mZ>=250 GeV)	0.011 * 1.3 pb	33740	102250
Z($\to\mu^+\mu^-$)+3lp incl. (mZ>=250 GeV)	0.0066/1.5 * 1.3 pb	33741	105750
Z($\to\mu^+\mu^-$)+2b+0lp excl.	0.97 * 1.5 pb	32356, 32806, 32807	342000
Z($\to\mu^+\mu^-$)+2b+1lp excl.	0.36 * 1.5 pb	32357	52750
Z($\to\mu^+\mu^-$)+2b+2lp incl.	0.21/1.5 * 1.5 pb	32257	25000
$t\bar{t}$ inclusive (M_{top}=170-175 GeV)	7.0 pb	35833, 35834, 35835, 35437, 35438, 35439, 34873, 34874, 33810, 33811	1615030
WZ inclusive	3.6 pb	30488, 30489, 33685, 33684, 42212, 38491	724250
ZZ inclusive	1.423 pb	30486, 30487, 33687, 33686, 42213, 38492	711000
Pythia Z($\to\mu^+\mu^-$) (mZ=15-60 GeV)	479139.25 fb	40687 40686 40685 40684 40683, 40682 40681 40680 40679 40678, 36595 36594 36593 36592 36591	3107250
Pythia Z($\to\mu^+\mu^-$) (mZ=60-130 GeV)	255203.33 fb	38912 38911 38910 38909 38908, 38907 38906 38905 38904 38903, 38902 38901 38900 38899 38898	2821282
Pythia Z($\to\mu^+\mu^-$) (mZ=130-250 GeV)	1875.78 fb	41252 41251	413521
Pythia Z($\to\mu^+\mu^-$) (mZ=250-500 GeV)	476. fb	41256	102750
Pythia Z($\to\mu^+\mu^-$) (mZ>=500 GeV)	24.7 fb	41259	51500

Table 1: The MC samples used, and their cross-sections (corrected with NLO k-factors, where noted), SAM request ID's, and number of events generated. "lp" stands for "light-parton" in ALPGEN, and indicates the number of hard jets at the parton level for each ALPGEN+Pythia sub-sample. "excl." means that the sub-sample is exclusive and requires exactly the number of light partons indicated, whereas "incl." denotes that all higher parton multiplicity states were also allowed. The Pythia Z($\to\mu^+\mu^-$) samples were only used as a cross-check for the Z + Drell Yan (DY) $\mu\mu$ invariant mass distribution.

5 QCD

A sample of QCD events is selected by reversing the muon isolation criteria, i.e. requiring that the product scaled isolation of the two muons forming the Z candidate is >0.01. In addition, no isolated Z candidate (of any di-muon invariant mass) can be present in the event.

The QCD event fraction is determined by fitting a combination of the QCD and MC di-muon invariant mass distributions (in the range 40–500 GeV) to the data. Fits are performed to the data in events with at least two jets (since the QCD fraction was observed to depend on the jet multiplicity). A separate fit is performed for events with at least 0, 1, 2 L4 b-tagged jets, and at least 0 or 1 VERYTIGHT b-tagged jets (but not two or more L4 b-tagged jets) as seen in Figures 2 – 6. The QCD fractions in the 0, 1, 2 L4 b-tagged, and 0, 1 VERYTIGHT b-tagged categories are found to be 0.8%, 0.7%, 2.6%, 1.3%, and 0.3% respectively. The uncertainty on the size of the QCD background is taken from the error on the background fit, about 50% (relative) in the double L4 and single VERYTIGHT b-tagged channels. A cross-check with the Pythia Z($\rightarrow\mu\mu$) samples gives very similar fits and QCD fractions for all channels, well within the systematic uncertainties quoted. The Pythia fits are shown in the bottom half of Figures 2 – 6 for comparison.

The rise in the QCD fraction in b-tagged data is assumed to be due to the presence of $b\bar{b}$ events, which can often (10%) of the time decay to a leading muon which may pass isolation cuts. Also note the presence of $t\bar{t}$ (shown as the magenta line), particularly in the b-tagged channels, which must be properly accounted for during the fit.

6 Results Using M_{jj} Selection

Before investigating the more complicated NN-based search, we first perform a simple M_{jj}-based selection as a sanity check and to compare with earlier results. Since the Higgs is decaying to $b\bar{b}$, we attempt to isolate the signal by selecting events where the two leading p_T jets form an invariant mass close to that expected for a given Higgs mass. Invariant mass is calculated using the 4-vector formula, which accounts for the non-zero mass of each individual jet[1]. The actual value of the invariant mass reconstructed in full MC is always less, by about 20% on average, than the actual Higgs mass in each sample. This lowering of the reconstructed mass is due to final-state radiation of particles and jets outside the reconstructed jet cones. The leading-p_T di-jet mass distribution in each Higgs MC sample is fit to a Gaussian, in the 1T and 2L b-tagged channels, separately. The search window then extends from mean-1.5*width to mean+1.5*width. The final fit values are shown in Table 2.

Systematics are identical to the p17 ZH→ee analysis [15]. The total background uncertainty is 20%, and the signal efficiency uncertainty is 8%.

The total amount of data, various backgrounds, and expected signal are shown for a representative di-jet mass range of interest (70-110 GeV), after 0, 1, and at least 2 L4

[1]In ROOT notation, where 'jet' is an array of p_T-sorted TMBJet objects: $m_{j0,j1}$ = (jet[0]+jet[1]).Mag()

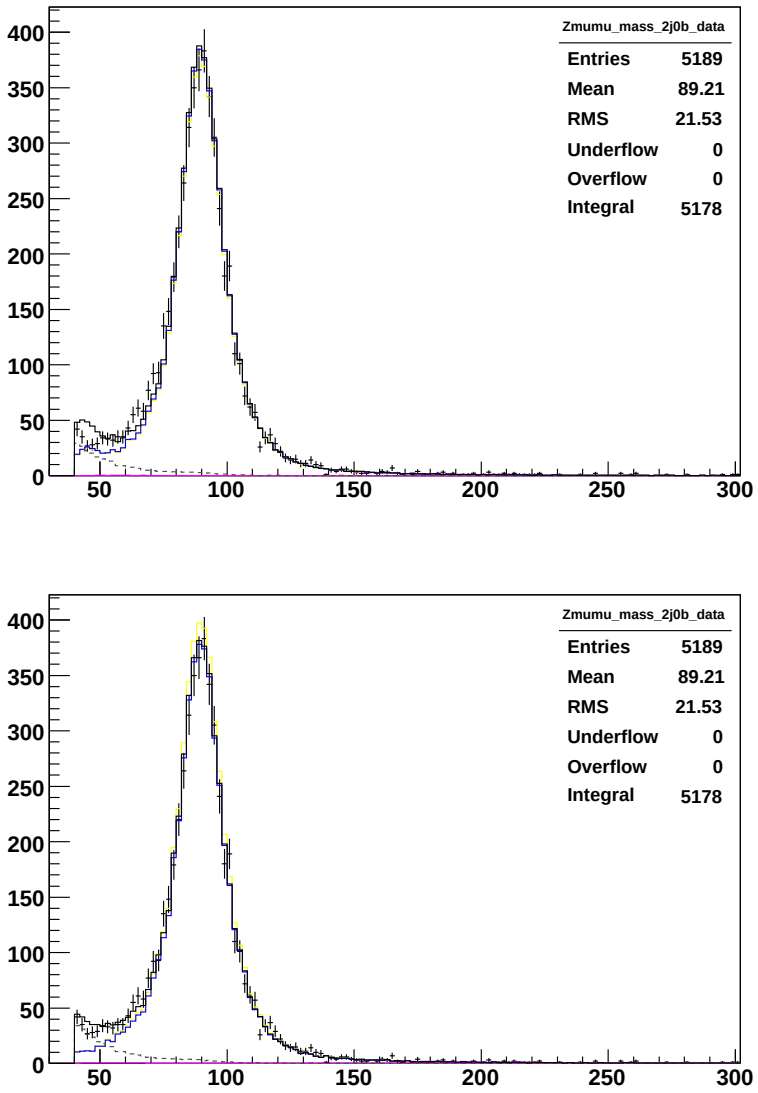

Figure 2: A fit of the di-mu mass spectrum (after requiring at least two jets) and 0 L4 b-tagged jets. Data are the points. The dashed line is QCD, solid yellow is the Z+DY shape from MC before scaling to data in the range $70<M_{\mu\mu}<110$ GeV, solid magenta is $t\bar{t}$, solid blue is total MC, and solid black is total MC plus QCD. The upper plot is the ALPGEN simulation and the lower is Pythia.

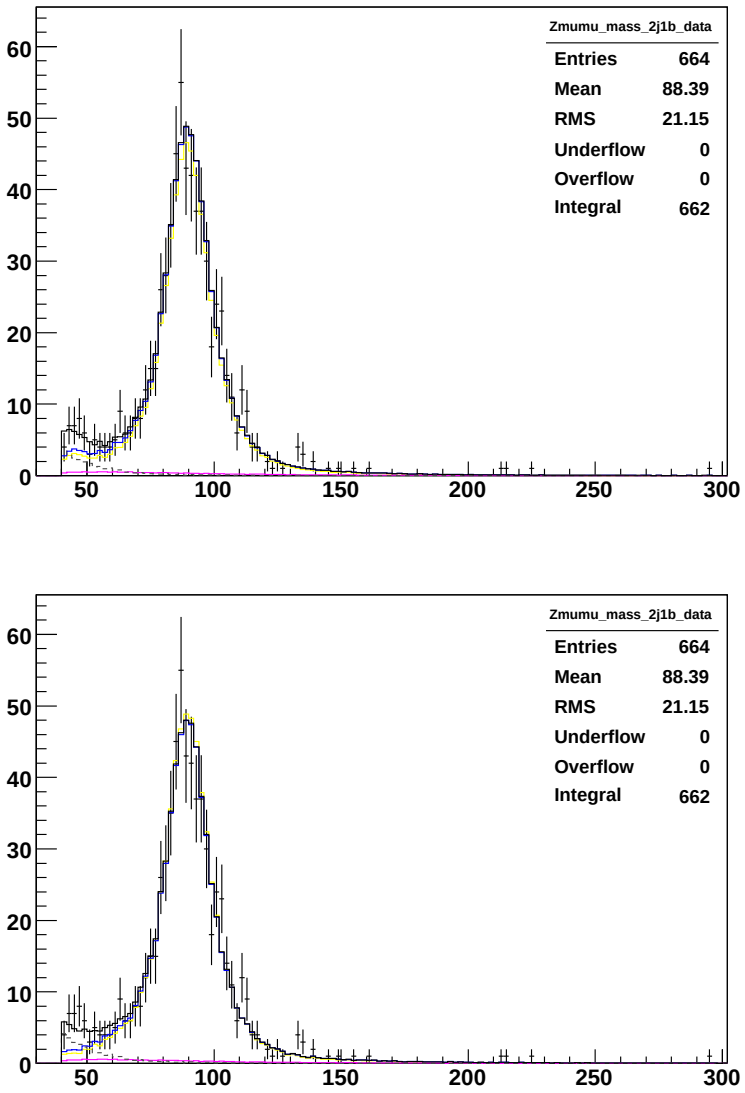

Figure 3: A fit of the di-mu mass spectrum (after requiring at least two jets) and 1 L4 b-tagged jets. Data are the points. The dashed line is QCD, solid yellow is the Z+DY shape from MC before scaling to data in the range $70<M_{\mu\mu}<110$ GeV, solid magenta is $t\bar{t}$, solid blue is total MC, and solid black is total MC plus QCD. The upper plot is the ALPGEN simulation and the lower is Pythia.

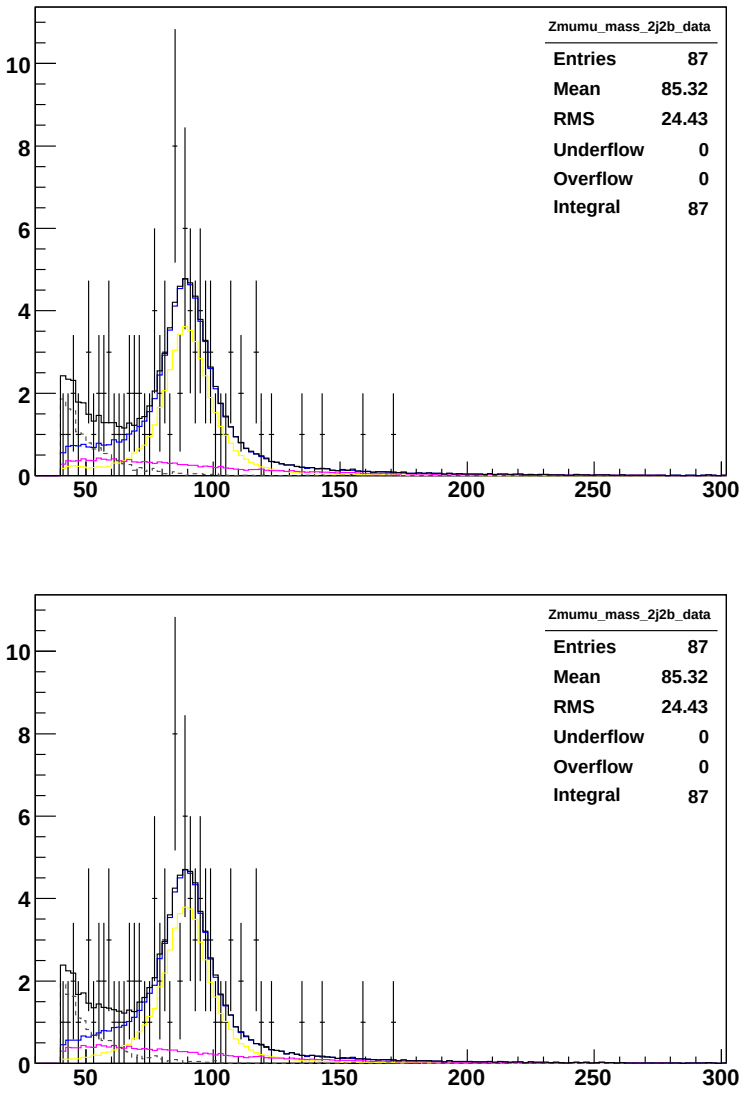

Figure 4: A fit of the di-mu mass spectrum (after requiring at least two jets) and at least 2 L4 b-tagged jets. Data are the points. The dashed line is QCD, solid yellow is the Z+DY shape from MC before scaling to data in the range $70<M_{\mu\mu}<110$ GeV, solid magenta is $t\bar{t}$, solid blue is total MC, and solid black is total MC plus QCD. The upper plot is the ALPGEN simulation and the lower is Pythia.

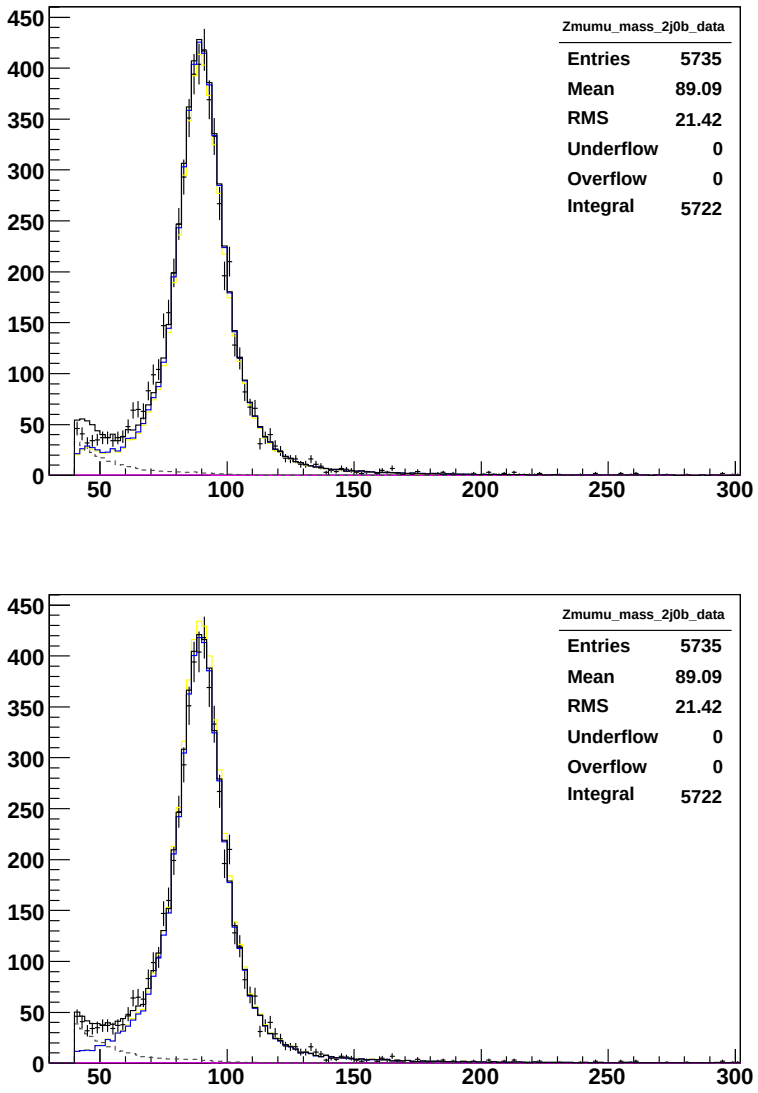

Figure 5: A fit of the di-mu mass spectrum (after requiring at least two jets) and 0 VERYTIGHT b-tagged jets, and not 2 or more L4 b-tagged jets. Data are the points. The dashed line is QCD, solid yellow is the Z+DY shape from MC before scaling to data in the range $70<M_{\mu\mu}<110$ GeV, solid magenta is $t\bar{t}$, solid blue is total MC, and solid black is total MC plus QCD. The upper plot is the ALPGEN simulation and the lower is Pythia.

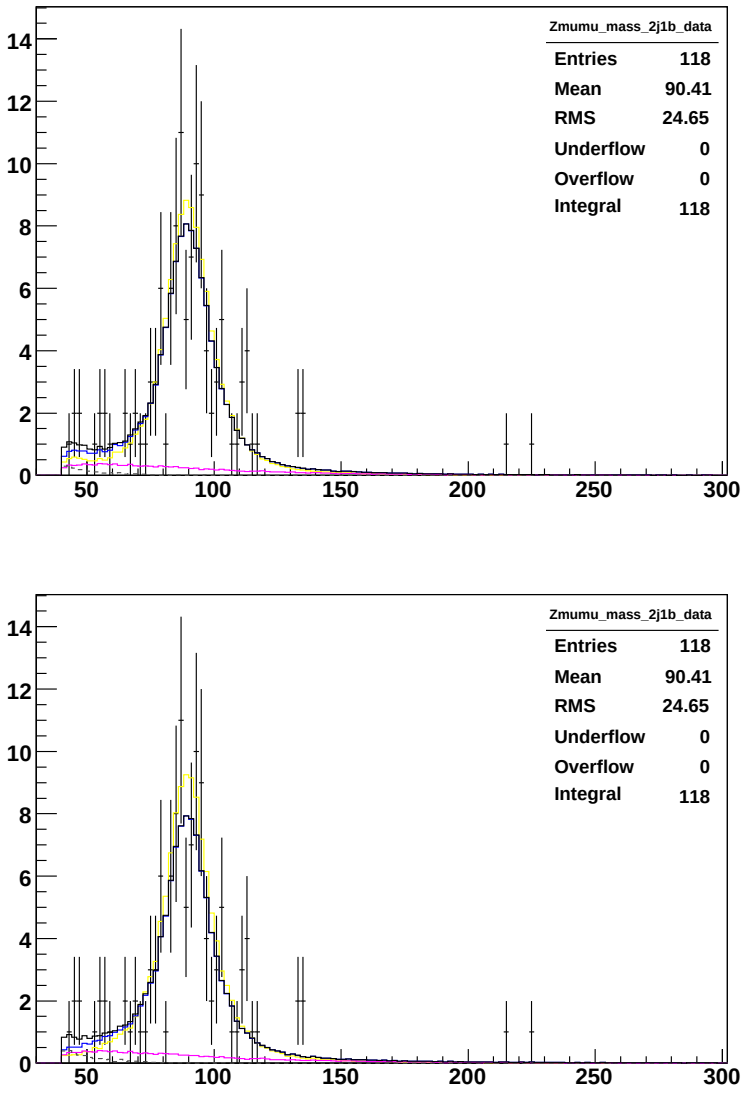

Figure 6: A fit of the di-mu mass spectrum (after requiring at least two jets) and 1 VERYTIGHT b-tagged jets, and not 2 or more L4 b-tagged jets. Data are the points. The dashed line is QCD, solid yellow is the Z+DY shape from MC before scaling to data in the range $70<M_{\mu\mu}<110$ GeV, solid magenta is $t\bar{t}$, solid blue is total MC, and solid black is total MC plus QCD. The upper plot is the ALPGEN simulation and the lower is Pythia.

m_H (GeV)	Mean (GeV)	Width (GeV)	Search Window (GeV)
ZZ	77.0	19.3	48.1-105.9
105	84.1	22.6	50.2-118.0
115	91.9	24.6	55.0-128.9
125	98.7	27.1	58.1-139.4
135	106.0	29.3	62.0-149.9
145	113.9	31.4	66.8-161.0
155	121.5	32.9	72.1-170.9
ZZ	79.0	18.1	51.8-106.2
105	88.0	19.8	58.3-117.7
115	96.2	21.9	63.3-129.0
125	103.5	24.0	67.4-139.5
135	111.3	26.1	72.1-150.5
145	119.7	27.7	78.2-161.3
155	127.1	29.6	82.7-171.6

Table 2: The mean, width, and -1.5,+1.5 sigma search window for each signal mass tested in the 1T (top) and 2L (bottom) channels.

b-tagged jets are required in Table 3. The same for 0, 1, and at least 2 VERYTIGHT b-tagged jets and not 2 or more L4 b-tagged jets is shown in Table 4. Tables 5 and 6 show the same over the entire di-jet mass range. Figures 7–9 show the invariant mass distributions of the two leading-p_T jets, after requiring at least 0, 1, 2 L4 b-tagged jets in the events. Figures 11 and 12 show the invariant mass distribution after requiring at least 0 and 1 VERYTIGHT b-tagged jets and not 2 or more L4 b-tagged jets.

Sample	0 tag	1 tag	2 tag
Data	915	139	13
Total background	873.023	124.188	12.403
QCD	9.284	0.633	0.178
ZH(115)	0.122	0.256	0.180
ZZ	9.449	2.688	0.900
WZ	9.540	2.019	0.110
$t\bar{t}$	1.139	2.303	1.610
Z+(light)	824.653	97.910	4.845
Z+2b	18.959	18.634	4.761

Table 3: The data, backgrounds, and expected SM signal for a representative di-jet mass range (70-110 GeV), after exactly 0, 1, and at least 2 L4 b-tagged jets are required.

Sample	0 tag	1 tag	2 tag
Data	1028	26	0
Total background	964.015	25.728	0.000
QCD	9.243	0.050	0.000
ZH(115)	0.200	0.175	0.000
ZZ	11.016	1.037	0.000
WZ	11.069	0.409	0.000
$t\bar{t}$	1.860	1.558	0.000
Z+(light)	904.915	11.254	0.000
Z+2b	25.912	11.420	0.000

Table 4: The data, backgrounds, and expected SM signal for a representative di-jet mass range (70-110 GeV), after exactly 0, 1, and at least 2 VERYTIGHT b-tagged jets are required, and not 2 or more L4 b-tagged jets.

Sample	0 tag	1 tag	2 tag
Data	4145	524	53
Total background	4186.598	518.991	45.685
QCD	46.056	3.142	0.882
ZH(115)	0.237	0.461	0.301
ZZ	16.670	4.915	1.475
WZ	20.273	4.068	0.238
$t\bar{t}$	3.559	7.153	5.340
Z+(light)	4010.256	420.657	19.207
Z+2b	89.783	79.056	18.544

Table 5: The data, backgrounds, and expected SM signal for the entire di-jet mass range, after exactly 0, 1, and at least 2 L4 b-tagged jets are required.

Sample	0 tag	1 tag	2 tag
Data	4582	87	0
Total background	4569.977	101.415	0.000
QCD	47.024	0.252	0.000
ZH(115)	0.381	0.313	0.000
ZZ	19.484	1.951	0.000
WZ	23.354	0.818	0.000
$t\bar{t}$	5.798	4.841	0.000
Z+(light)	4354.202	46.001	0.000
Z+2b	120.116	47.552	0.000

Table 6: The data, backgrounds, and expected SM signal for the entire di-jet mass range, after exactly 0, 1, and at least 2 VERYTIGHT b-tagged jets are required, and not 2 or more L4 b-tagged jets.

m_H (GeV)	Data	QCD	Total Bgnd.	Sig.	Eff(%).	Exp.(pb) (Exp./SM)	Obs.(pb)
ZZ	48	0.08	50.51	1.53	0.10	23.892 (16.79)	22.500
105	51	0.09	53.88	0.36	8.82	8.524 (74.10)	8.054
115	51	0.10	52.14	0.26	9.29	8.052 (102.03)	7.819
125	49	0.10	51.95	0.17	9.57	7.611 (153.38)	7.179
135	46	0.10	49.00	0.09	9.76	7.321 (269.76)	6.680
145	47	0.11	46.52	0.04	9.35	7.225 (587.39)	7.458
155	47	0.10	41.46	0.01	9.45	6.550 (1666.56)	8.058
ZZ	22	0.28	19.66	1.21	0.08	15.100 (10.61)	18.213
105	21	0.27	19.04	0.34	8.20	4.497 (39.09)	5.106
115	20	0.29	19.25	0.25	9.03	4.056 (51.39)	4.323
125	16	0.30	18.85	0.17	9.51	3.653 (73.61)	3.194
135	19	0.31	17.73	0.10	10.01	3.363 (123.90)	3.853
145	18	0.30	16.32	0.04	9.88	3.334 (271.02)	3.844
155	17	0.31	15.58	0.01	10.21	3.075 (782.53)	3.566

Table 7: The quantities used for setting limits, and the derived expected and observed limits for each Higgs mass, using only a simple M_{jj} event selection, in the 1T (top) and 2L (bottom) channels. The limits account for the BR of Z$\to\mu\mu$ of 0.03366.

Limits are set using the "limit_calculators" Bayesian package [16], by counting the number of events of data, total expected background (from MC and QCD), and expected signal in each invariant mass search window derived above. Table 7 shows the expected and observed limits on the ZH cross-section, accounting for the BR of Z$\to\mu\mu$ of 0.03366 [18].

The ZH cross-section limits derived are about a factor of 2.6 more restrictive than those from the DØ p14 analysis, which used only 317 pb^{-1}(using the old luminosity constants) of data [19]. For instance, there was an expected limit of 10.5 pb for a Higgs mass of 115 GeV, compared to 4.0 pb in this analysis. Assuming that results would simply scale by the square-root of integrated luminosity, a factor of $\sim$1.7 would be expected. The extra factor of 2.6/1.7 = 1.5 of added sensitivity is most likely due to the improved b-tagging, which now uses the NN algorithm.

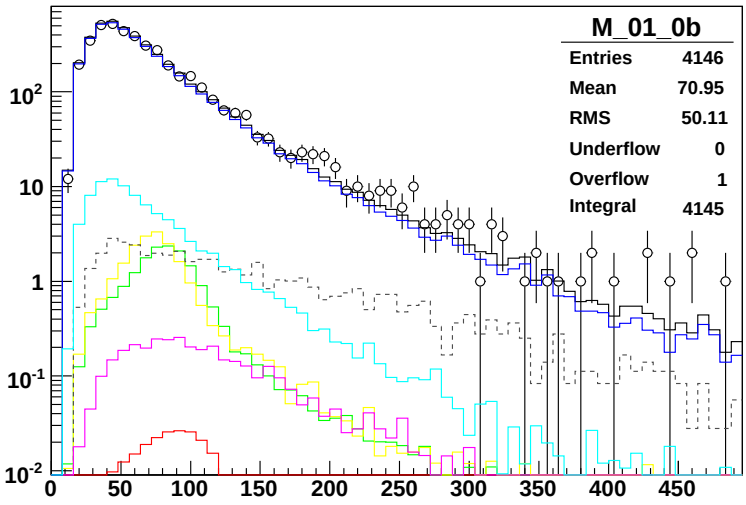

Figure 7: The leading p_T di-jet invariant mass distribution in the events with 0 or more L4 b-tagged jets. For the backgrounds from MC: blue is Z+Xlp, light blue is Z+2b, light green is ZZ, yellow is WZ, magenta is $t\bar{t}$, and red is Higgs signal for m_h=115 GeV. QCD, from non-isolated muon data, is shown as a dashed grey line. The data are shown as circles, with Poisson uncertainties. The total background (including QCD) is the black histogram.

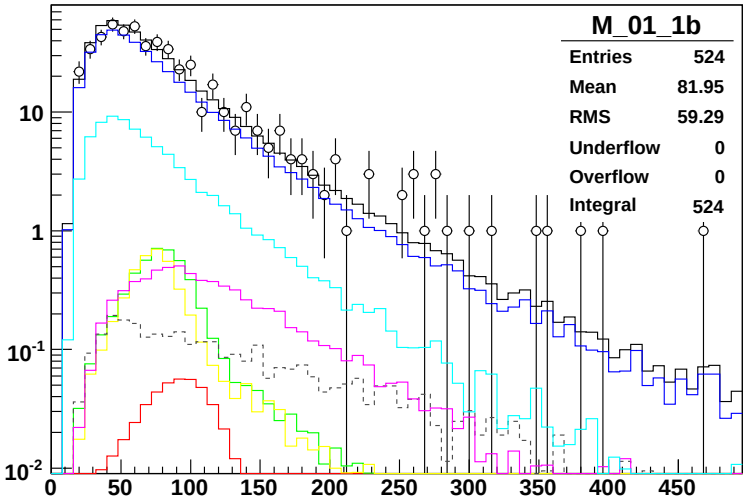

Figure 8: The leading p_T di-jet invariant mass distribution in the events with 1 or more L4 b-tagged jets. For the backgrounds from MC: blue is Z+Xlp, light blue is Z+2b, light green is ZZ, yellow is WZ, magenta is $t\bar{t}$, and red is Higgs signal for m_h=115 GeV. QCD, from non-isolated muon data, is shown as a dashed grey line. The data are shown as circles, with Poisson uncertainties. The total background (including QCD) is the black histogram.

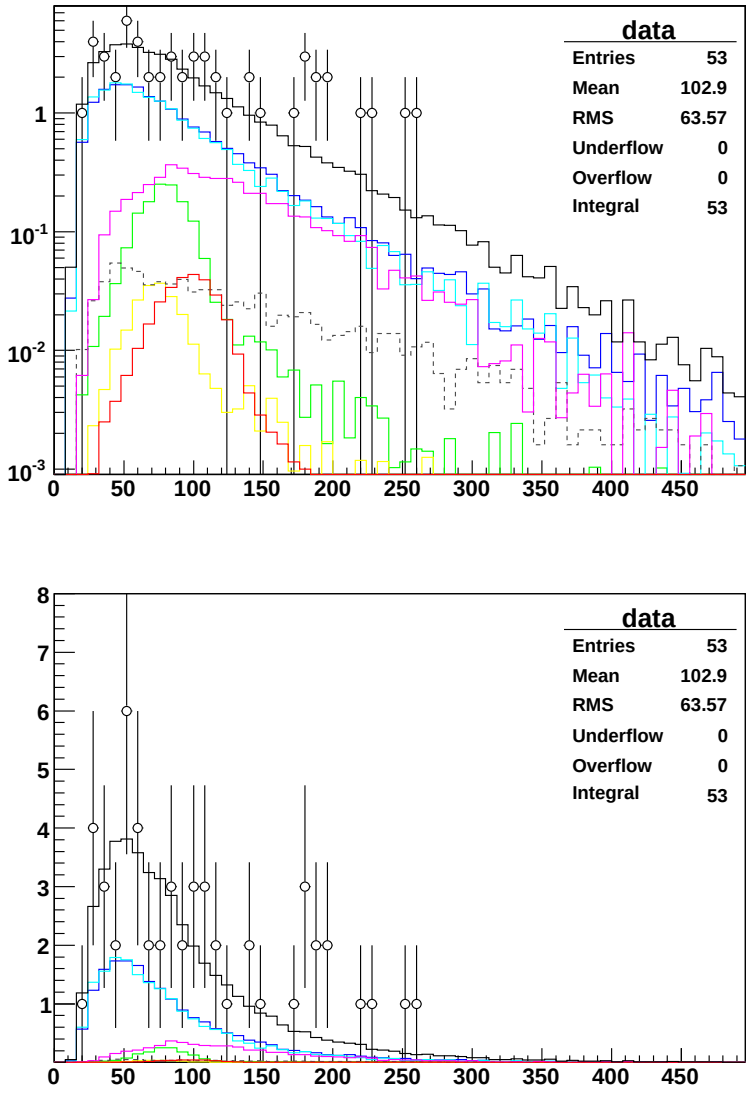

Figure 9: The leading p_T di-jet invariant mass distribution in the events with 2 or more L4 b-tagged jets (the 2L channel). For the backgrounds from MC: blue is Z+Xlp, light blue is Z+2b, light green is ZZ, yellow is WZ, magenta is $t\bar{t}$, and red is Higgs signal for m_h=115 GeV. QCD, from non-isolated muon data, is shown as a dashed grey line. The data are shown as circles, with Poisson uncertainties. The total background (including QCD) is the black histogram. (The top is a log plot, and the bottom is not.)

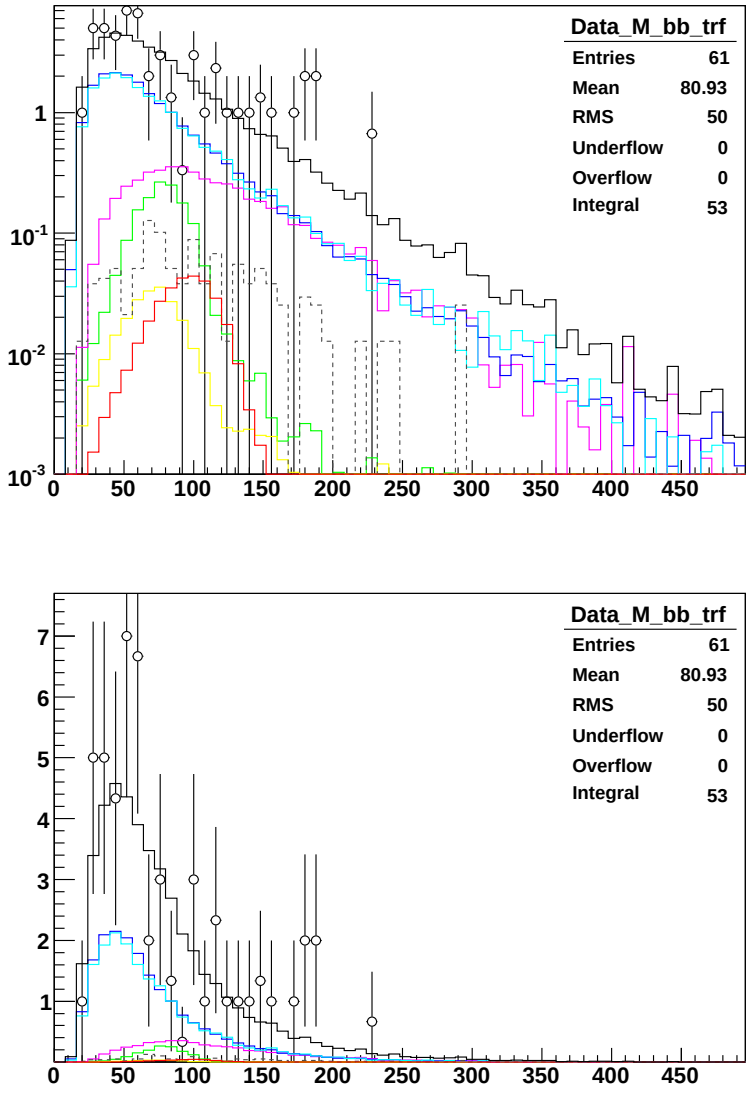

Figure 10: The di-jet invariant mass of all L4 b-tagged jet pairs in the events with 2 or more L4 b-tagged jets (the 2L channel). For the backgrounds from MC: blue is Z+Xlp, light blue is Z+2b, light green is ZZ, yellow is WZ, magenta is $t\bar{t}$, and red is Higgs signal for m_h=115 GeV. QCD, from non-isolated muon data, is shown as a dashed grey line. The data are shown as circles, with Poisson uncertainties. The total background (including QCD) is the black histogram. (The top is a log plot, and the bottom is not.)

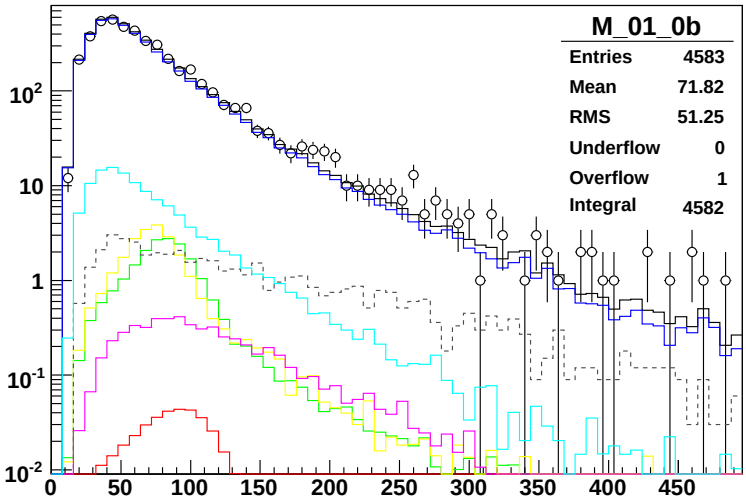

Figure 11: The leading p_T di-jet invariant mass distribution in the events with 0 or more VERYTIGHT b-tagged jets and not 2 or more L4 b-tagged jets. For the backgrounds from MC: blue is Z+Xlp, light blue is Z+2b, light green is ZZ, yellow is WZ, magenta is $t\bar{t}$, and red is Higgs signal for m_h=115 GeV. QCD, from non-isolated muon data, is shown as a dashed grey line. The data are shown as circles, with Poisson uncertainties. The total background (including QCD) is the black histogram.

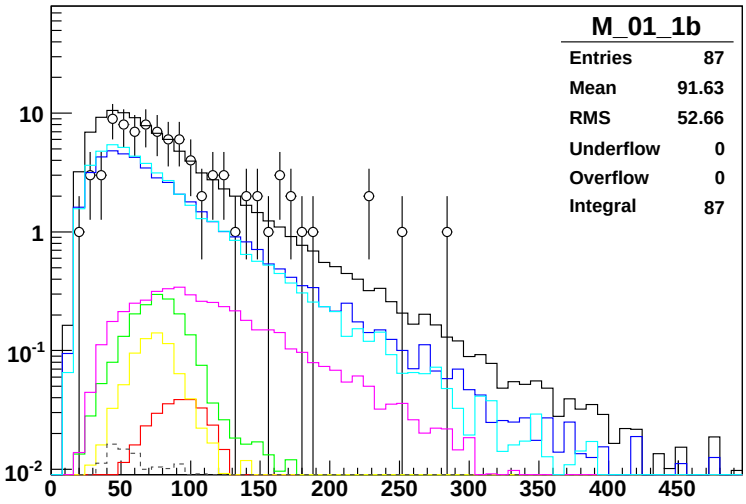

Figure 12: The leading p_T di-jet invariant mass distribution in the events with 1 or more VERYTIGHT b-tagged jets and not 2 or more L4 b-tagged jets (the 1T channel). For the backgrounds from MC: blue is Z+Xlp, light blue is Z+2b, light green is ZZ, yellow is WZ, magenta is $t\bar{t}$, and red is Higgs signal for m_h=115 GeV. QCD, from non-isolated muon data, is shown as a dashed grey line. The data are shown as circles, with Poisson uncertainties. The total background (including QCD) is the black histogram.

Sample	1T	2L
QCD	535	491
ZH	9392	9257
ZZ	5781	5654
WZ	2465	2402
$t\bar{t}$	1565	1516
Z+(light)	74393	66550
Z+2b	13754	12132

Table 8: The number of events used for training in each sample, for a Higgs mass of 115 GeV.

7 NN Event Selection

To improve the separation of signal from backgrounds, an artificial neural network was used, based on the TMultiLayerPerceptron class in ROOT. The network was trained using approximately half of the background and signal events, the rest being used to test the network performance and derive limits. The background events came from MC simulation for all backgrounds, except for QCD, which came from non-isolated muon data as in the standard M_{jj}-based analysis. Separate NN's were trained for the 1T and 2L channels. The number of events available for training from each sample are shown in Table 8, for a Higgs mass of 115 GeV. The number of events used for training depends slightly on the Higgs mass because only events within a $\pm 3\sigma$ around the Higgs di-jet invariant mass peak were used for training, since this was shown to slightly improve the performance of the NN.

Background events were weighted such that the total contribution of each sample made up that expected from it in either the 1T or 2L channel. During NN training, signal events were weighted such that it's integral equaled that of the background events. This technique provided for better significance and NN output values that ranged nicely from 0–1. For testing and limit setting, of course, signal events were weighted such that the integral made up that expected from it in either the 1T or 2L channel. For testing, events could also be weighted such that each sample contributed the amount expected from it in before b-tagging. And again, signal events could also be weighted such that their integral equaled that expected from backgrounds, in order to see the difference in shapes of signal and background.

The parameters of the NN were roughly optimized to give the best signal significance, defined as $S/\sqrt{B}$, by counting the number of signal (S) and background (B) events which pass the optimal NN output cut. Sensitive variables were hypothesized based on physical reasoning of the signal vs. background processes, and then added, in order of their ability to improve the NN significance, until the NN significance failed to improve further. The final set of NN input variables are (in order of separation power):

1. M_{bb}: The invariant mass of a randomly chosen b-tagged jet pair. For the 1T channel, this variable was set to the invariant mass of the b-tagged jet and the

highest p_T non-b-tagged jet. Note that the 4-vector invariant mass calculation was used throughout this analysis, which takes into account the mass of each individual jet.

2. $p_T(1)$: The p_T of the leading p_T jet.
3. $p_T(2)$: The p_T of the second-leading p_T jet.
4. ZΔR: ΔR between the two muons in the Z candidate.
5. $|\Delta\eta|$: The absolute value of the difference in η between the two highest p_T jets.
6. $|\Delta\phi|$: The absolute value of the difference in ϕ between the two highest p_T jets.
7. $\Delta R(Z, jet1)$: The ΔR between the Z candidate and the highest p_T jet.
8. $|\eta_Z|$: The $|\eta|$ of the Z candidate.
9. $\not{E}_T$: The missing E_T of the event (useful against $t\bar{t}$).
10. SE_T: The scalar E_T of the event.

Each NN was trained using the BFGS technique, for 150 epochs. 6 hidden neurons were used (in a single layer), and one output neuron. A separate NN was trained against each candidate signal Higgs mass, as well as for ZZ, and for $t\bar{t}$ as a test. When a sample which is normally a background, such as ZZ or $t\bar{t}$, was used as a signal, it was not considered as a background sample. For $t\bar{t}$, an additional test was performed where the $M_{\mu\mu}$ window was opened from the usual 70–110 GeV to 40–500 GeV, in order to accept more $t\bar{t}$ 'signal'. The NN outputs for each NN trained are shown in Figures 13–21. Additional plots of each NN input variable and some other variables (for $M_H = 115$ GeV) are shown in Figures 22–43.

With both the larger Z mass window and the standard one, good agreement is seen between expected background, $t\bar{t}$ signal, and data, as seen in Figures 13 and 14, respectively. This agreement gives credence to the entire analysis chain, including the b-tagging and NN selection techniques.

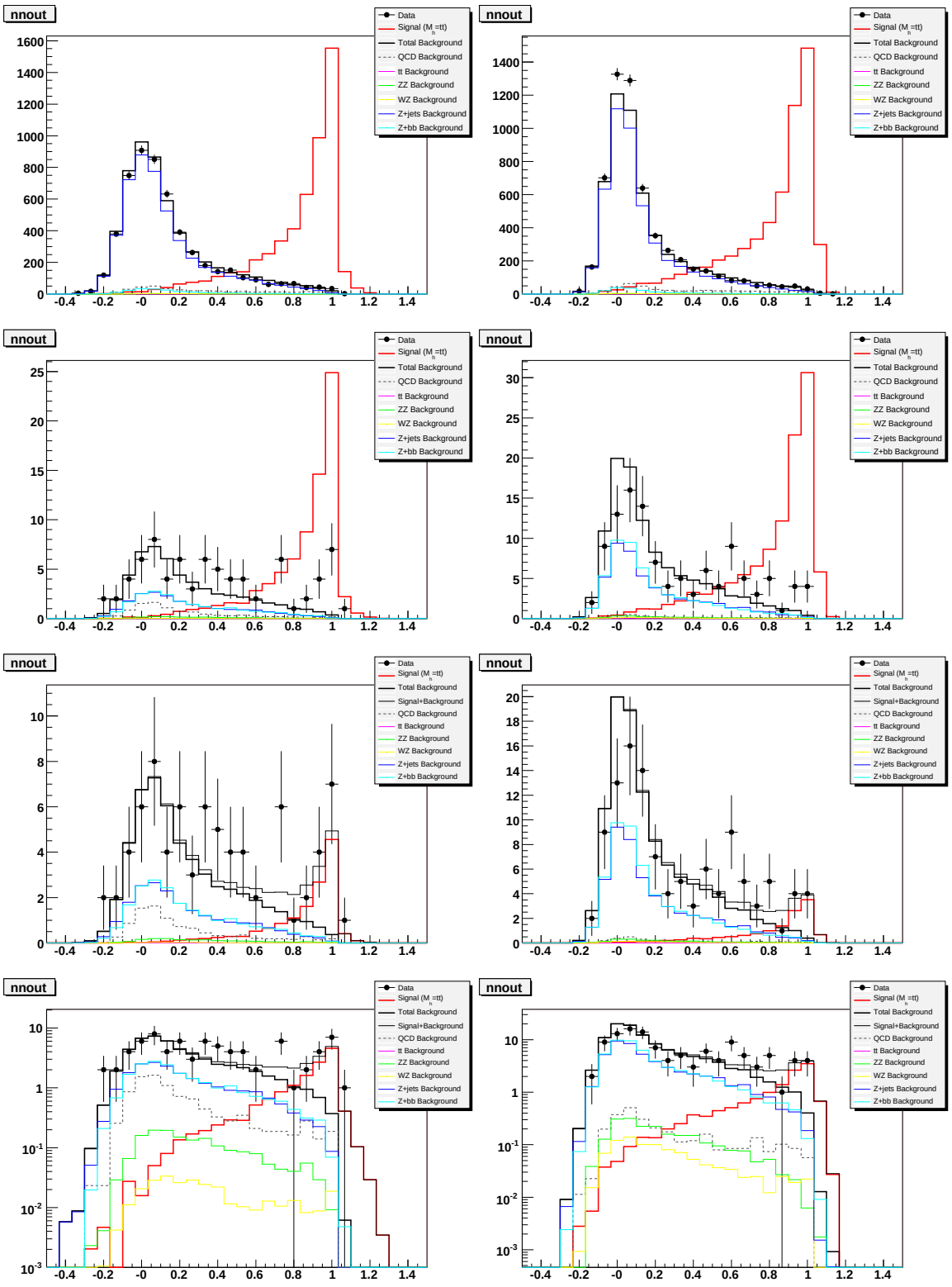

Figure 13: The NN output for $t\bar{t}$ (with wide $M_{\mu\mu}$ selection cuts from 40–500 GeV) in the 2L (left) and 1T (right) channels: before b-tagging with signal scaled to background (top), after b-tagging with signal scaled to background (middle), and after b-tagging with signal scaled according to its expected cross section (bottom).

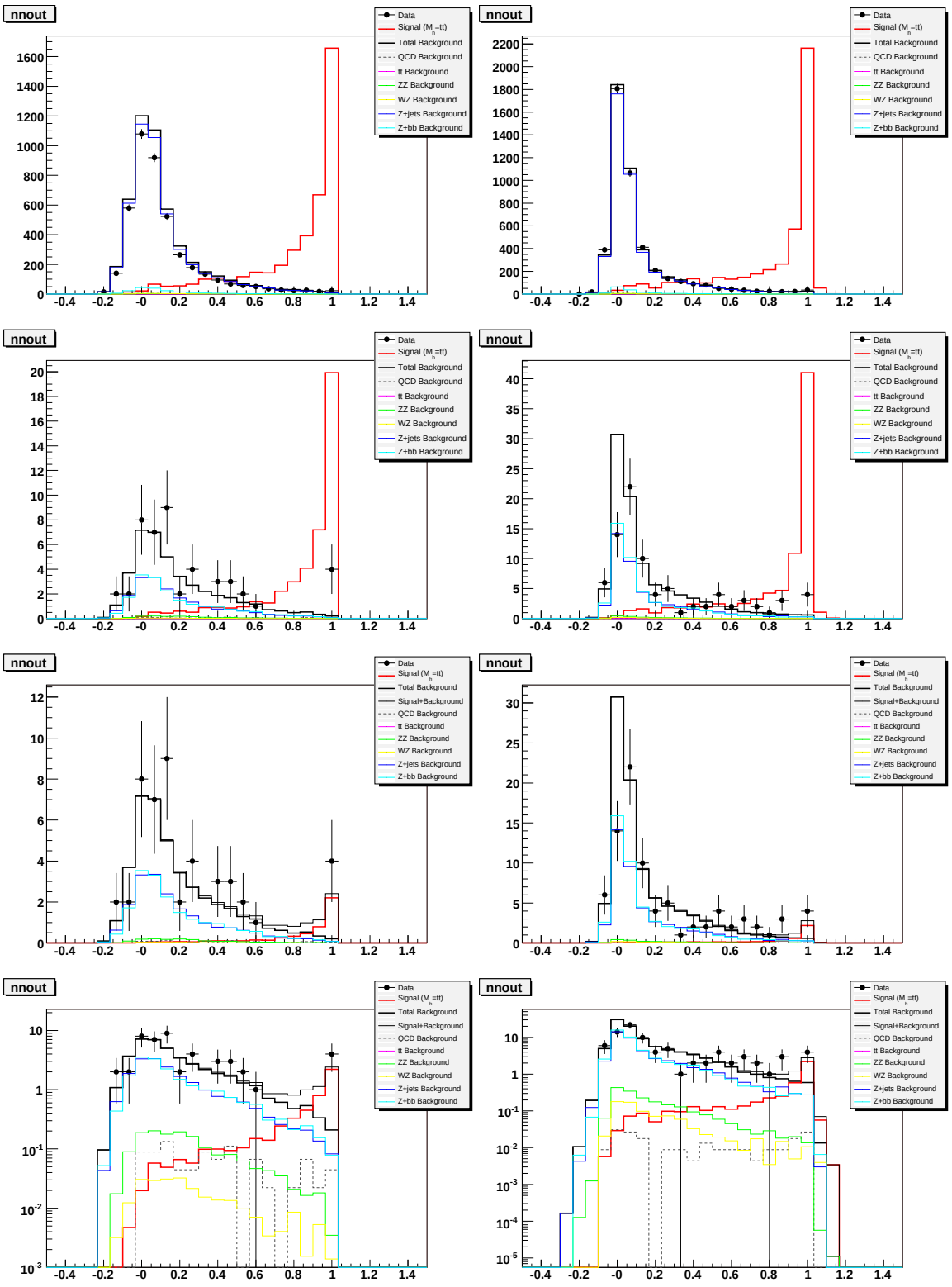

Figure 14: The NN output for $t\bar{t}$ in the 2L (left) and 1T (right) channels: before b-tagging with signal scaled to background (top), after b-tagging with signal scaled to background (middle), and after b-tagging with signal scaled according to its expected cross section (bottom).

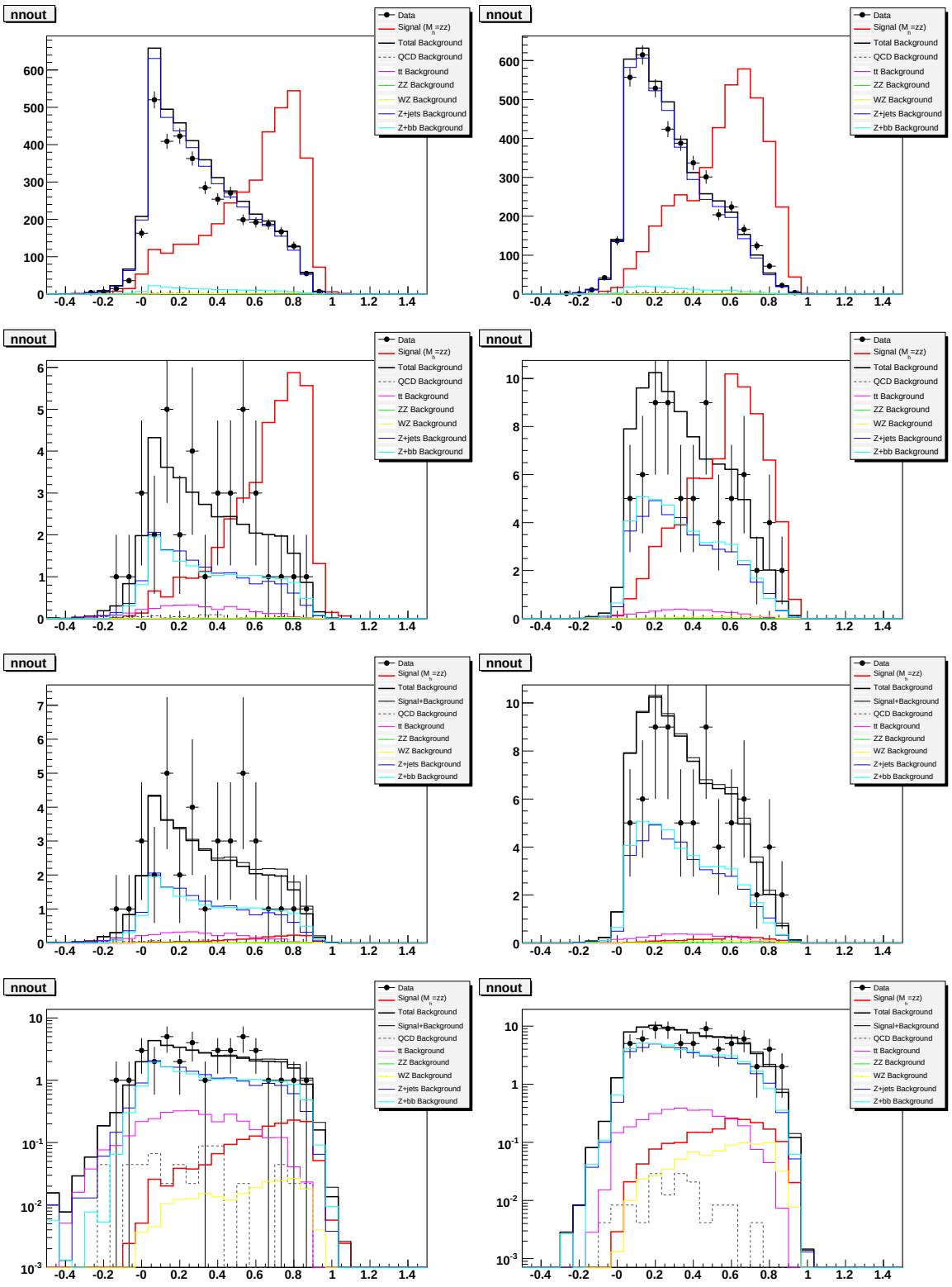

Figure 15: The NN output for ZZ in the 2L (left) and 1T (right) channels: before b-tagging with signal scaled to background (top), after b-tagging with signal scaled to background (middle), and after b-tagging with signal scaled according to its expected cross section (bottom).

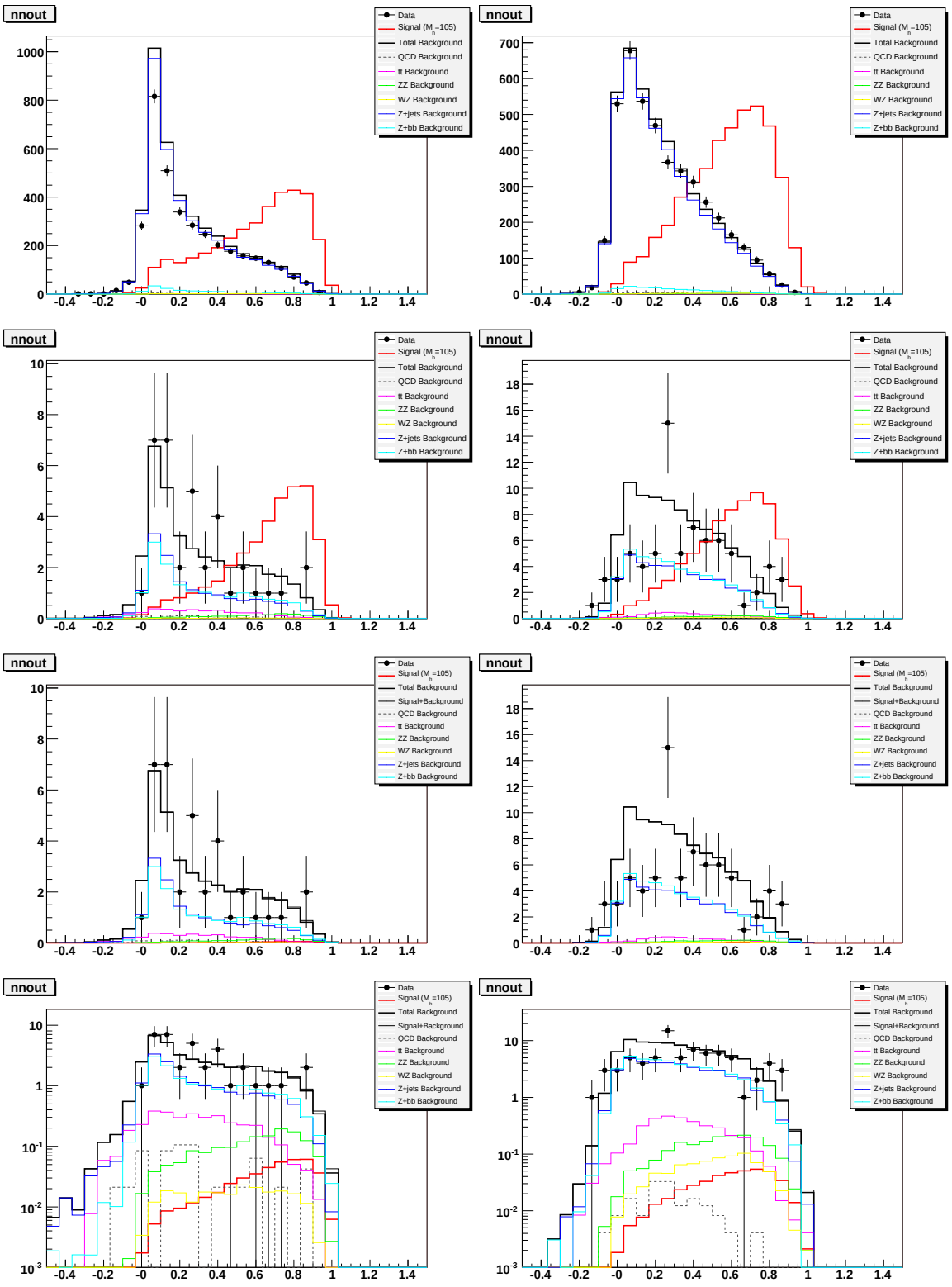

Figure 16: The NN output for ZH(105) in the 2L (left) and 1T (right) channels: before b-tagging with signal scaled to background (top), after b-tagging with signal scaled to background (middle), and after b-tagging with signal scaled according to its expected cross section (bottom).

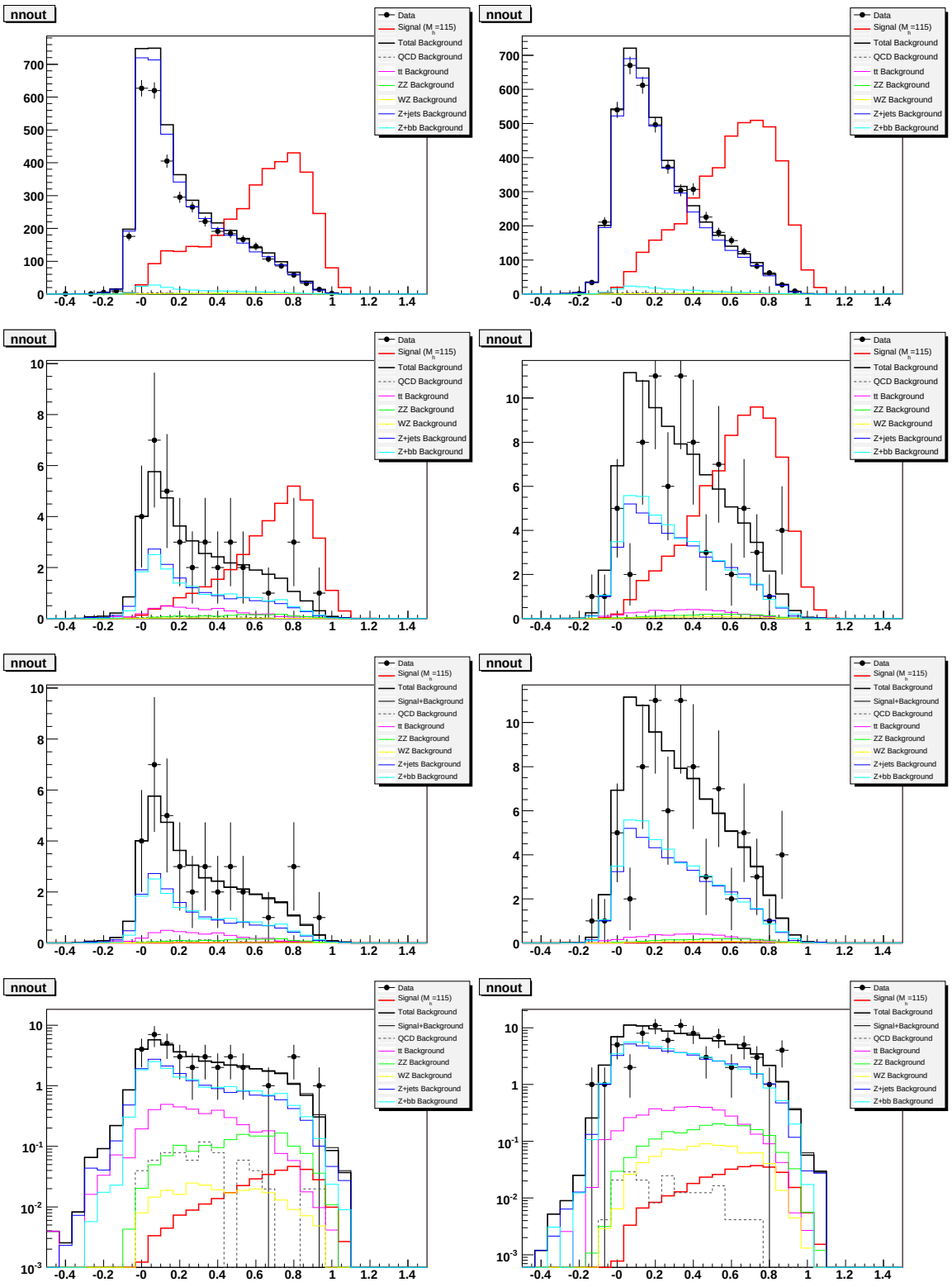

Figure 17: The NN output for ZH(115) in the 2L (left) and 1T (right) channels: before b-tagging with signal scaled to background (top), after b-tagging with signal scaled to background (middle), and after b-tagging with signal scaled according to its expected cross section (bottom).

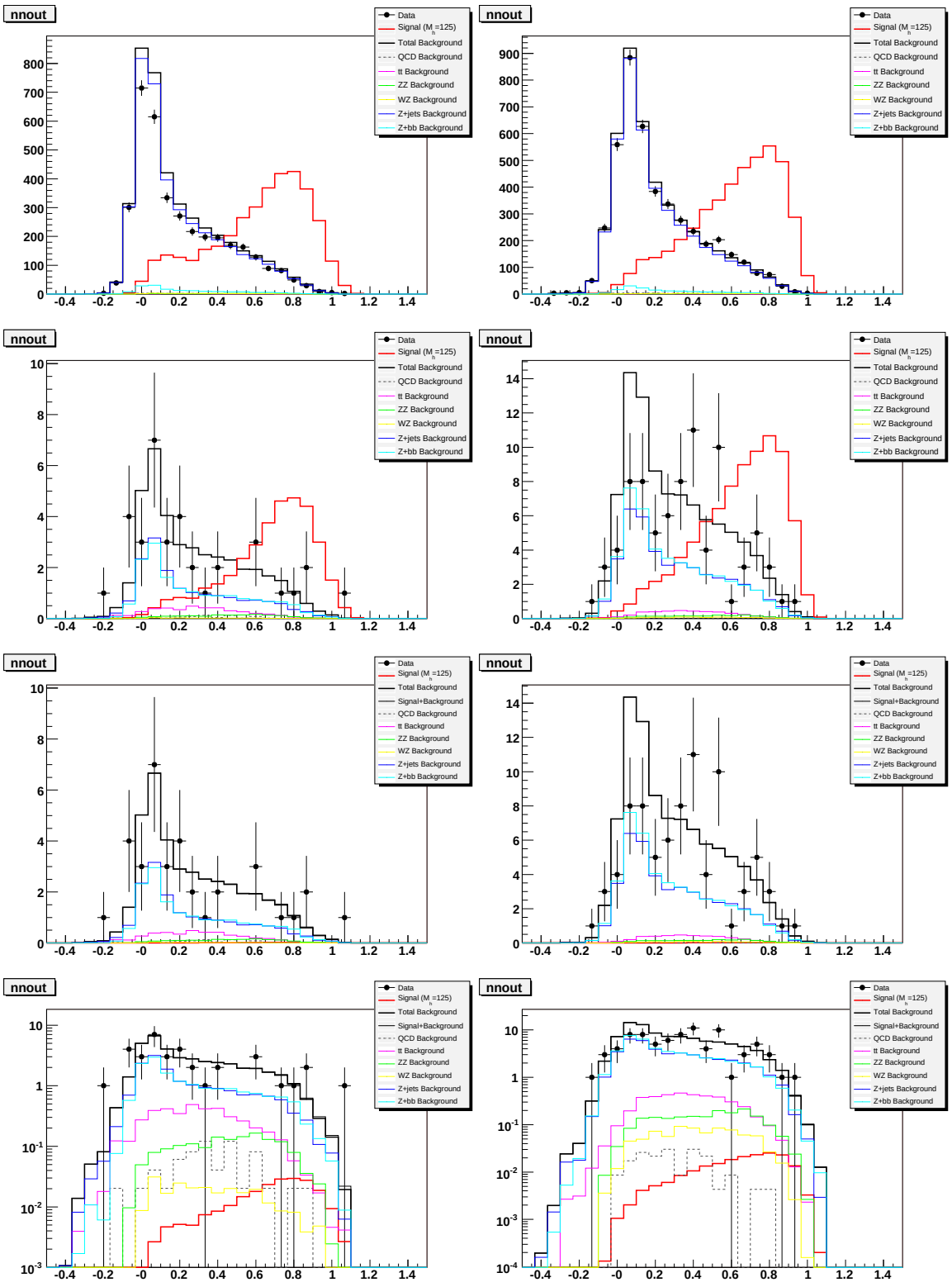

Figure 18: The NN output for ZH(125) in the 2L (left) and 1T (right) channels: before b-tagging with signal scaled to background (top), after b-tagging with signal scaled to background (middle), and after b-tagging with signal scaled according to its expected cross section (bottom).

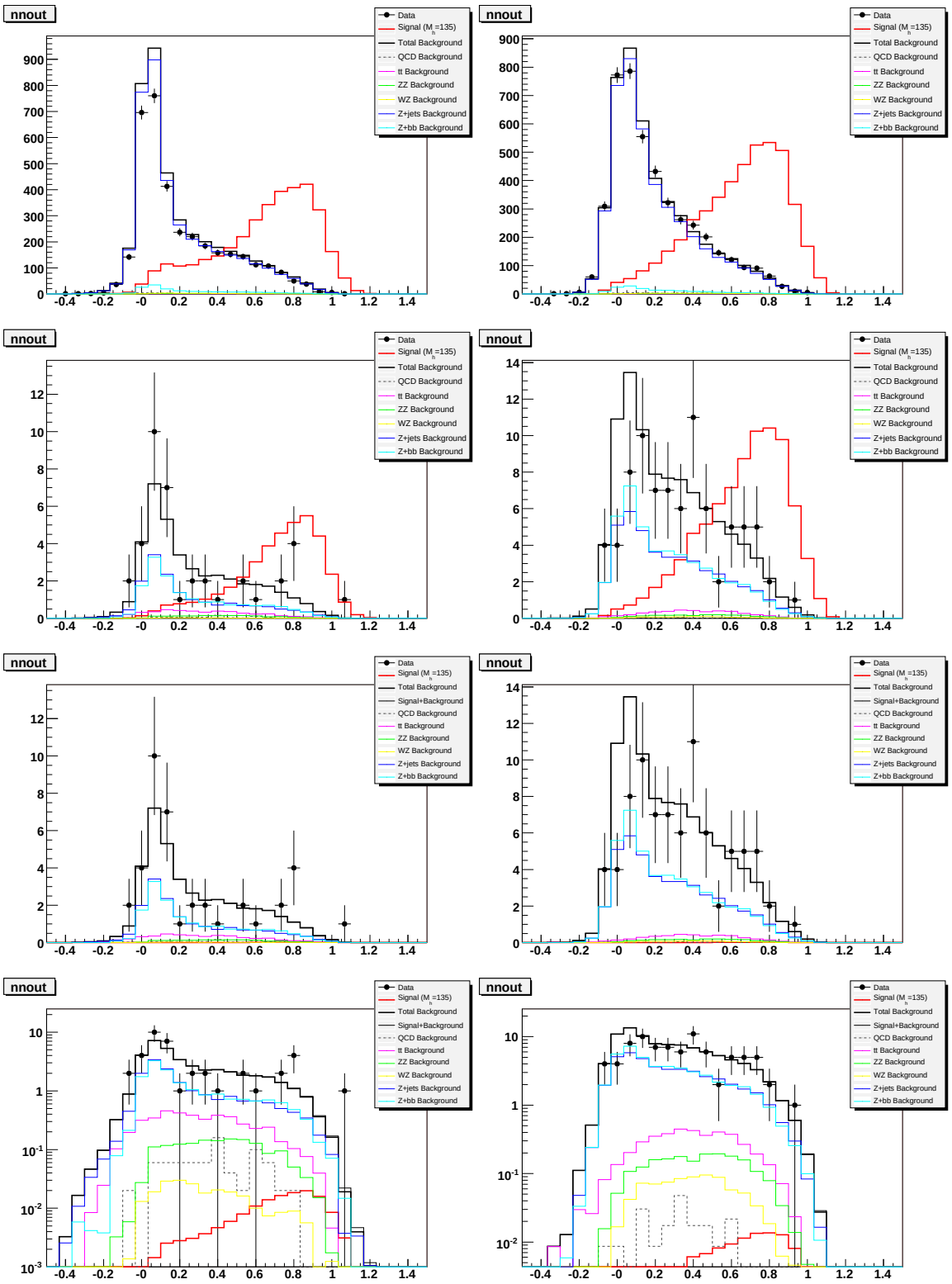

Figure 19: The NN output for ZH(135) in the 2L (left) and 1T (right) channels: before b-tagging with signal scaled to background (top), after b-tagging with signal scaled to background (middle), and after b-tagging with signal scaled according to its expected cross section (bottom).

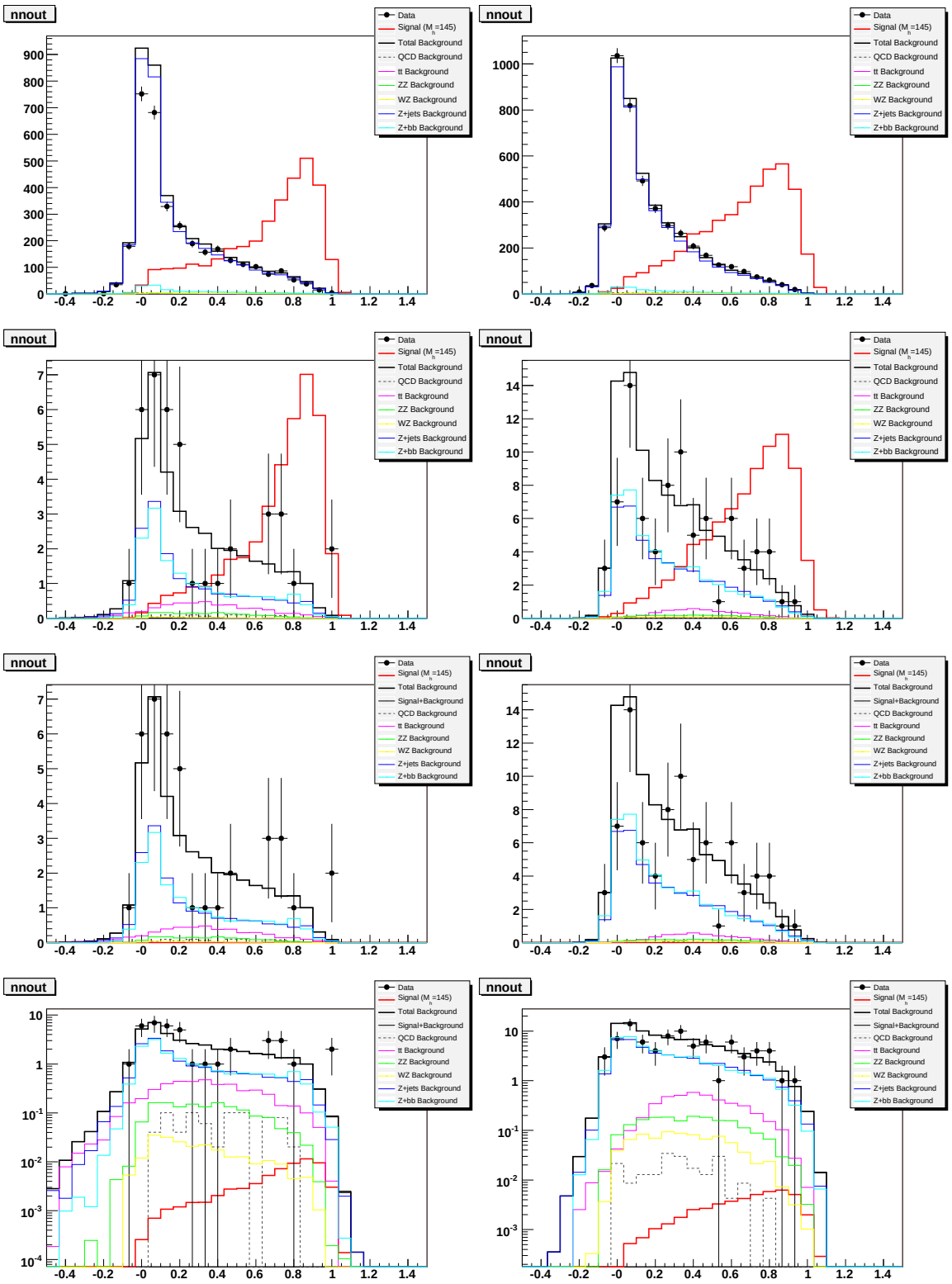

Figure 20: The NN output for ZH(145) in the 2L (left) and 1T (right) channels: before b-tagging with signal scaled to background (top), after b-tagging with signal scaled to background (middle), and after b-tagging with signal scaled according to its expected cross section (bottom).

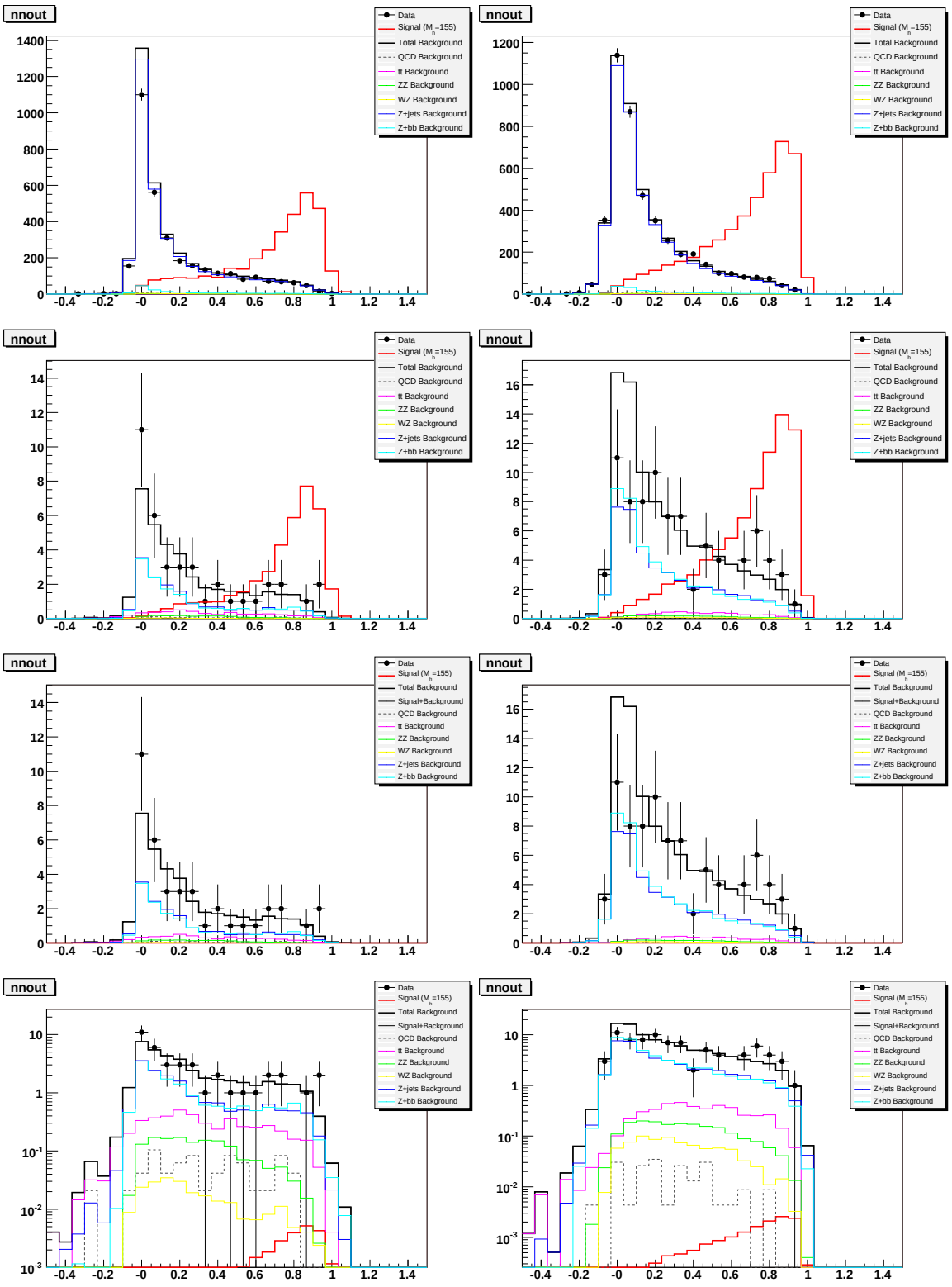

Figure 21: The NN output for ZH(155) in the 2L (left) and 1T (right) channels: before b-tagging with signal scaled to background (top), after b-tagging with signal scaled to background (middle), and after b-tagging with signal scaled according to its expected cross section (bottom).

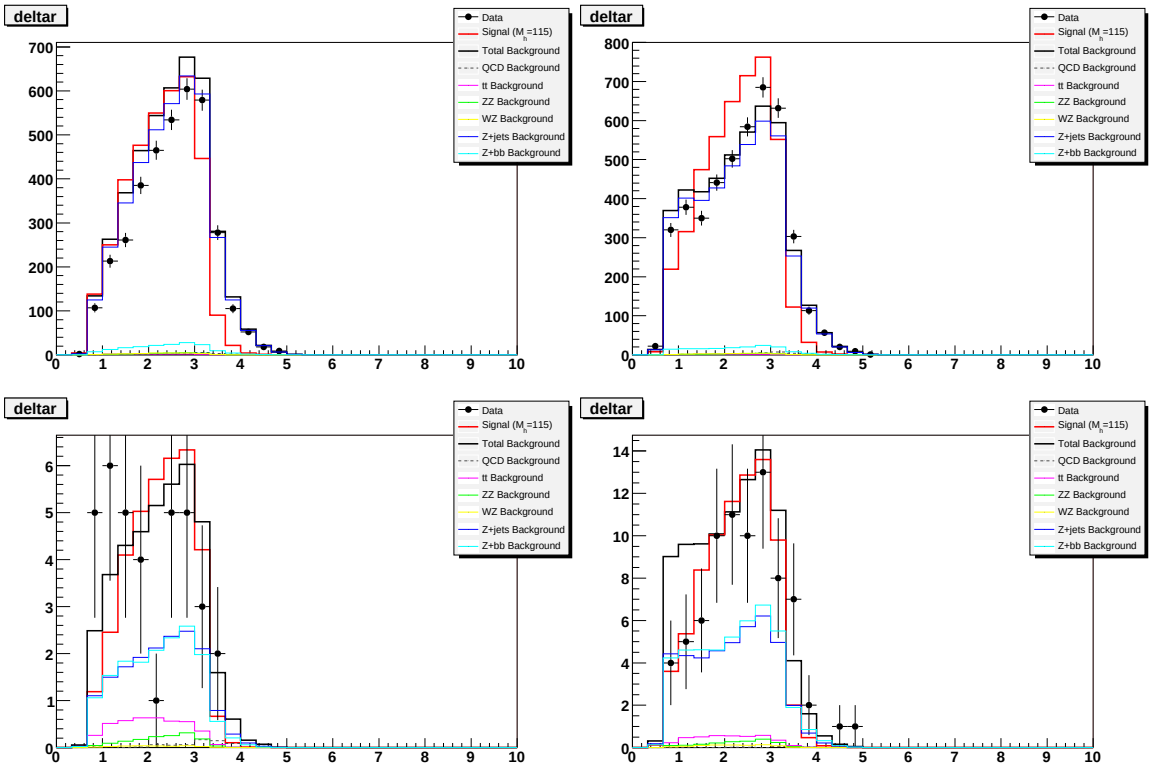

Figure 22: The ΔR between the two leading p_T jets for ZH(115) in the 2L (left) and 1T (right) channels: before b-tagging with signal scaled to background (top) and after b-tagging with signal scaled to background (bottom).

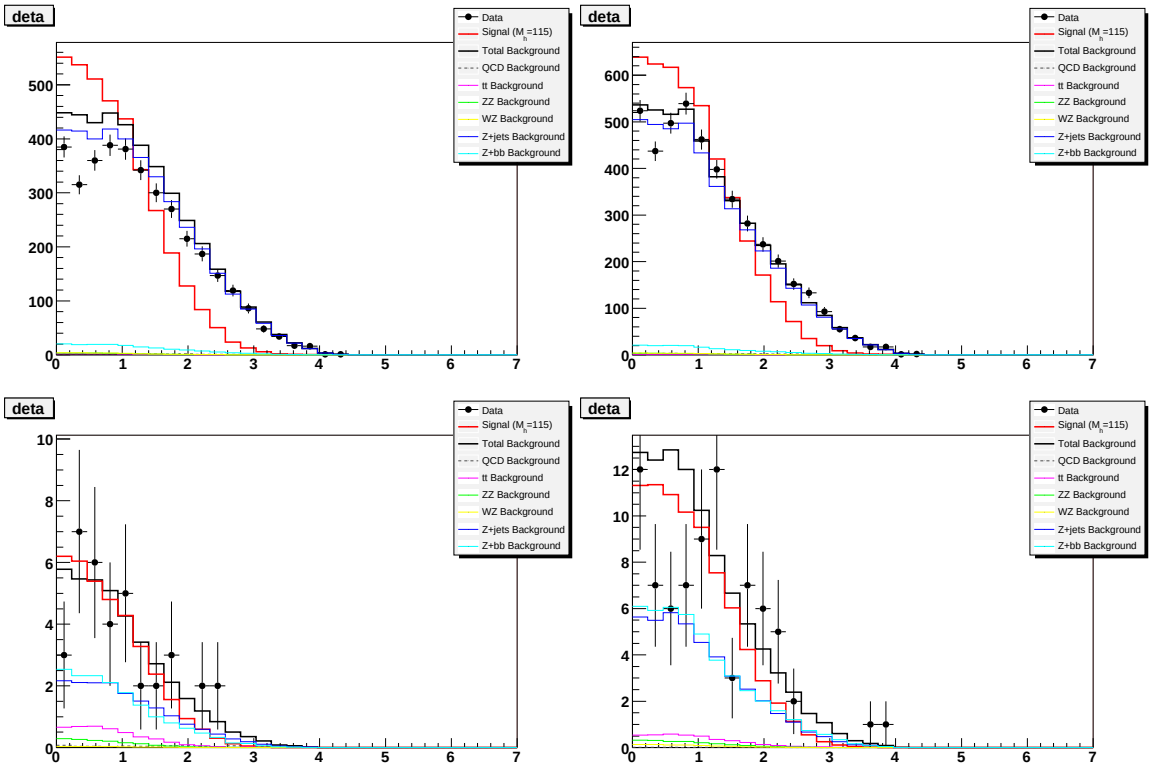

Figure 23: The absolute value of the $\Delta\eta$ between the two leading p_T jets for ZH(115) in the 2L (left) and 1T (right) channels: before b-tagging with signal scaled to background (top) and after b-tagging with signal scaled to background (bottom).

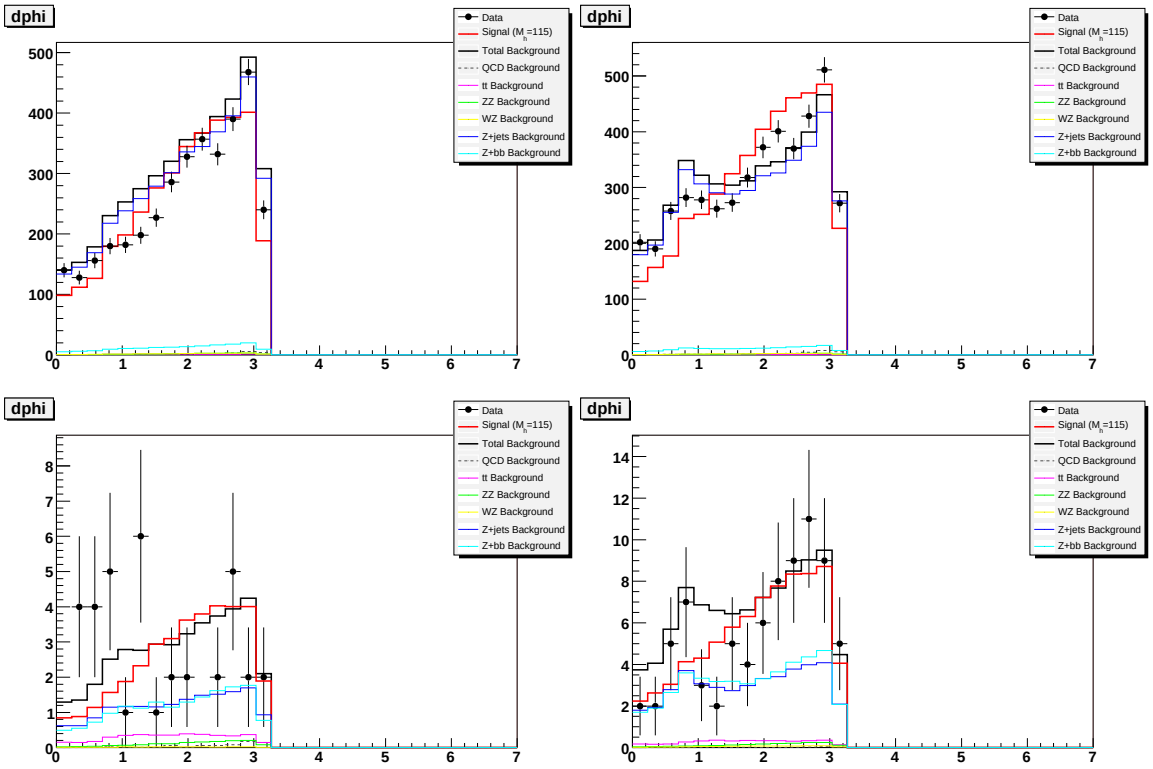

Figure 24: The absolute value of the $\Delta\phi$ between the two leading p_T jets for ZH(115) in the 2L (left) and 1T (right) channels: before b-tagging with signal scaled to background (top) and after b-tagging with signal scaled to background (bottom).

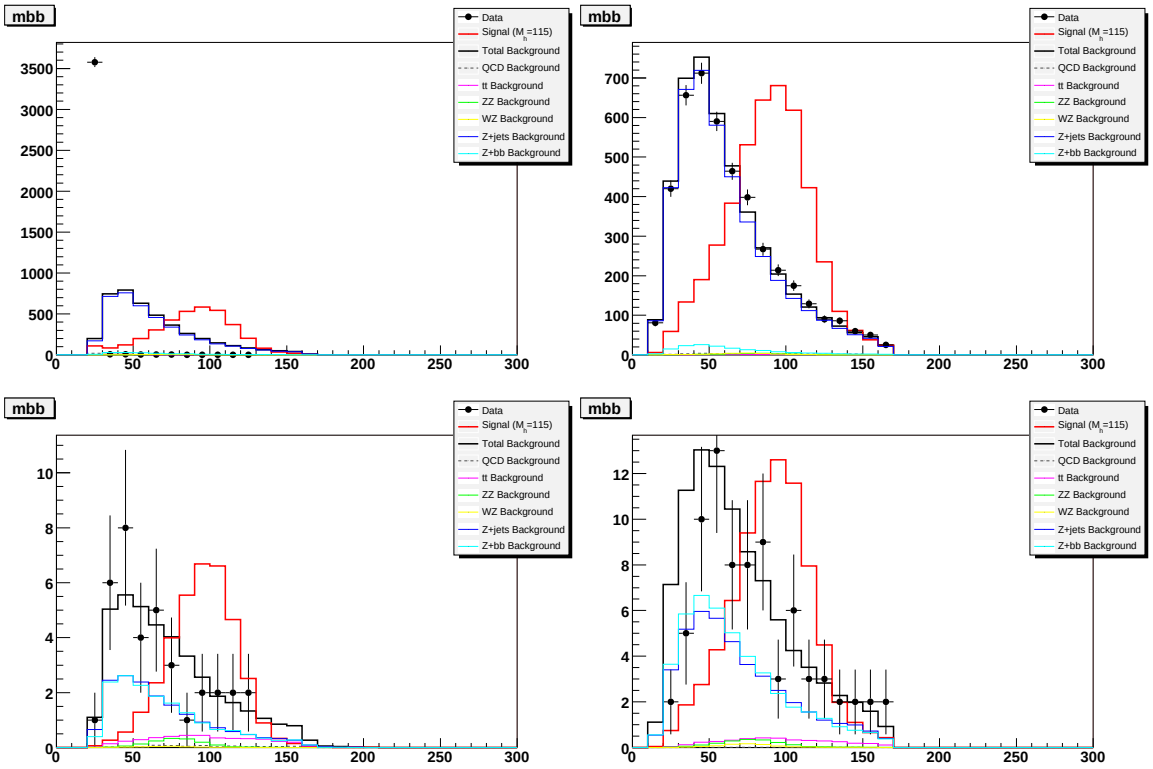

Figure 25: The invariant mass of two b-tagged jets for ZH(115) in the 2L (left) and 1T (right) channels: before b-tagging with signal scaled to background (top) and after b-tagging with signal scaled to background (bottom).

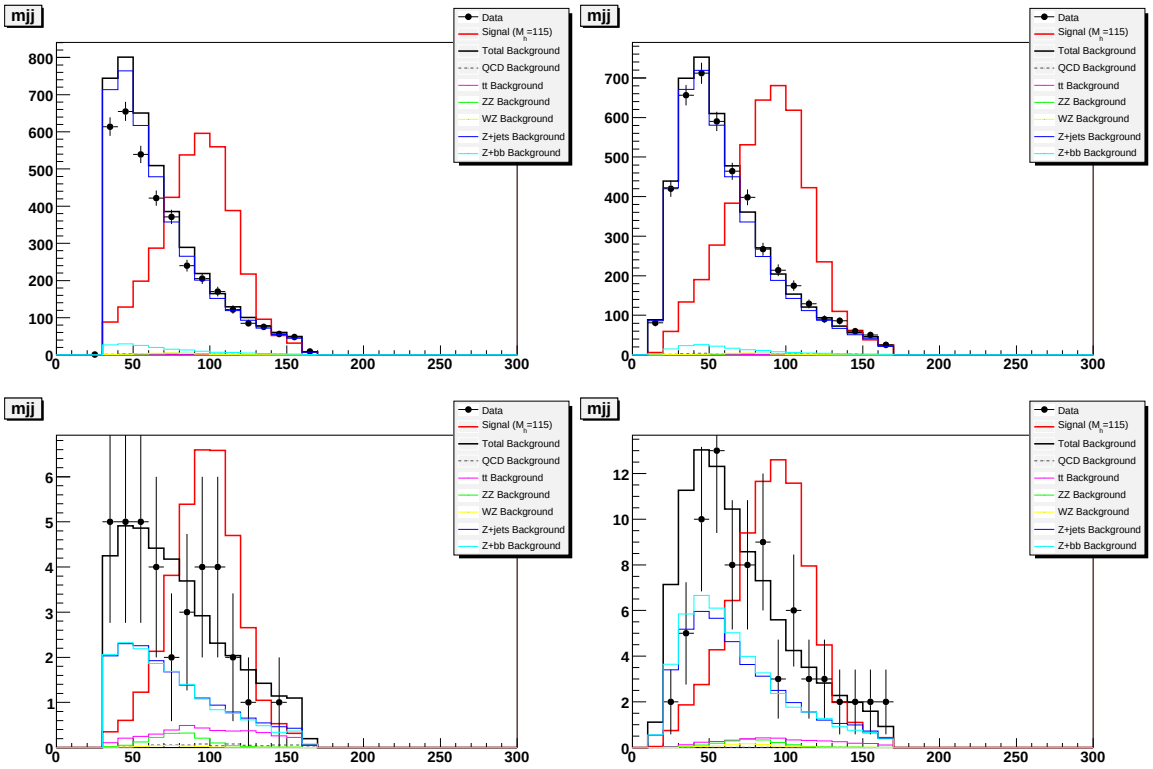

Figure 26: The invariant mass of the two leading p_T jets for ZH(115) in the 2L (left) and 1T (right) channels: before b-tagging with signal scaled to background (top) and after b-tagging with signal scaled to background (bottom).

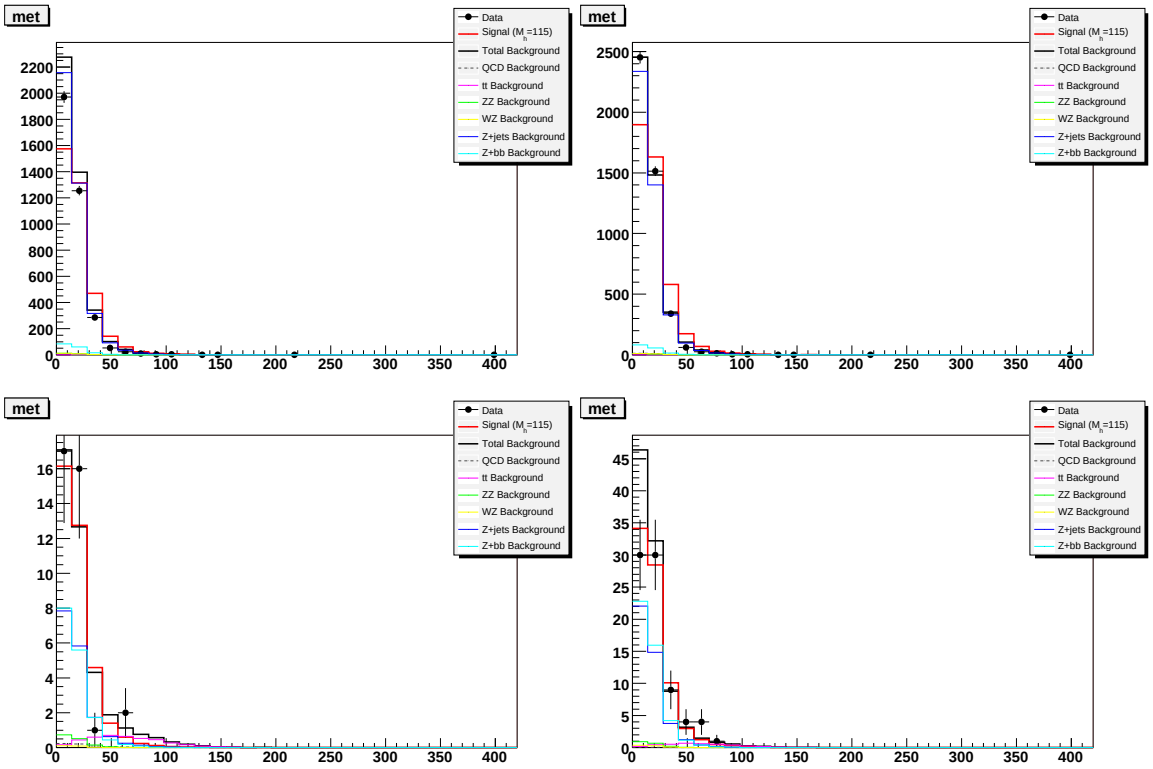

Figure 27: The $\not\!\!E_T$ for ZH(115) in the 2L (left) and 1T (right) channels: before b-tagging with signal scaled to background (top) and after b-tagging with signal scaled to background (bottom).

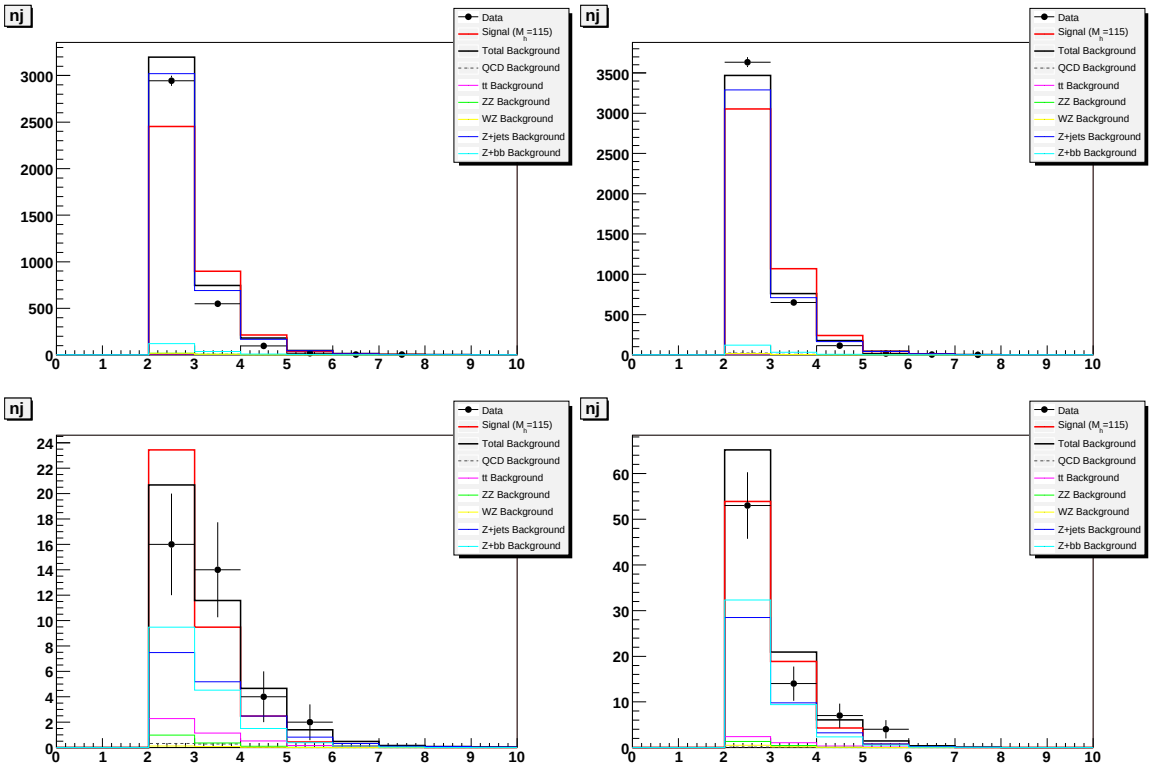

Figure 28: The number of jets (with p_T>15 GeV) for ZH(115) in the 2L (left) and 1T (right) channels: before b-tagging with signal scaled to background (top) and after b-tagging with signal scaled to background (bottom).

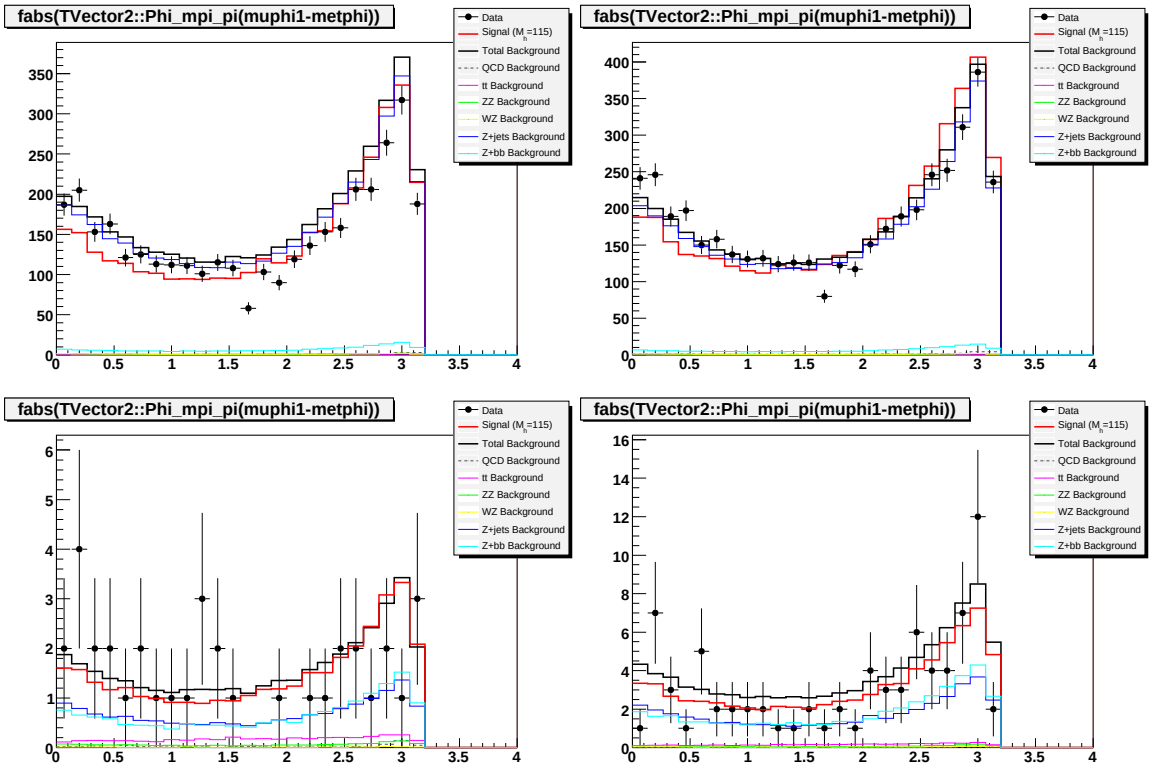

Figure 29: The $\Delta\phi$ between the leading p_T muon and the $\not\!\!E_T$ for ZH(115) in the 2L (left) and 1T (right) channels: before b-tagging with signal scaled to background (top) and after b-tagging with signal scaled to background (bottom).

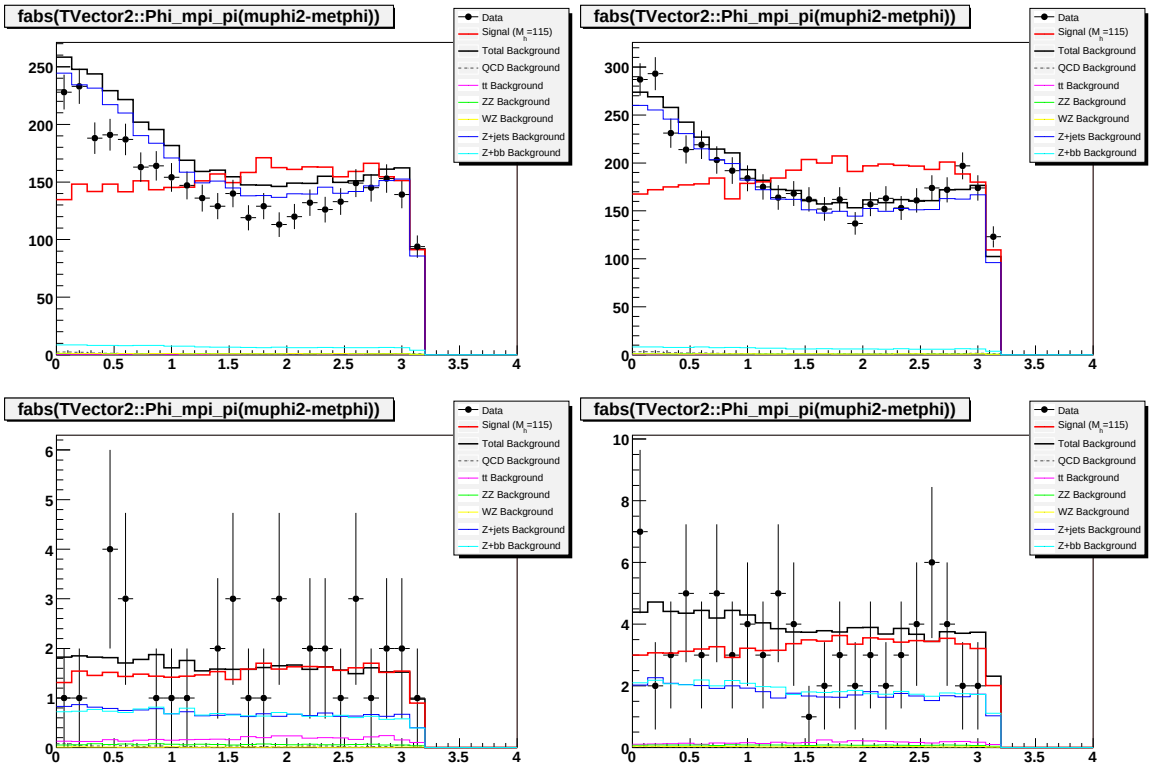

Figure 30: The $\Delta\phi$ between the second-leading p_T muon and the $\not\!\!E_T$ for ZH(115) in the 2L (left) and 1T (right) channels: before b-tagging with signal scaled to background (top) and after b-tagging with signal scaled to background (bottom).

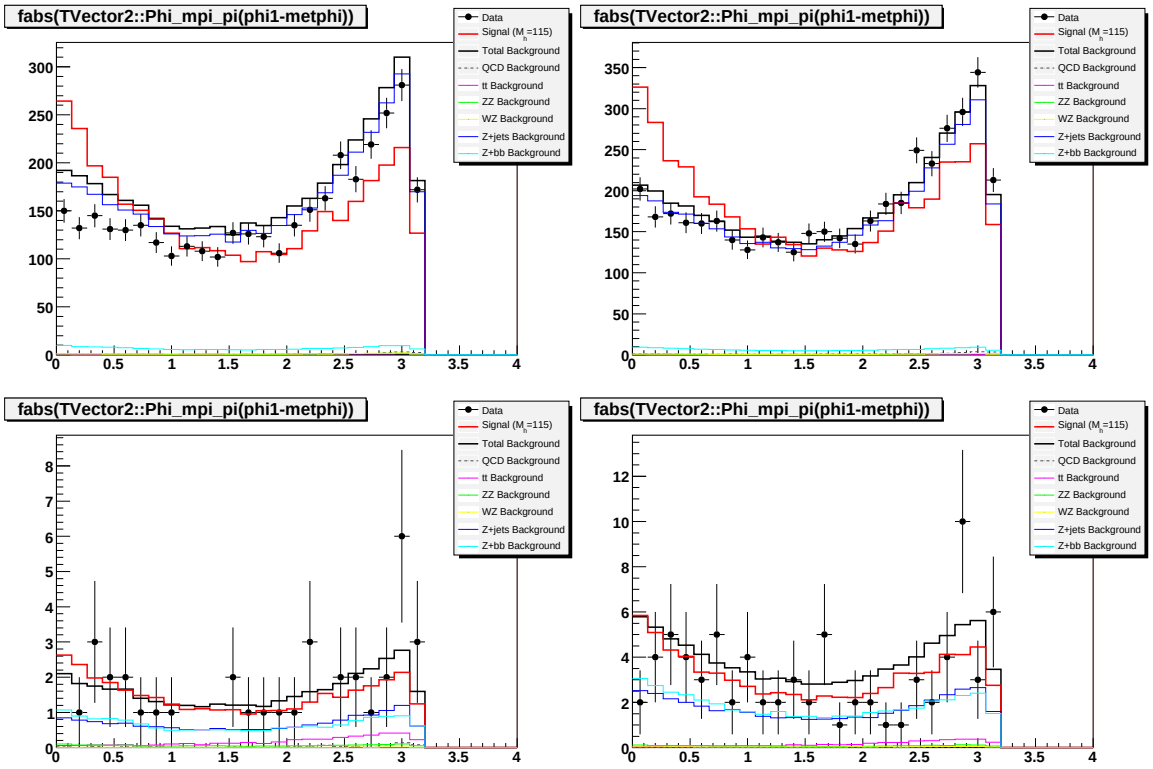

Figure 31: The $\Delta\phi$ between the leading p_T jet and the $\not\!\!E_T$ for ZH(115) in the 2L (left) and 1T (right) channels: before b-tagging with signal scaled to background (top) and after b-tagging with signal scaled to background (bottom).

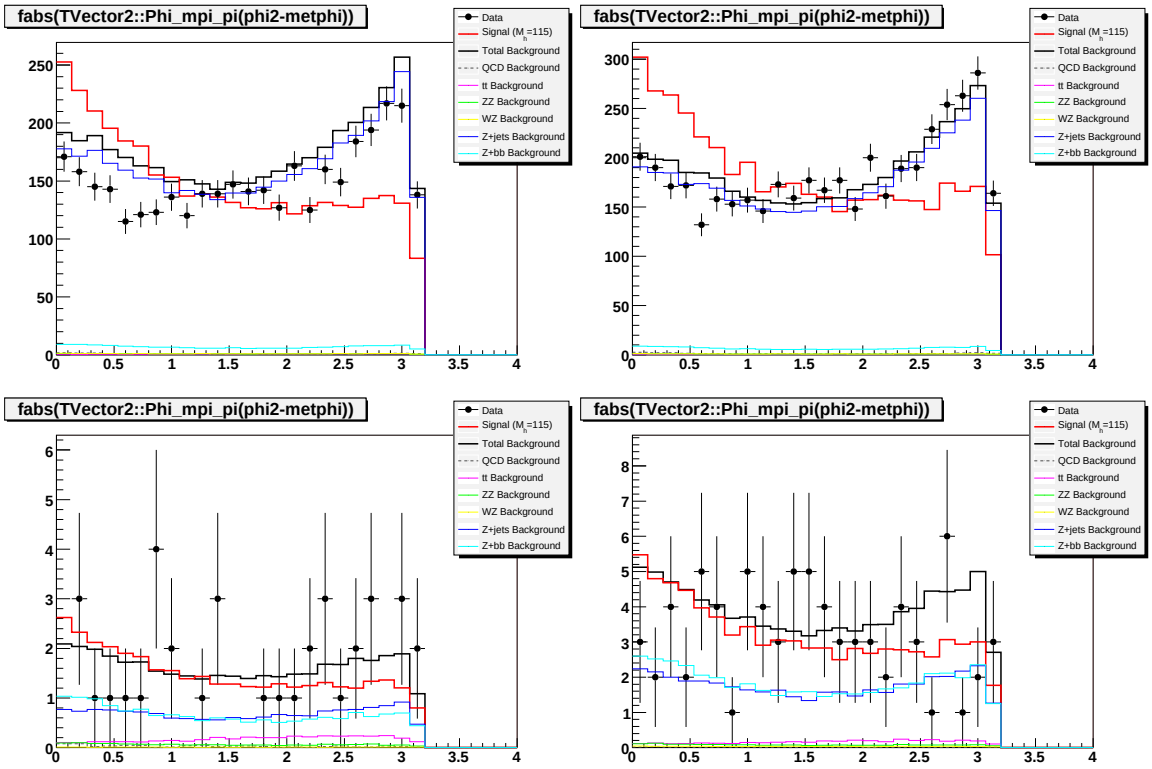

Figure 32: The $\Delta\phi$ between the second-leading p_T muon and the $\not\!\!E_T$ for ZH(115) in the 2L (left) and 1T (right) channels: before b-tagging with signal scaled to background (top) and after b-tagging with signal scaled to background (bottom).

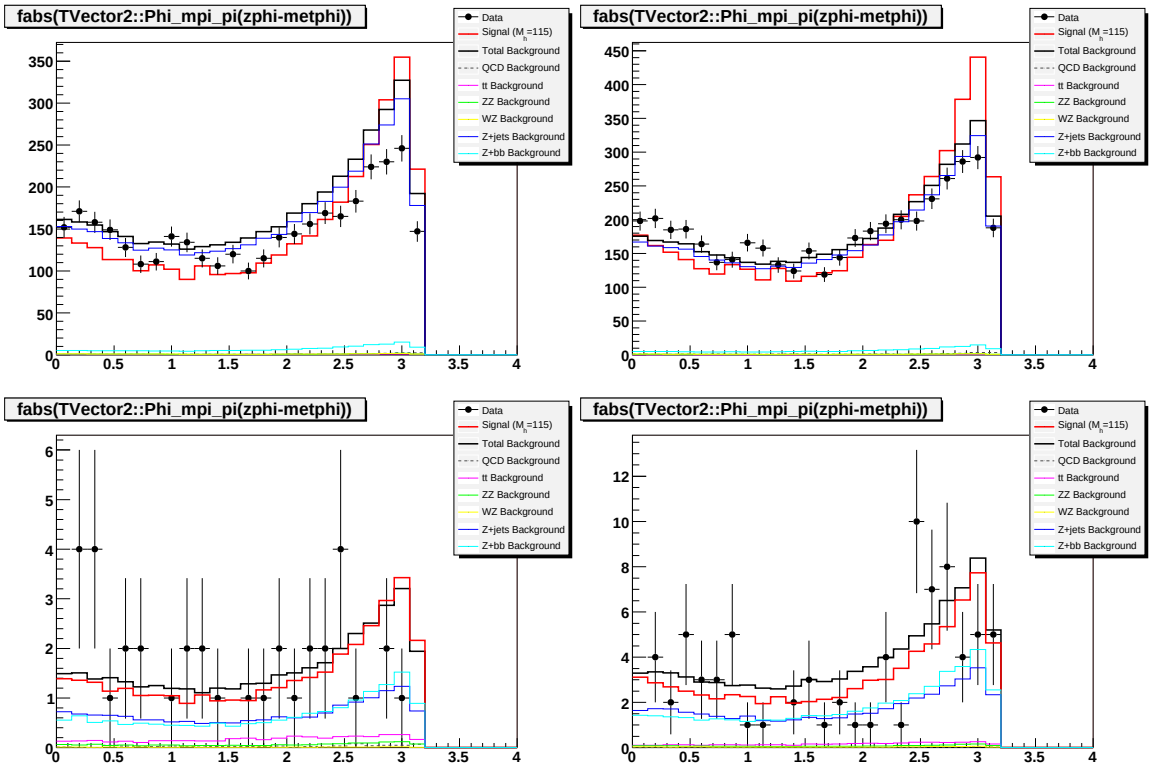

Figure 33: The $\Delta\phi$ between the Z and the $\not\!\!E_T$ for ZH(115) in the 2L (left) and 1T (right) channels: before b-tagging with signal scaled to background (top) and after b-tagging with signal scaled to background (bottom).

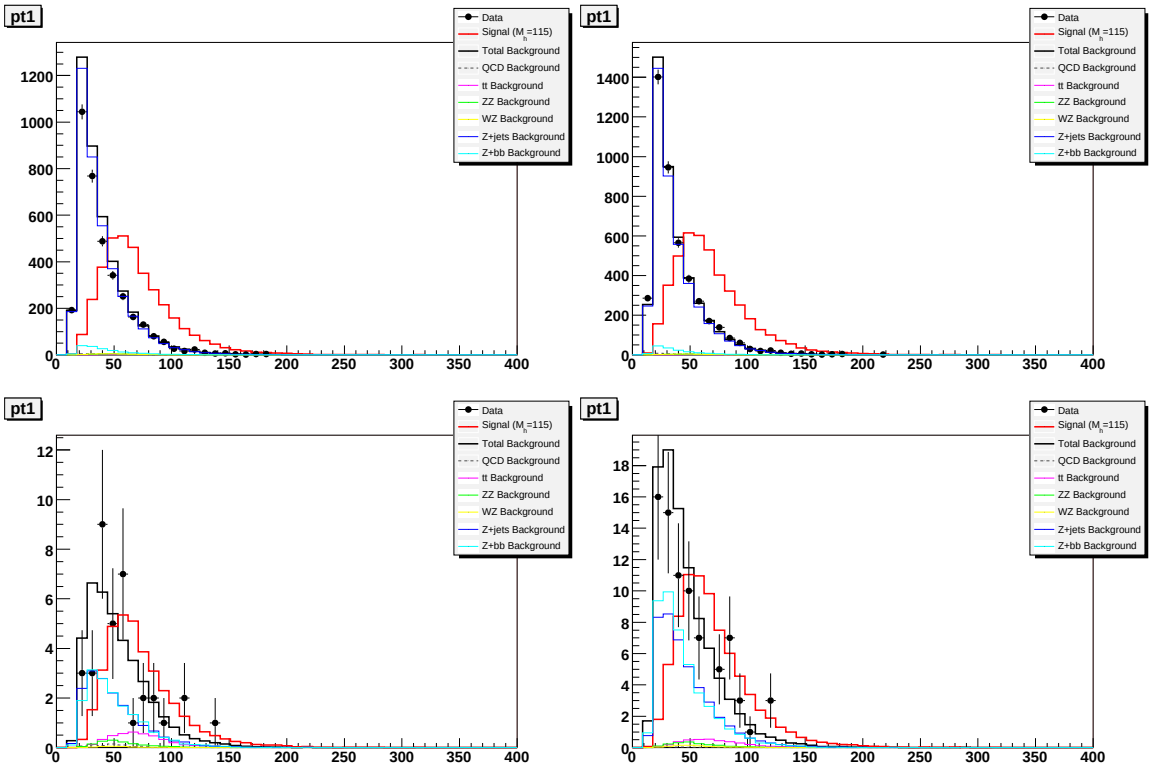

Figure 34: The p_T of the leading p_T jet for ZH(115) in the 2L (left) and 1T (right) channels: before b-tagging with signal scaled to background (top) and after b-tagging with signal scaled to background (bottom).

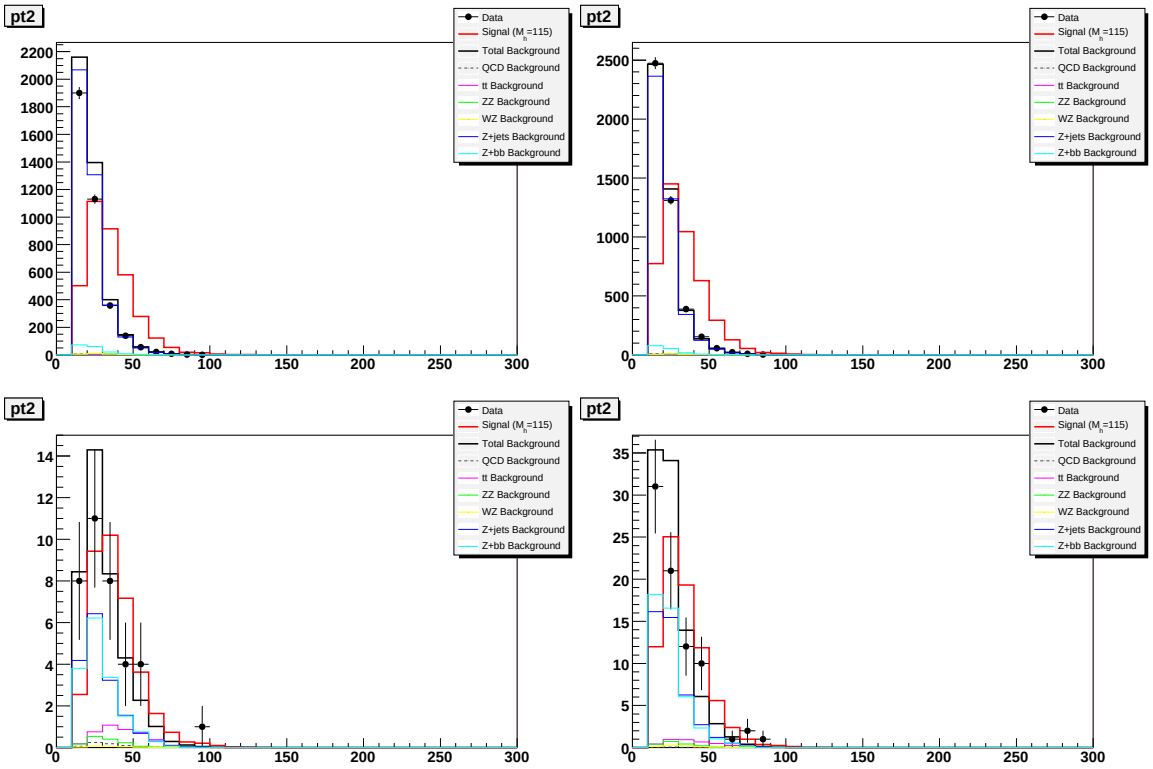

Figure 35: The p_T of the second-leading p_T jet for ZH(115) in the 2L (left) and 1T (right) channels: before b-tagging with signal scaled to background (top) and after b-tagging with signal scaled to background (bottom).

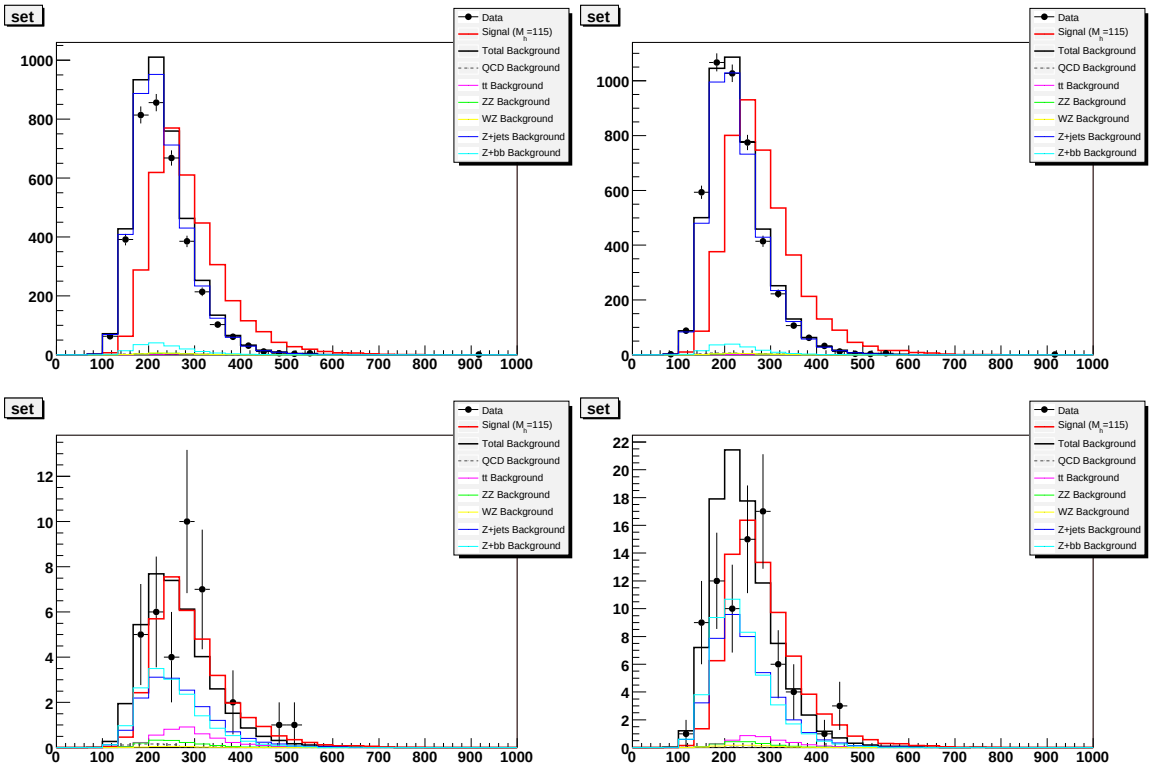

Figure 36: The scalar E_T for ZH(115) in the 2L (left) and 1T (right) channels: before b-tagging with signal scaled to background (top) and after b-tagging with signal scaled to background (bottom).

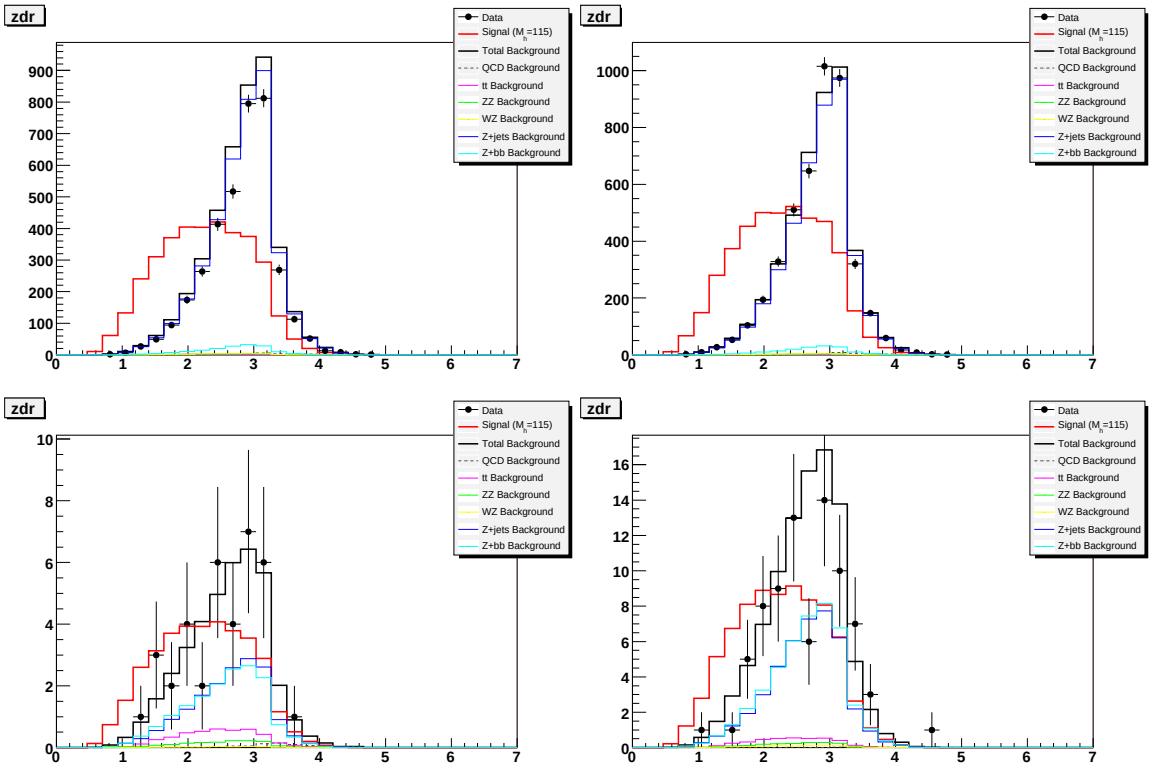

Figure 37: The ΔR between the two muons of the Z candidate for ZH(115) in the 2L (left) and 1T (right) channels: before b-tagging with signal scaled to background (top) and after b-tagging with signal scaled to background (bottom).

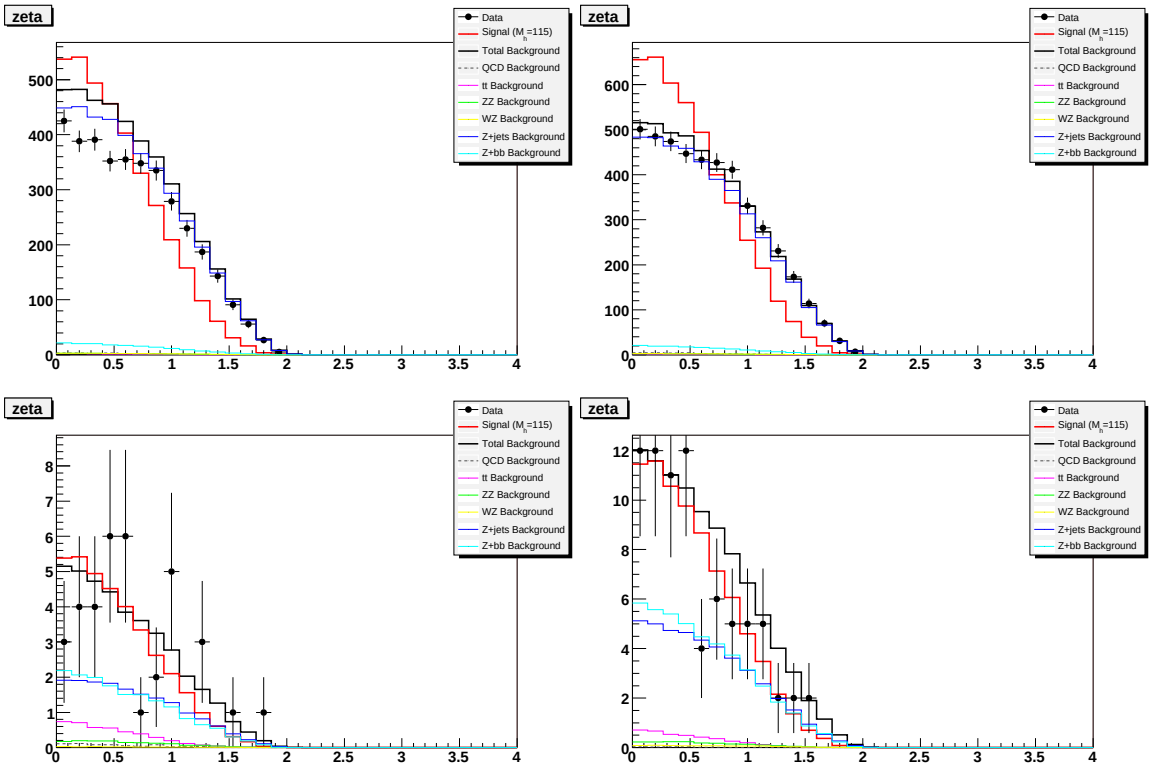

Figure 38: The $|\eta|$ of the Z candidate for ZH(115) in the 2L (left) and 1T (right) channels: before b-tagging with signal scaled to background (top) and after b-tagging with signal scaled to background (bottom).

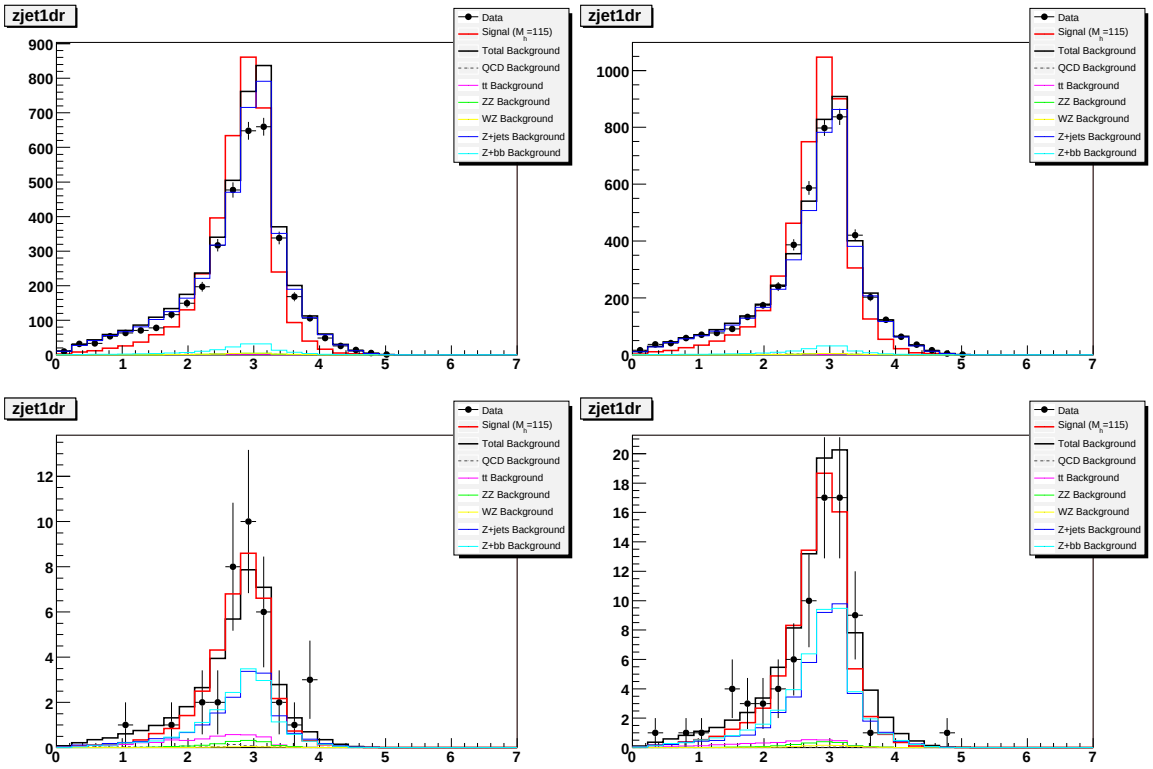

Figure 39: The ΔR between the Z candidate and the leading p_T jet for ZH(115) in the 2L (left) and 1T (right) channels: before b-tagging with signal scaled to background (top) and after b-tagging with signal scaled to background (bottom).

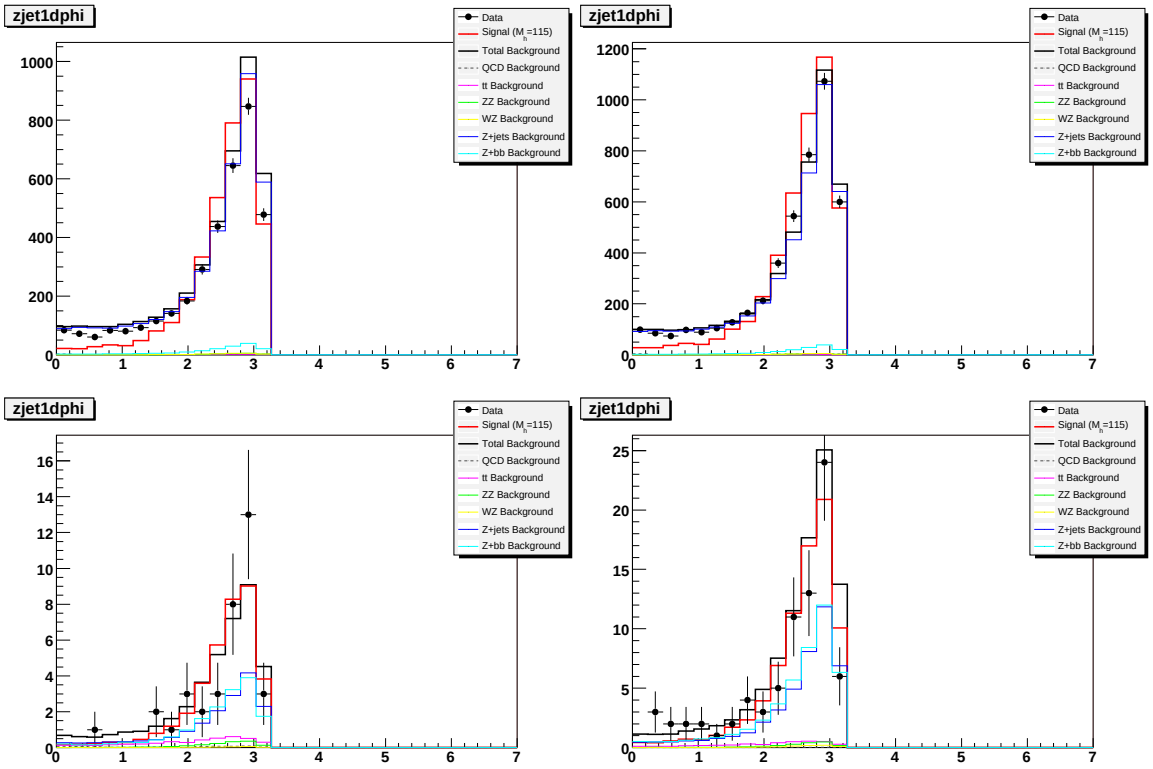

Figure 40: The $\Delta\phi$ between the Z candidate and the leading p_T jet for ZH(115) in the 2L (left) and 1T (right) channels: before b-tagging with signal scaled to background (top) and after b-tagging with signal scaled to background (bottom).

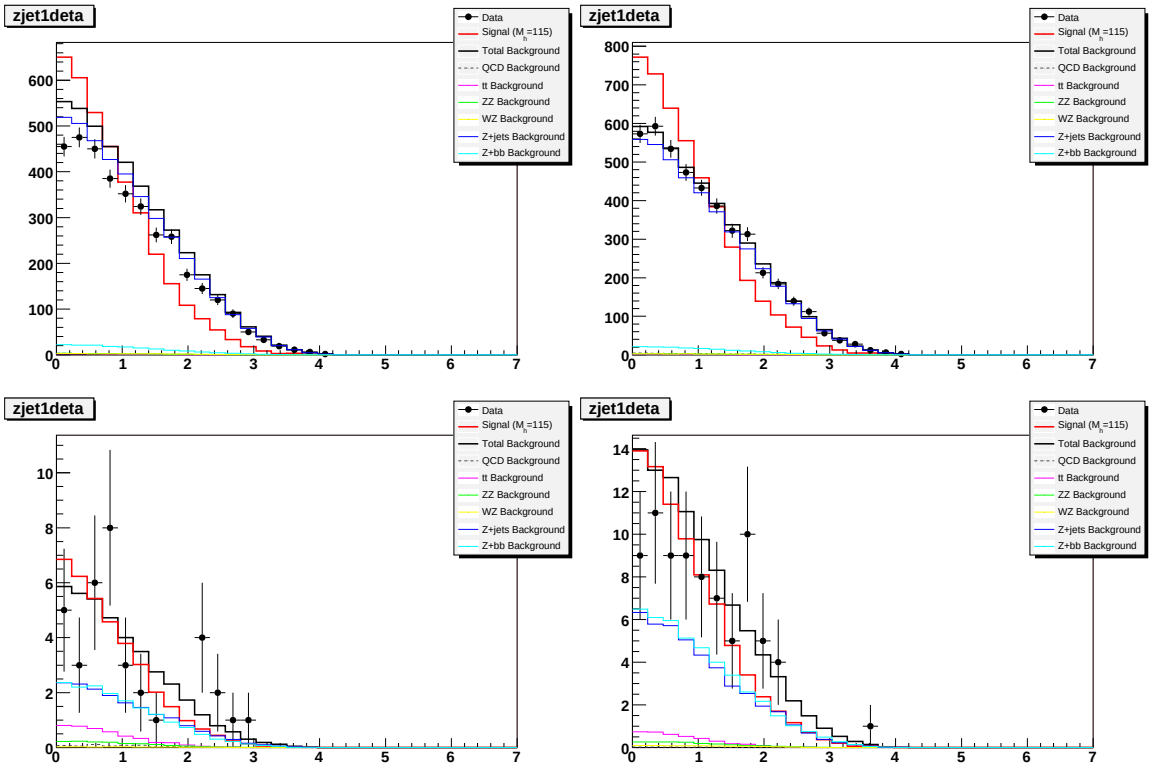

Figure 41: The $\Delta\eta$ between the Z candidate and the leading p_T jet for ZH(115) in the 2L (left) and 1T (right) channels: before b-tagging with signal scaled to background (top) and after b-tagging with signal scaled to background (bottom).

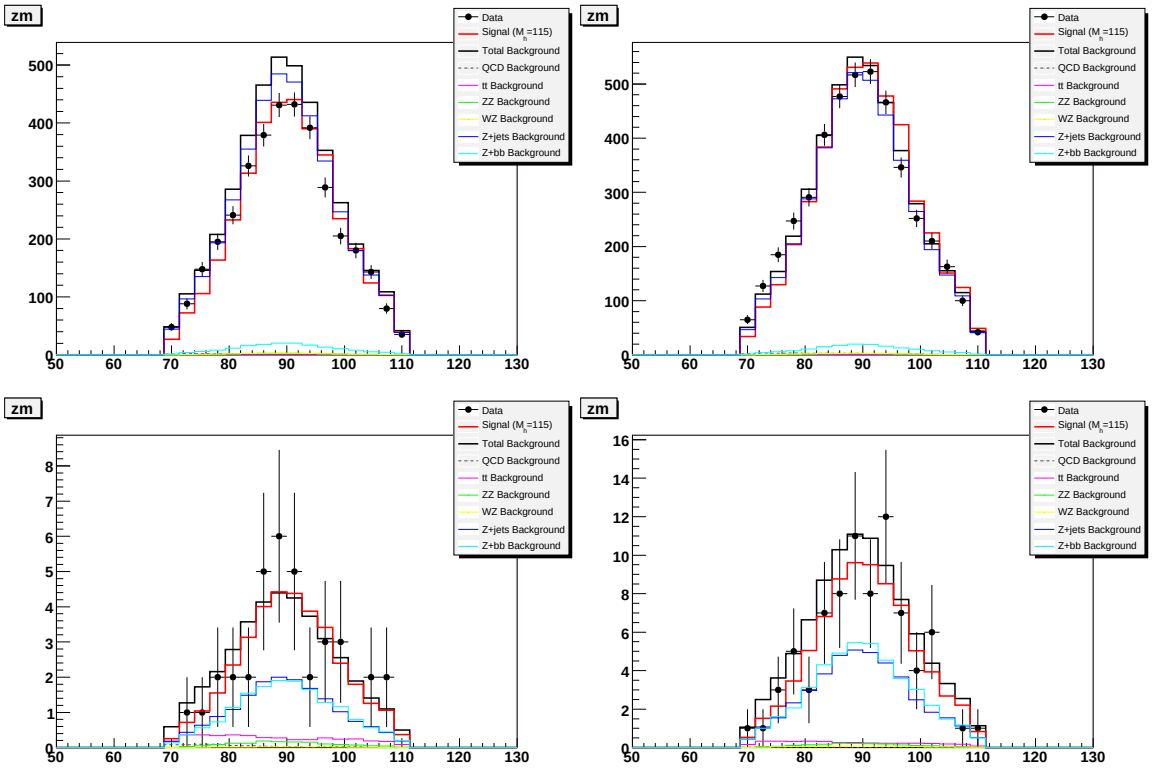

Figure 42: The mass of the Z candidate for ZH(115) in the 2L (left) and 1T (right) channels: before b-tagging with signal scaled to background (top) and after b-tagging with signal scaled to background (bottom).

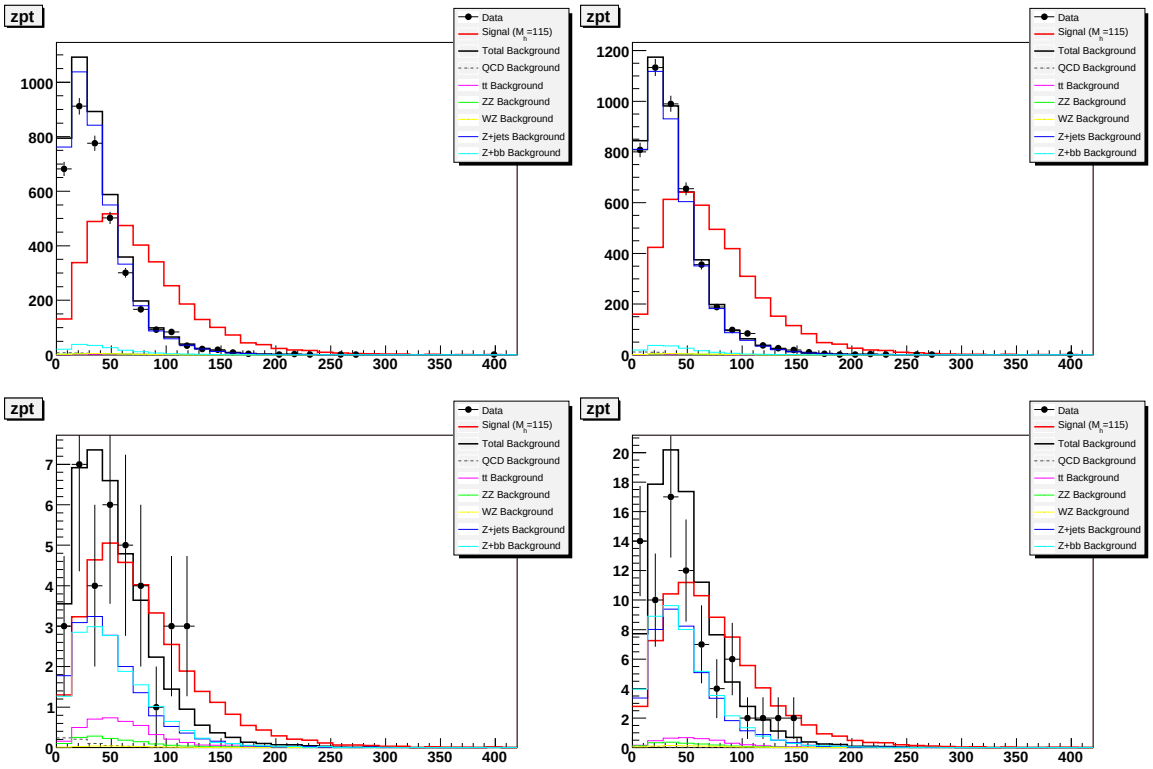

Figure 43: The p_T of the Z boson for ZH(115) in the 2L (left) and 1T (right) channels: before b-tagging with signal scaled to background (top) and after b-tagging with signal scaled to background (bottom).

m_H (GeV)	$\frac{S}{\sqrt{B}}$, no cut	$\frac{S}{\sqrt{B}}$, $M_{jj} \pm 1.5\sigma$ cut	$\frac{S}{\sqrt{B}}$, NN cut	$\frac{S}{\sqrt{B}}$ improvement
ZZ	0.147673	0.164123	0.189733	1.15604
105	0.0343727	0.040149	0.0508527	1.2666
115	0.0250861	0.0299971	0.0392238	1.30759
125	0.0164986	0.0203194	0.0275914	1.35788
135	0.0103027	0.0131932	0.0185488	1.40594
145	0.00492403	0.00656459	0.00958867	1.46067
155	0.00202224	0.00279023	0.00425873	1.5263
ZZ	0.172594	0.205798	0.246813	1.1993
105	0.0454573	0.0548417	0.0718437	1.31002
115	0.0343848	0.0424987	0.0580564	1.36607
125	0.02305	0.0284826	0.042001	1.47462
135	0.0148352	0.01932	0.0287515	1.48817
145	0.00736767	0.00962298	0.0151542	1.57479
155	0.0030547	0.00410121	0.0064064	1.56207

Table 9: The $S/\sqrt{B}$ using no cut, an $M_{jj} \pm 1.5\sigma$ cut, or an optimal NN output cut for each signal mass (and ZZ) in the 1T (top) and 2L (bottom) channels. Also shown is the improvement in $S/\sqrt{B}$ by using the NN output cut vs. the simpler $M_{jj} \pm 1.5\sigma$ cut.

8 Results Using NN Event Selection

Table 9 shows the sensitivity ($S/\sqrt{B}$) gained by each NN, using a simple method which places an optimal cut on the NN output and counts the number of S and B events remaining above the cut. Combined with the limits set using the M_{jj}-based method, one could then estimate the final sensitivity of each channel for each signal mass (and ZZ) after the NN has been applied.

Final limits are set using the full shape of the NN output for each signal and total background, using a LEP-like modified-frequentist approach [17]. This method also makes it trivial to combine the 1T and 2L channels. Figure 44 shows the log-likelihood sensitivities vs. mass for 1T+2L combined channels. The final limits on the cross-section for each signal mass (and ZZ) are shown in Table 10 and Figures 45 and 46.

These Higgs limits are still a factor of about 20 larger than the SM cross-section, at a Higgs mass of 115 GeV. However, this is just one channel, from one experiment, with about 10% of the final Run II integrated luminosity. And many further analysis improvements are still to be included, such as improved di-jet mass resolution, and optimization of b-tagging including the new silicon layer 0. We're still hopeful to discover a light SM Higgs boson by the end of Run II.

The expected limits on ZZ production are about a factor of 4 larger than the SM cross-section in this channel. Combined with the electron channel, we are only a factor

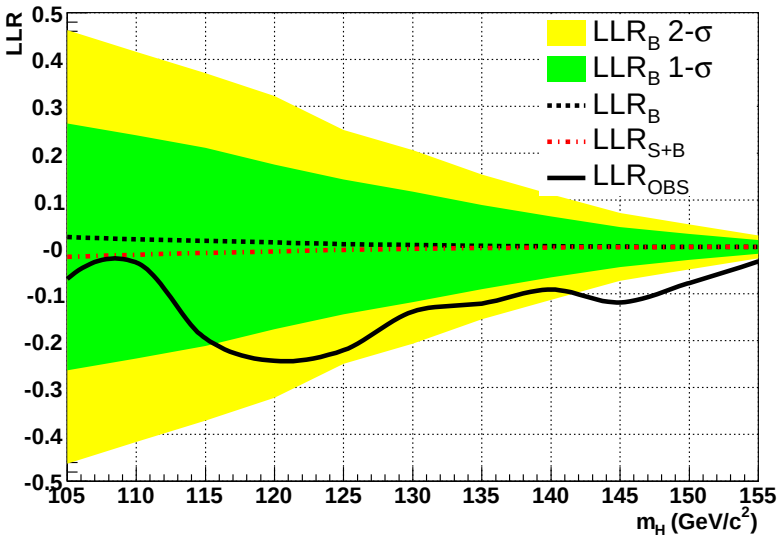

Figure 44: The sensitivity in the combined 1T+2L channels.

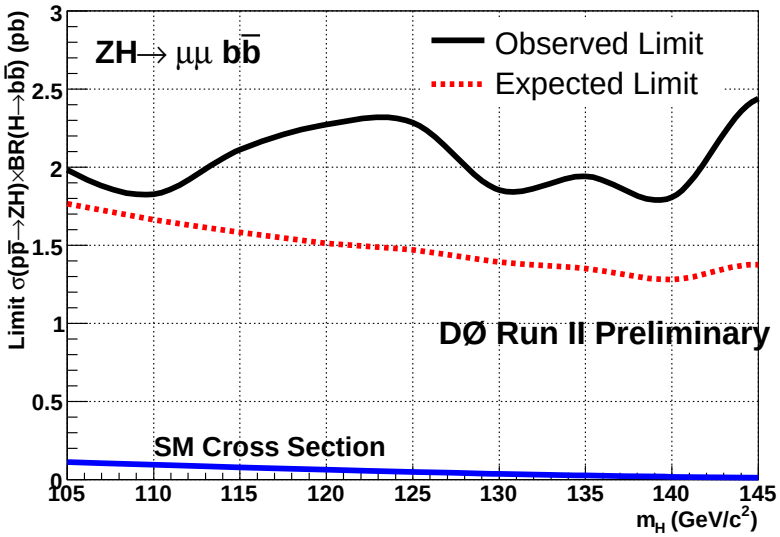

Figure 45: The limits on the cross section of $p\overline{p}\rightarrow$ZH$\rightarrow\mu\mu b\bar{b}$ in the combined 1T+2L channels.

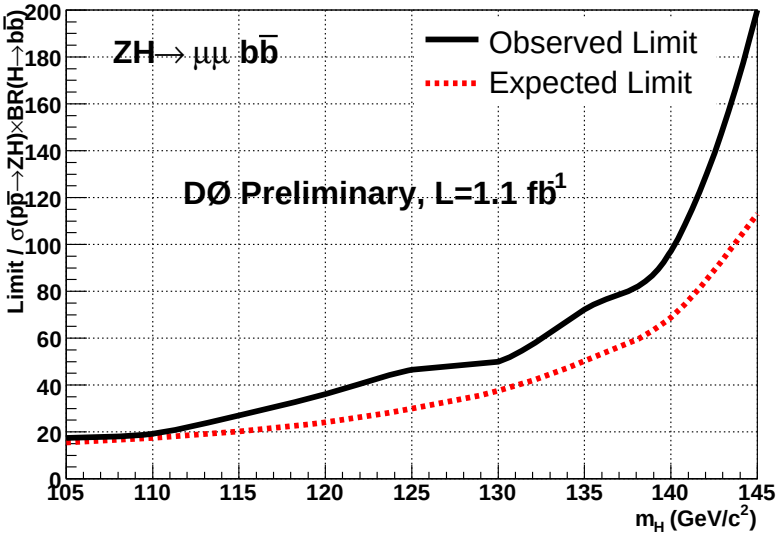

Figure 46: The ratio of the limits on the cross section of $p\overline{p}$→ZH→$\mu\mu b\bar{b}$ to the expected cross section in the SM in the combined 1T+2L channels.

m_H (GeV)	Expected (pb) (/SM)	Observed (pb) (/SM)
ZZ	5.77 (4.1)	7.54 (5.3)
105	1.77 (16)	1.98 (17)
115	1.58 (20)	2.11 (27)
125	1.47 (30)	2.29 (47)
135	1.35 (50)	1.94 (72)
145	1.38 (113)	2.44 (200)
155	1.29 (332)	2.30 (591)

Table 10: The cross section limits and ratios to the SM cross sections for ZZ and various Higgs signal masses.

of 2.7 away from the SM. The goal of observing $p\bar{p}\rightarrow$ZZ$\rightarrow$ll$b\bar{b}$ production by the end of Run II seems possible, but will be challenging. Of course, the observation of the ZZ signal would be a wonderful validation of the analysis assumptions and technique.

9 Extra Plots

Here are lots of extra plots showing the comparison between data and MC. As in previous plots, colors for the backgrounds from MC: blue is Z+Xlp, light blue is Z+2b, light green is ZZ, yellow is WZ, magenta is $t\bar{t}$, and red is Higgs signal for m_h=115 GeV. QCD, from non-isolated muon data, is shown as a dashed grey line. The data are shown as circles, with Poisson uncertainties. The total background (including QCD) is the black histogram.

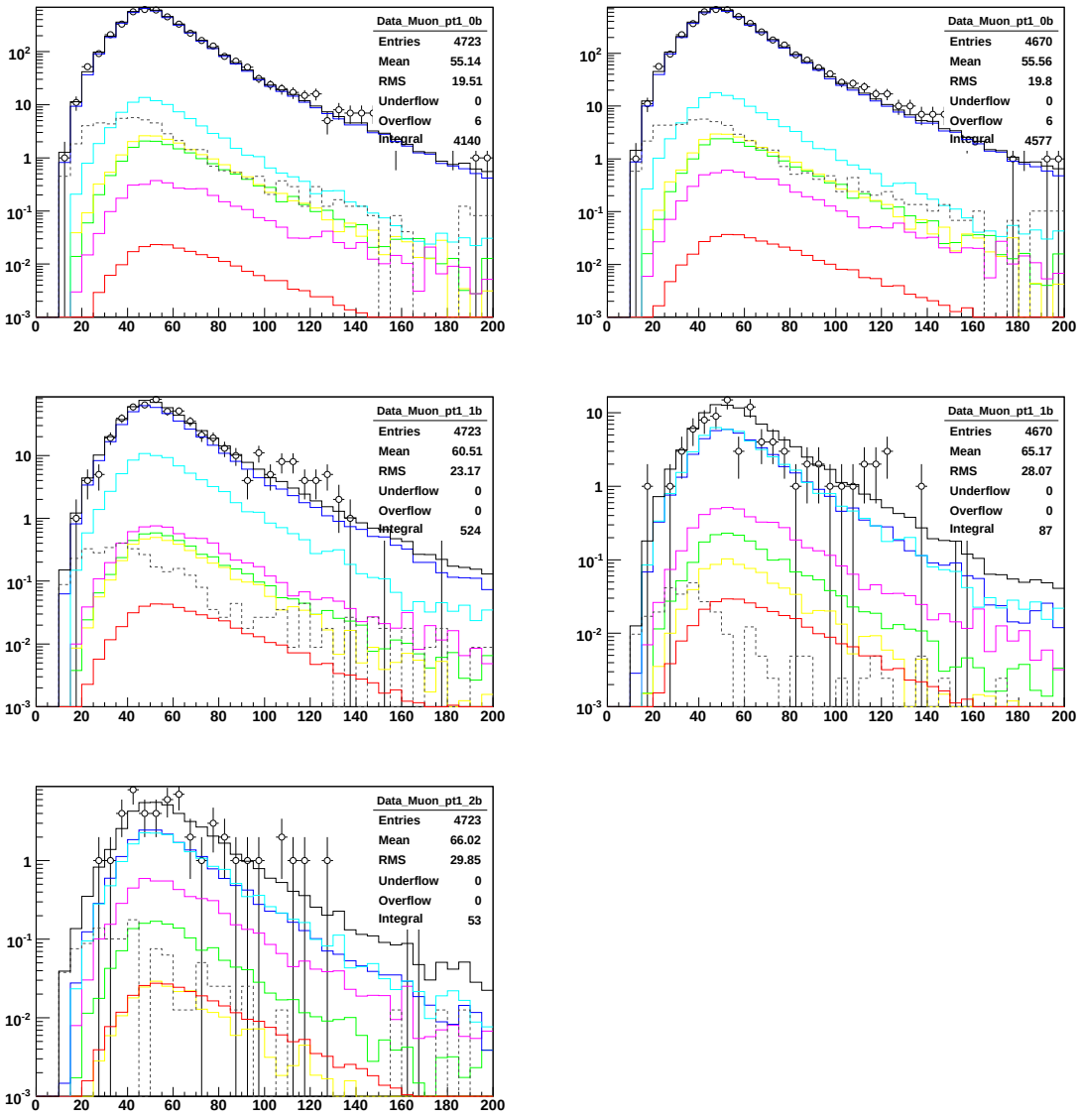

Figure 47: The leading muon p_T in events with 0, 1, and >=2 L4 b-tags (left) and 0, 1 VERYTIGHT b-tags but not 2 or more L4 b-tags (right).

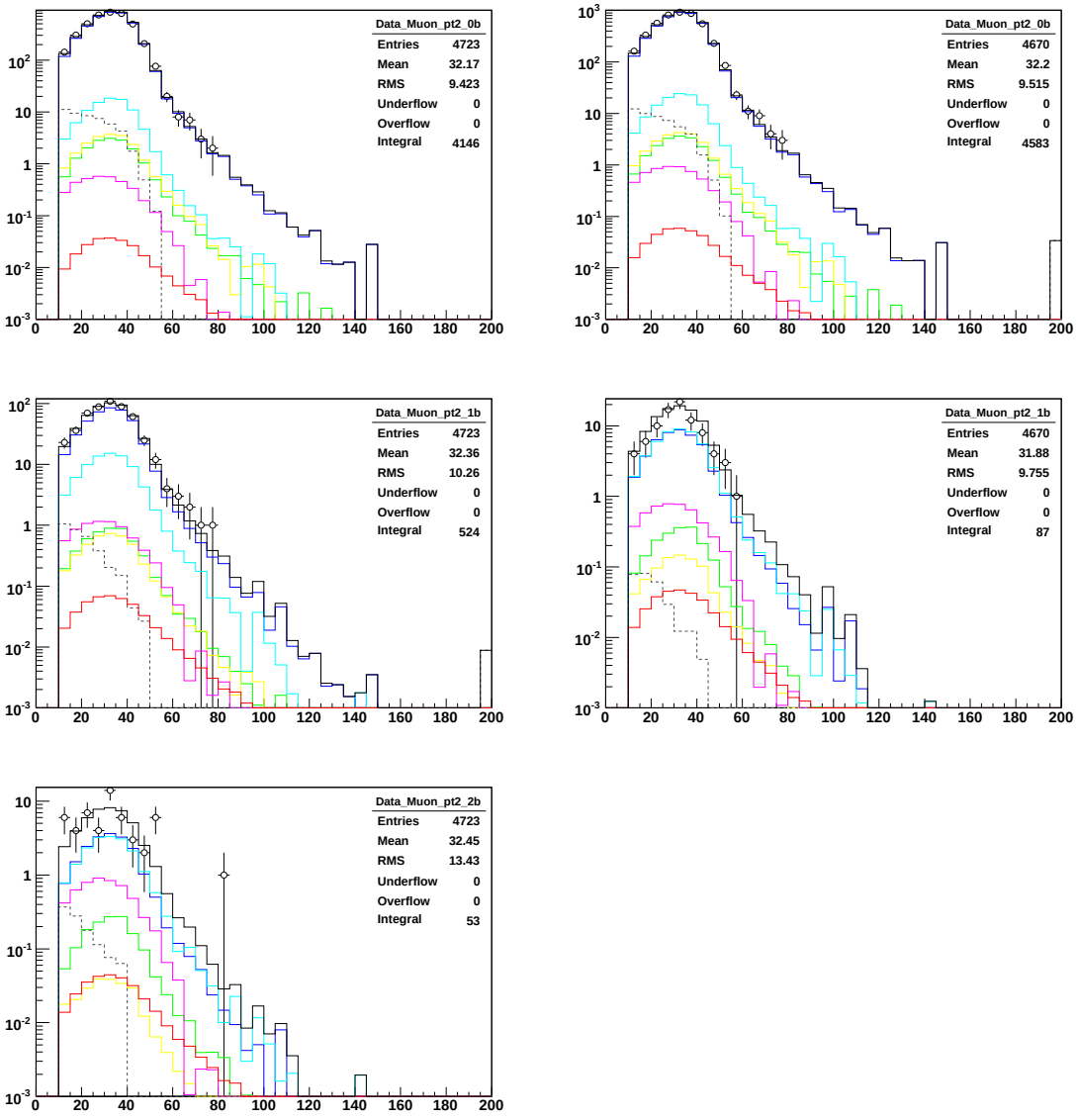

Figure 48: The second-leading muon p_T in events with 0, 1, and >=2 L4 b-tags (left) and 0, 1 VERYTIGHT b-tags but not 2 or more L4 b-tags (right).

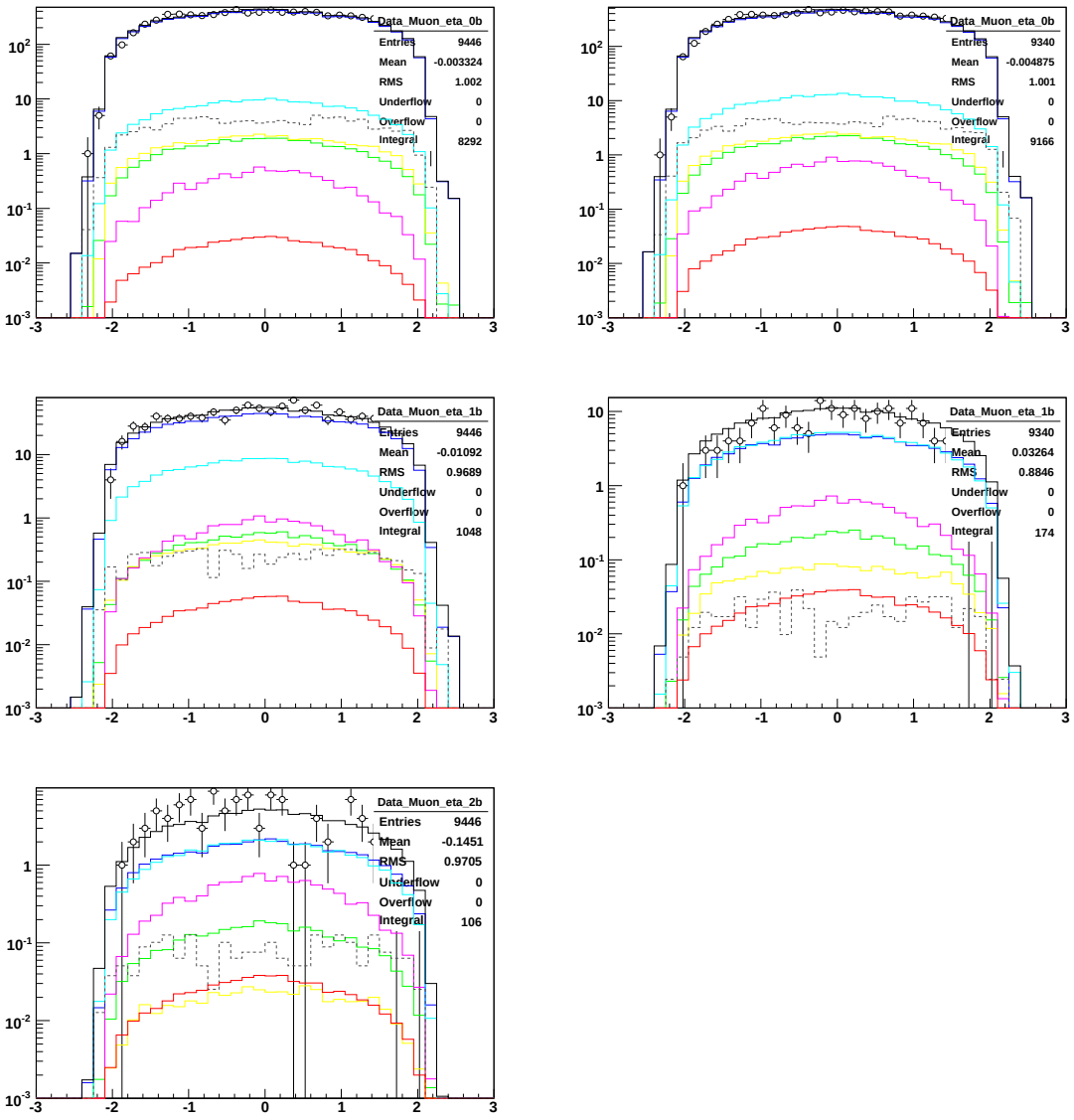

Figure 49: The η of the leading two p_T muons in events with 0, 1, and >=2 L4 b-tags (left) and 0, 1 VERYTIGHT b-tags but not 2 or more L4 b-tags (right).

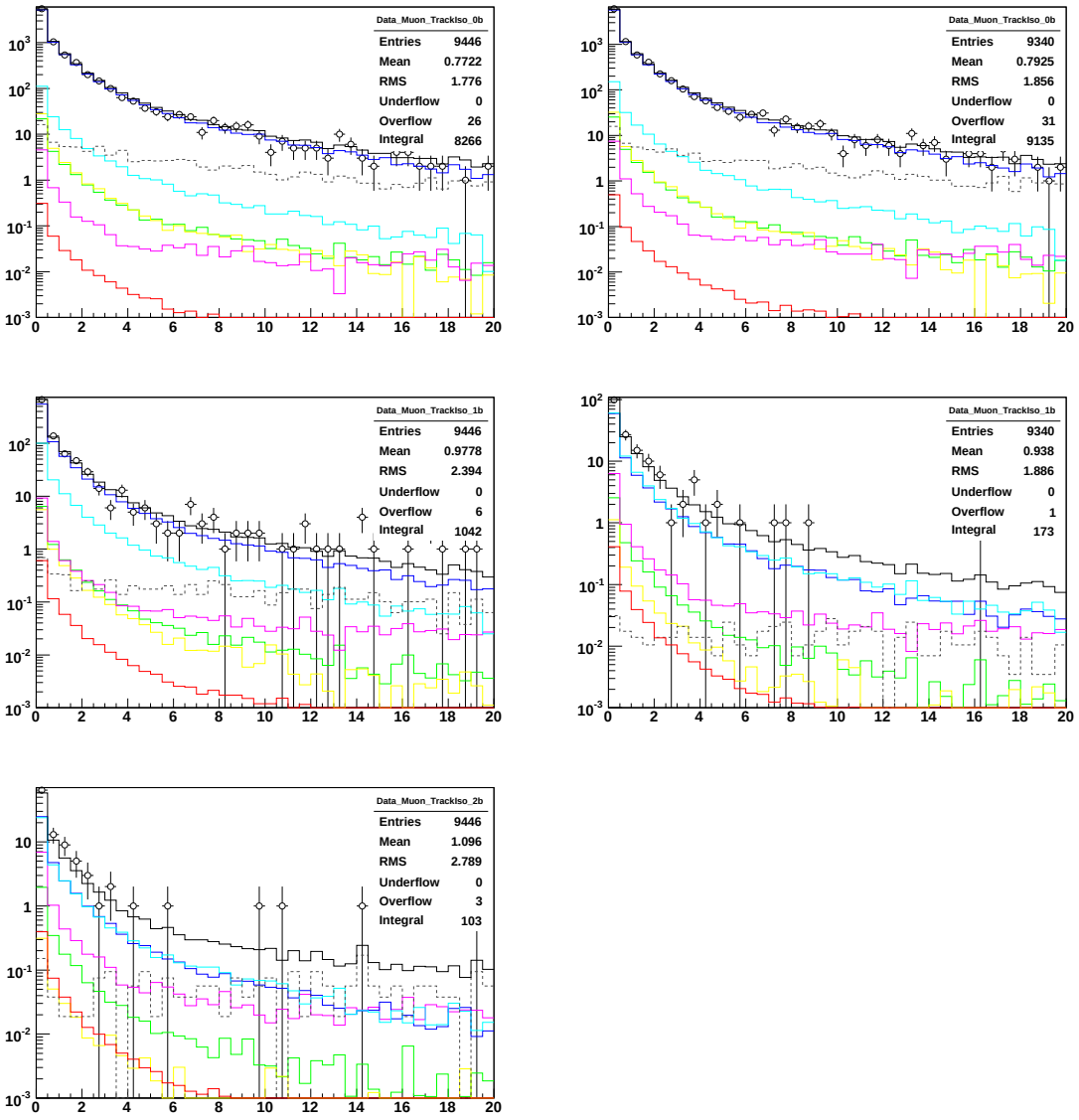

Figure 50: The Track isolation variable of the leading two p_T muons in events with 0, 1, and >=2 L4 b-tags (left) and 0, 1 VERYTIGHT b-tags but not 2 or more L4 b-tags (right).

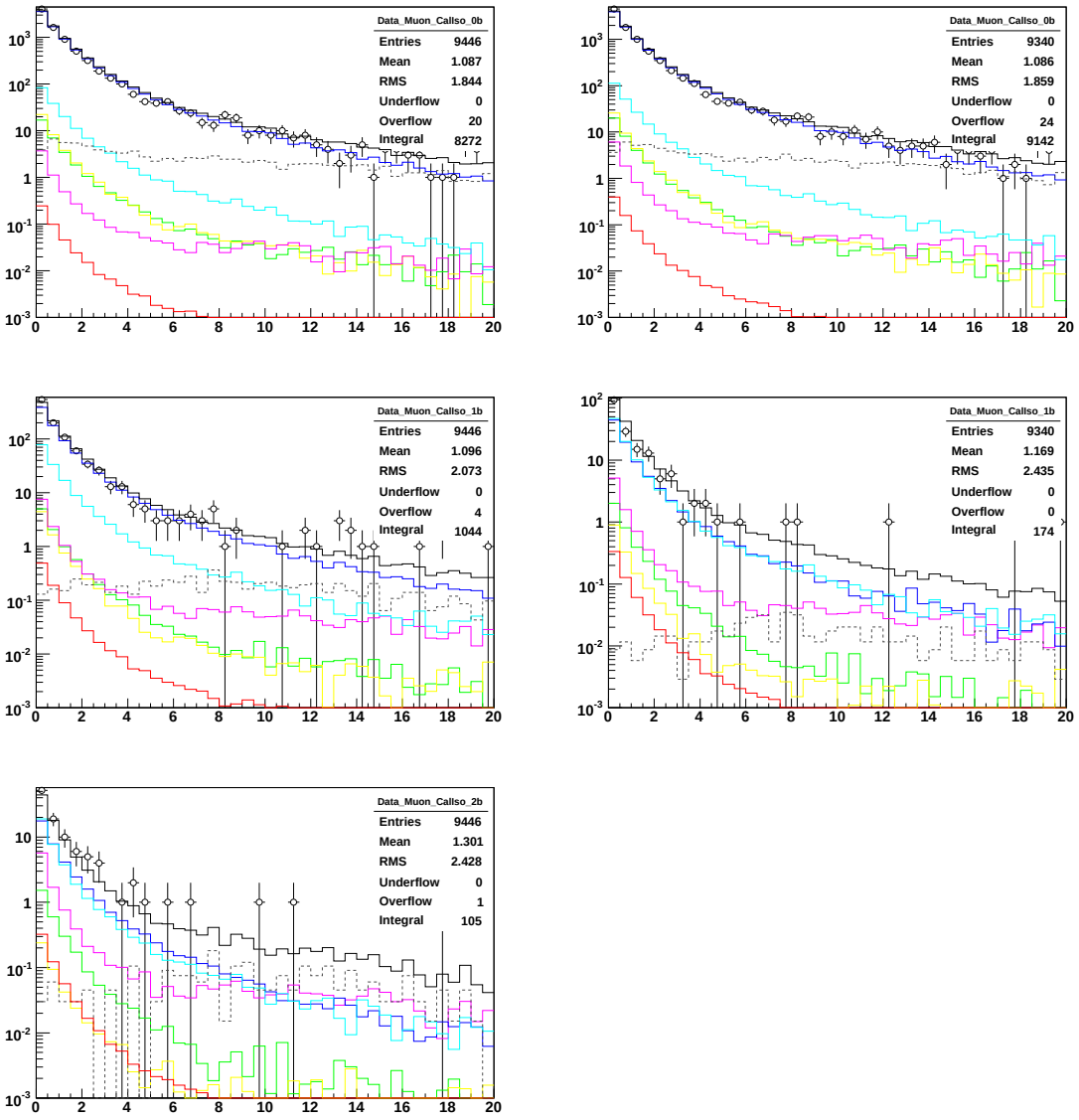

Figure 51: The Cal isolation variable of the leading two p_T muons in events with 0, 1, and >=2 L4 b-tags (left) and 0, 1 VERYTIGHT b-tags but not 2 or more L4 b-tags (right).

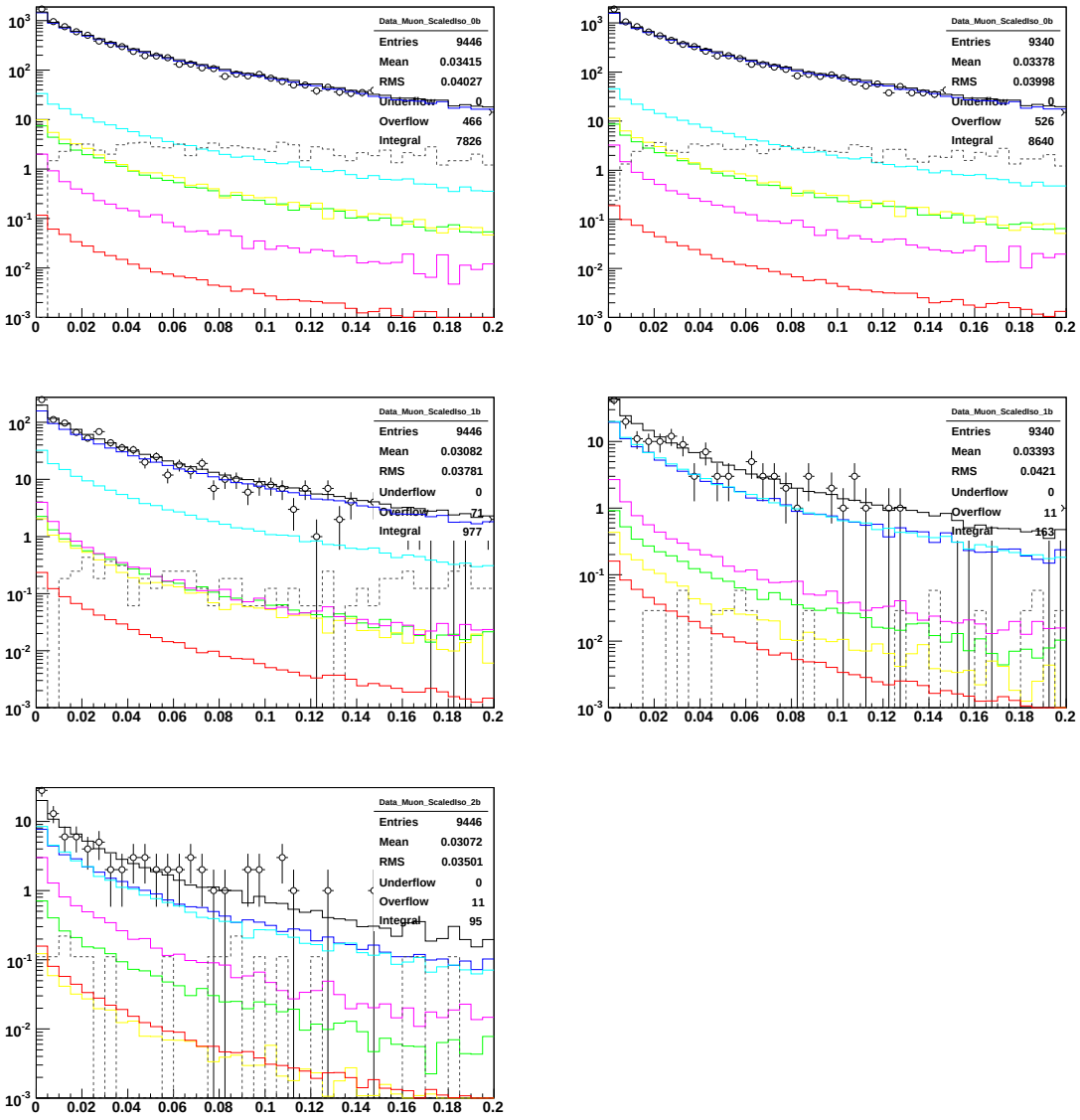

Figure 52: The Scaled isolation variable of the leading two p_T muons in events with 0, 1, and >=2 L4 b-tags (left) and 0, 1 VERYTIGHT b-tags but not 2 or more L4 b-tags (right).

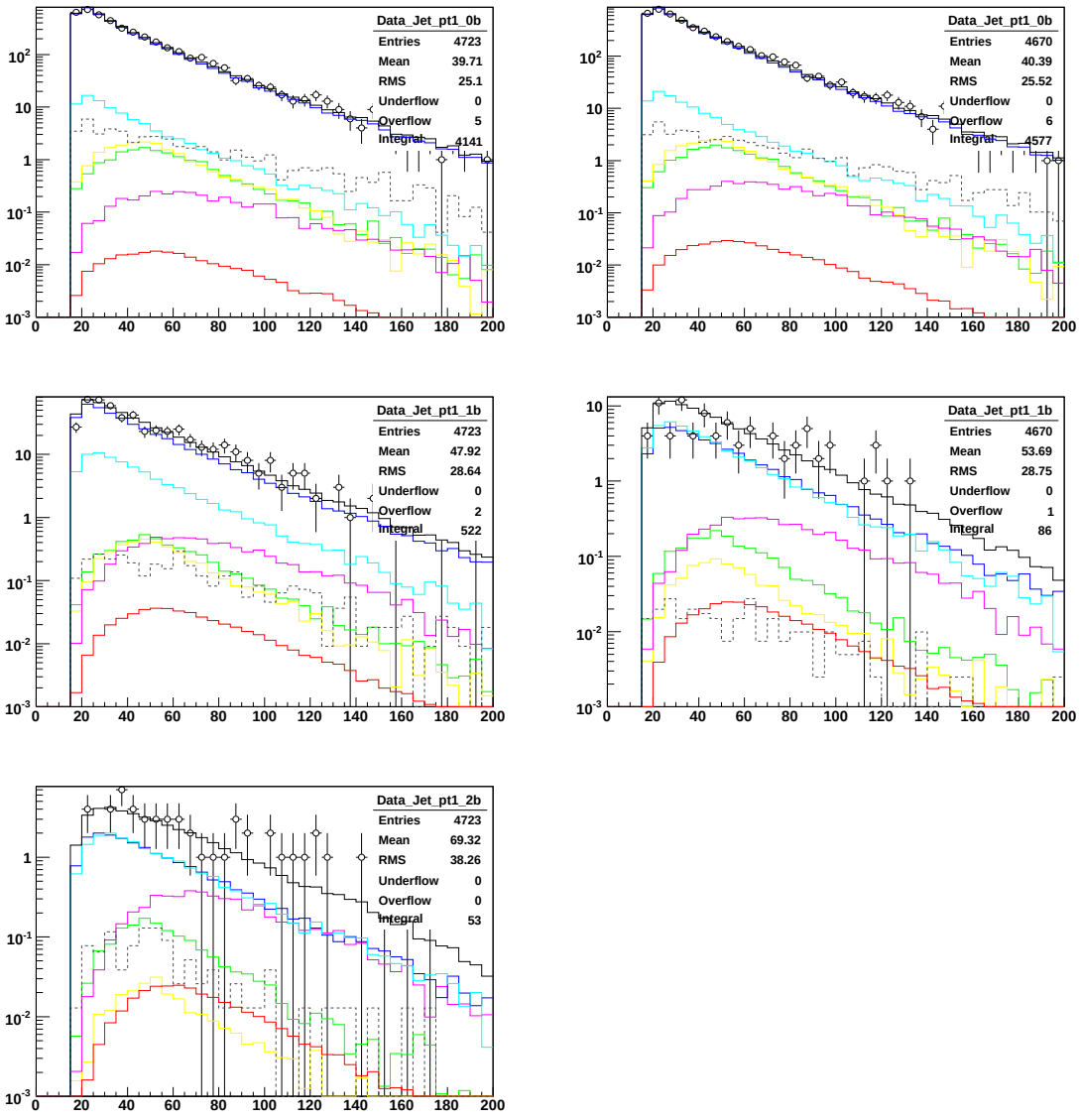

Figure 53: The leading jet p_T in events with 0, 1, and >=2 L4 b-tags (left) and 0, 1 VERYTIGHT b-tags but not 2 or more L4 b-tags (right).

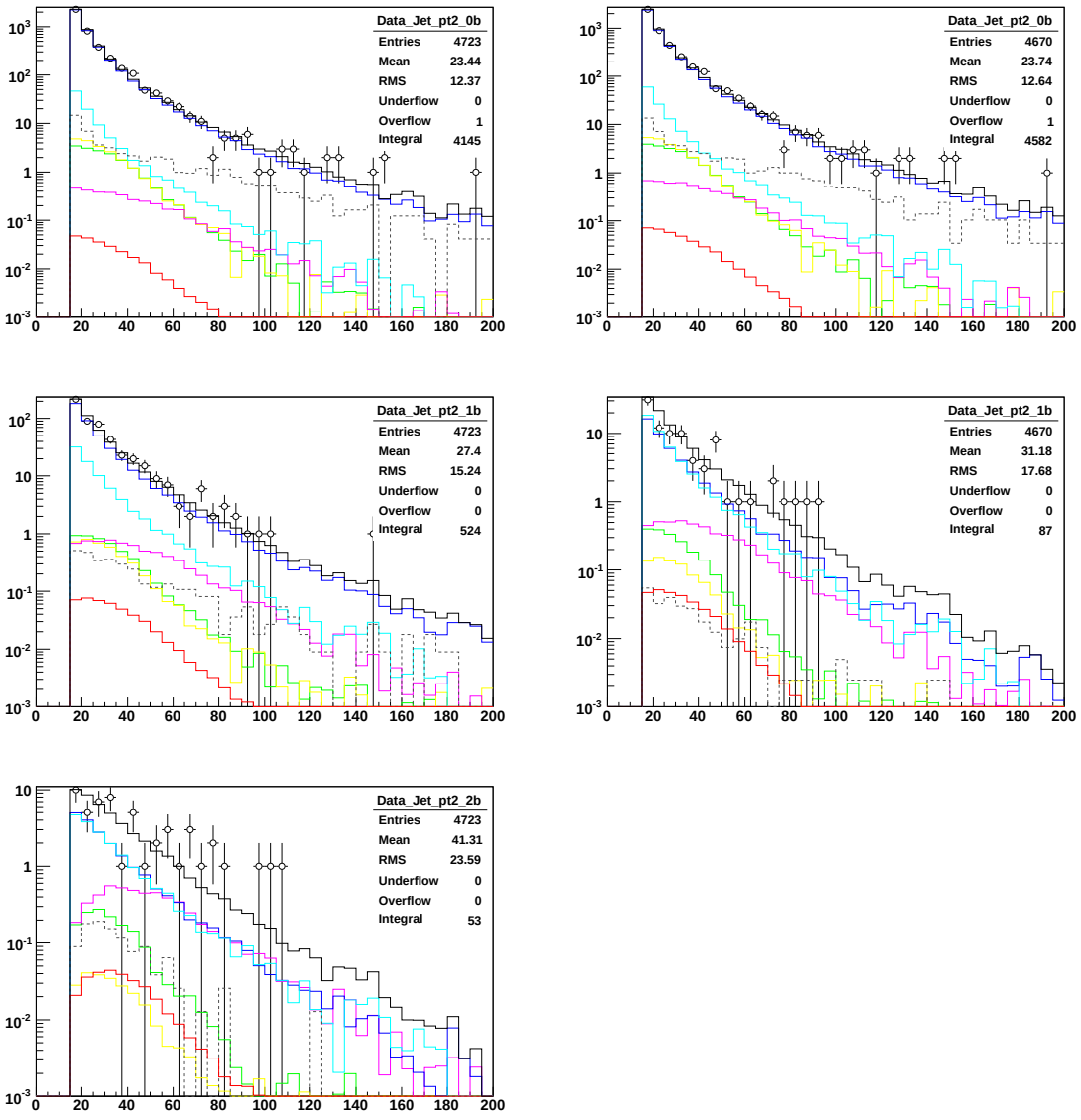

Figure 54: The second-leading jet p_T in events with 0, 1, and >=2 L4 b-tags (left) and 0, 1 VERYTIGHT b-tags but not 2 or more L4 b-tags (right).

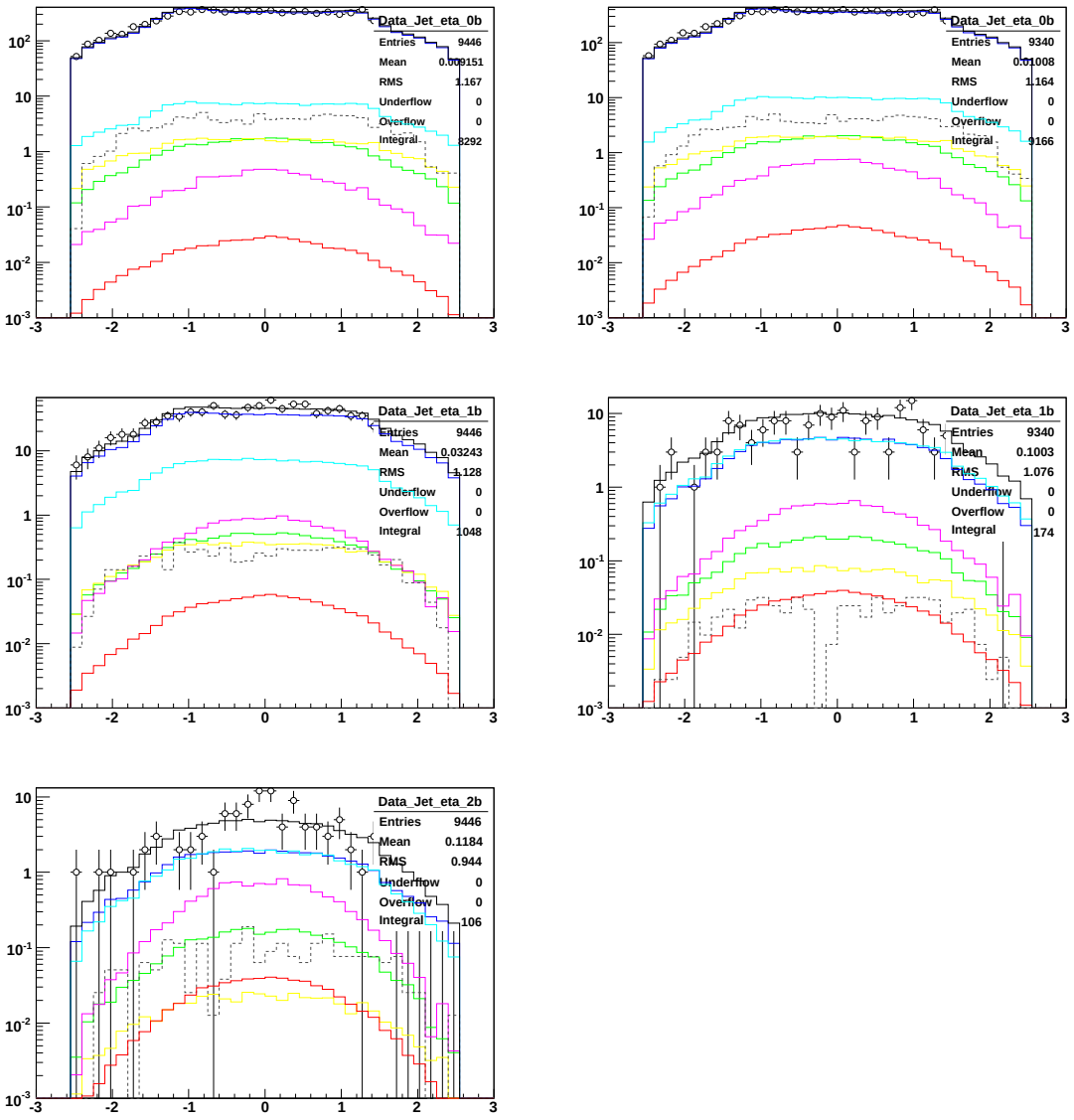

Figure 55: The η of the leading two p_T jets in events with 0, 1, and >=2 L4 b-tags (left) and 0, 1 VERYTIGHT b-tags but not 2 or more L4 b-tags (right).

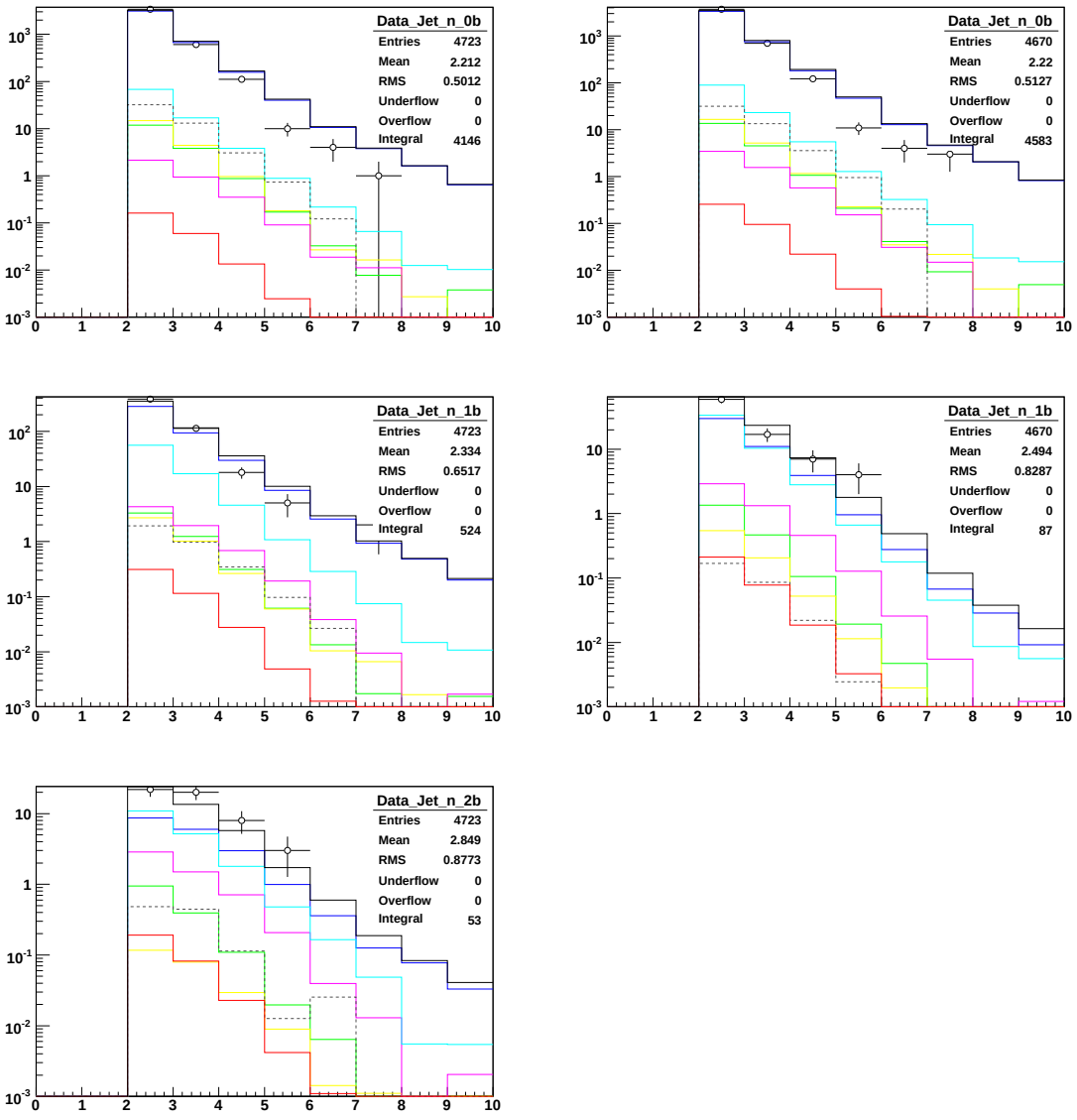

Figure 56: The jet multiplicity in events with 0, 1, and >=2 L4 b-tags (left) and 0, 1 VERYTIGHT b-tags but not 2 or more L4 b-tags (right).

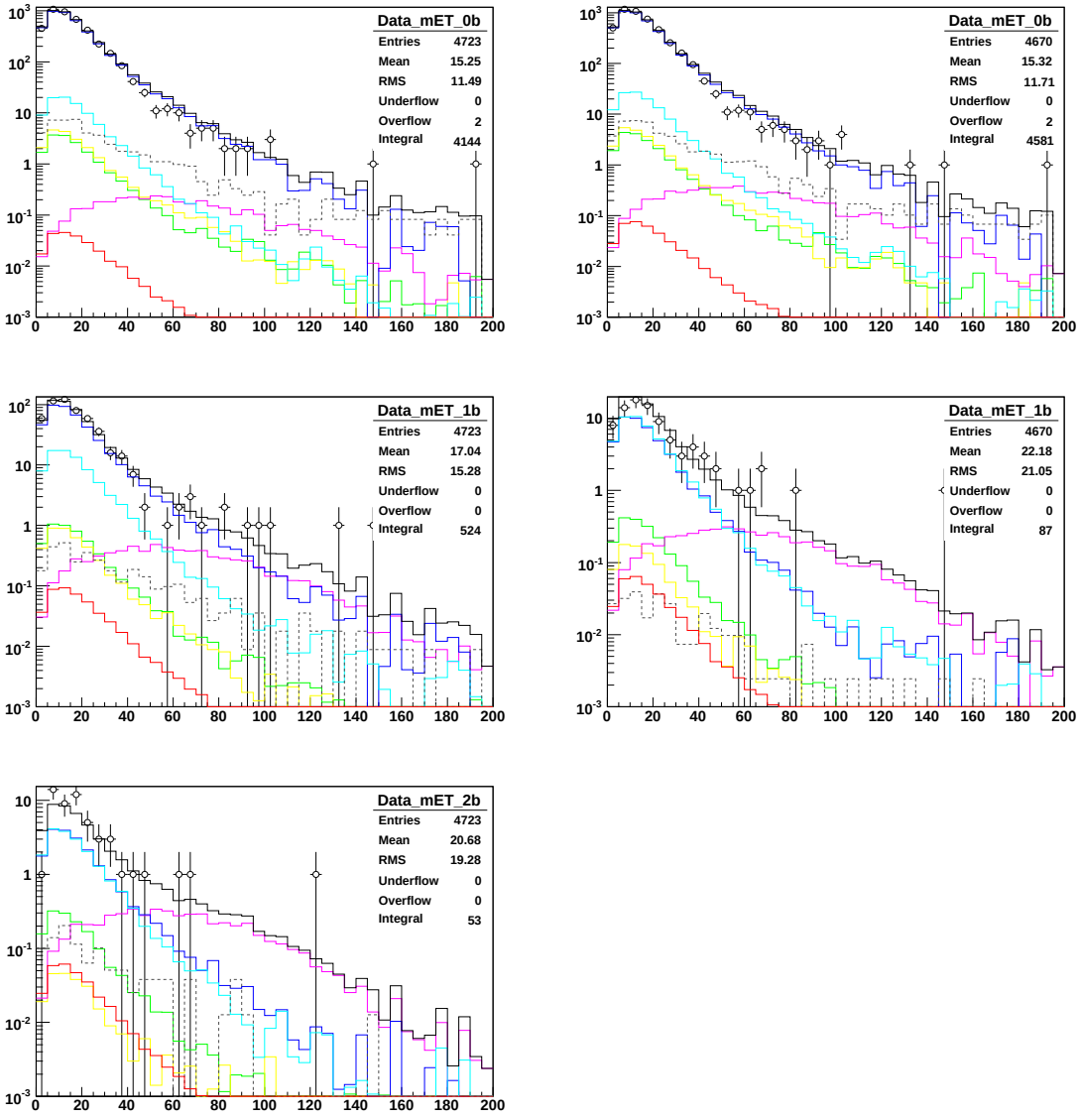

Figure 57: The missing E_T in events with 0, 1, and >=2 L4 b-tags (left) and 0, 1 VERYTIGHT b-tags but not 2 or more L4 b-tags (right).

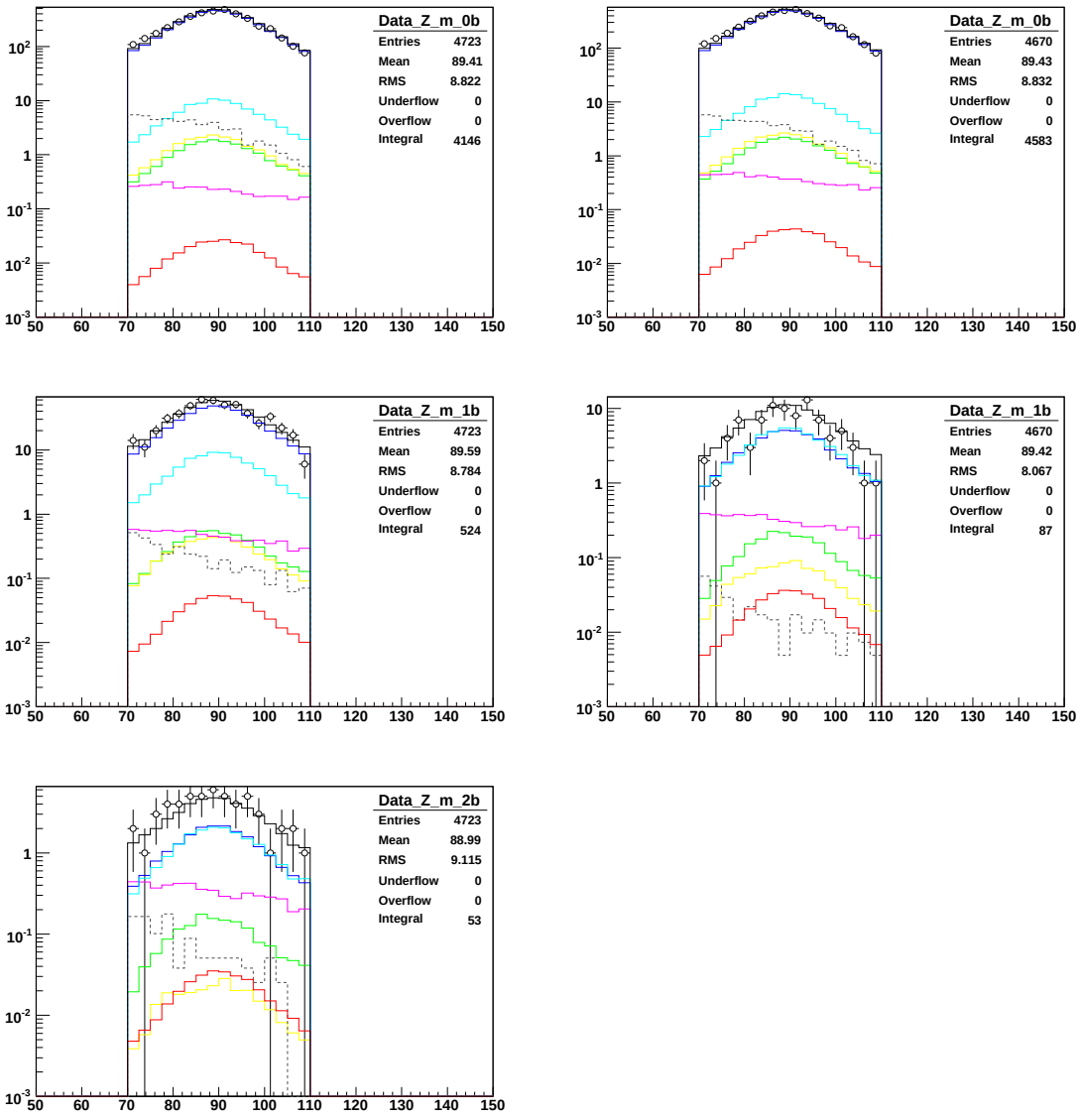

Figure 58: The Z-candidate invariant mass in events with 0, 1, and >=2 L4 b-tags (left) and 0, 1 VERYTIGHT b-tags but not 2 or more L4 b-tags (right).

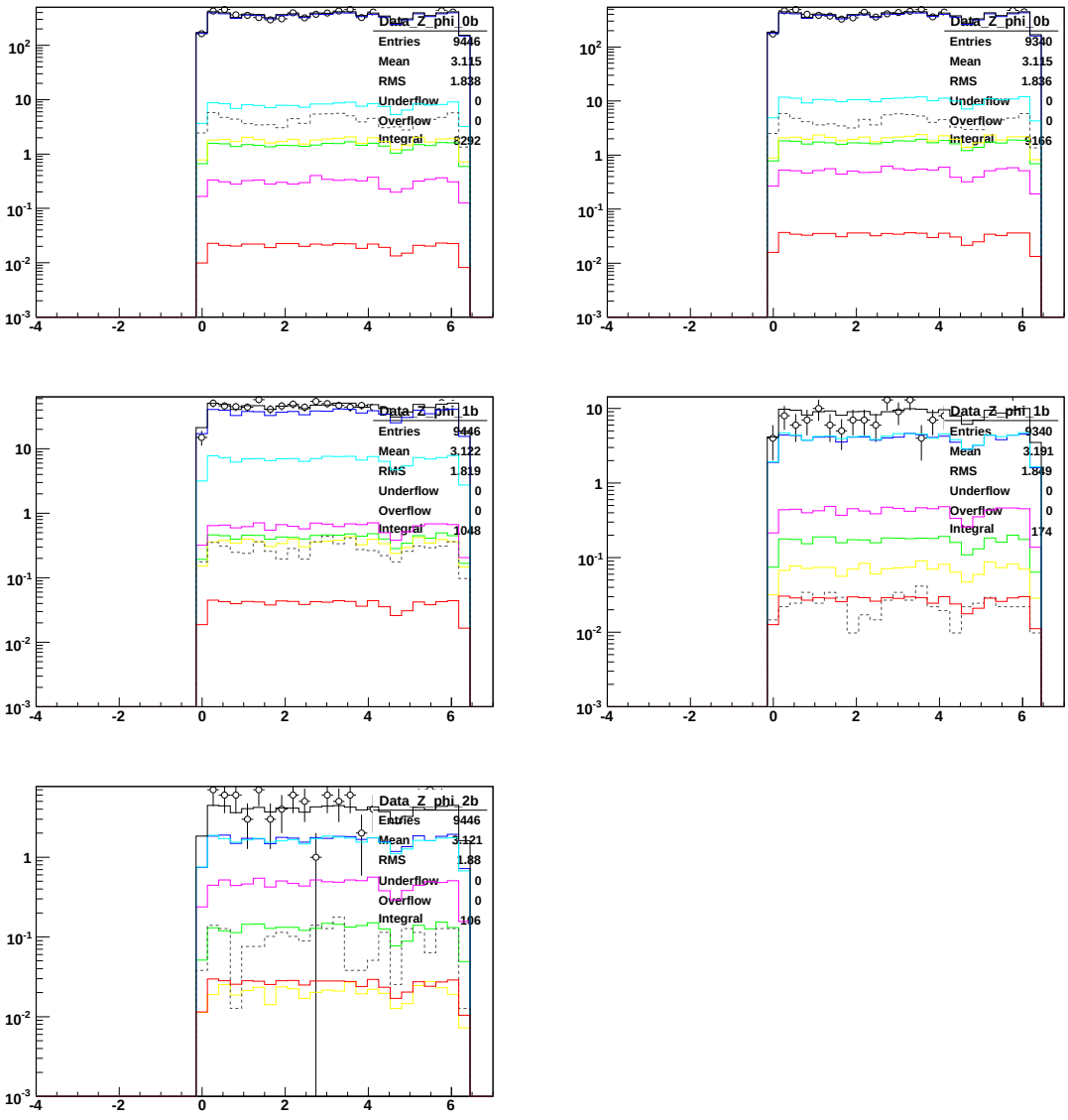

Figure 59: The Z-candidate ϕ in events with 0, 1, and >=2 L4 b-tags (left) and 0, 1 VERYTIGHT b-tags but not 2 or more L4 b-tags (right).

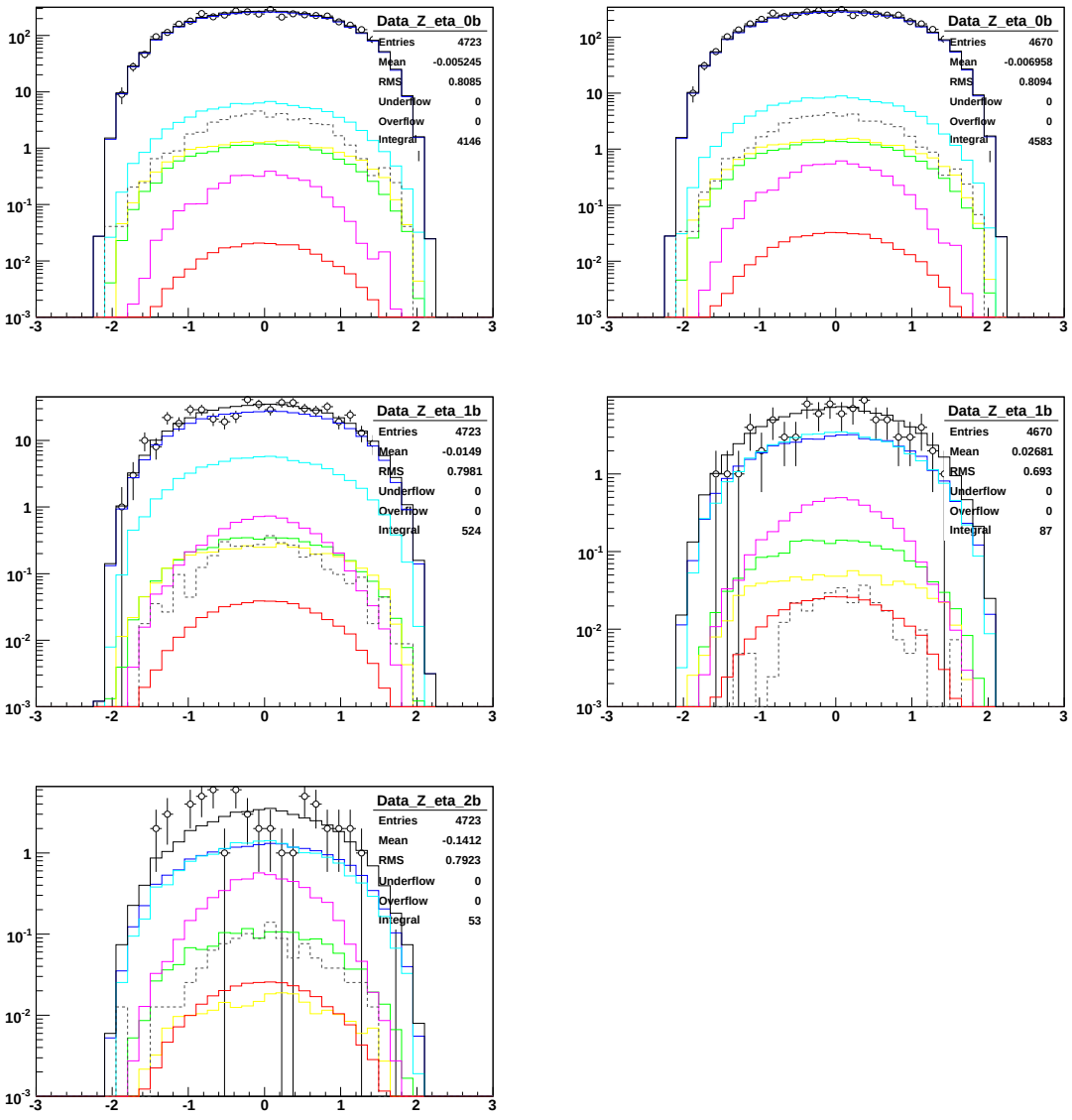

Figure 60: The Z-candidate η in events with 0, 1, and >=2 L4 b-tags (left) and 0, 1 VERYTIGHT b-tags but not 2 or more L4 b-tags (right).

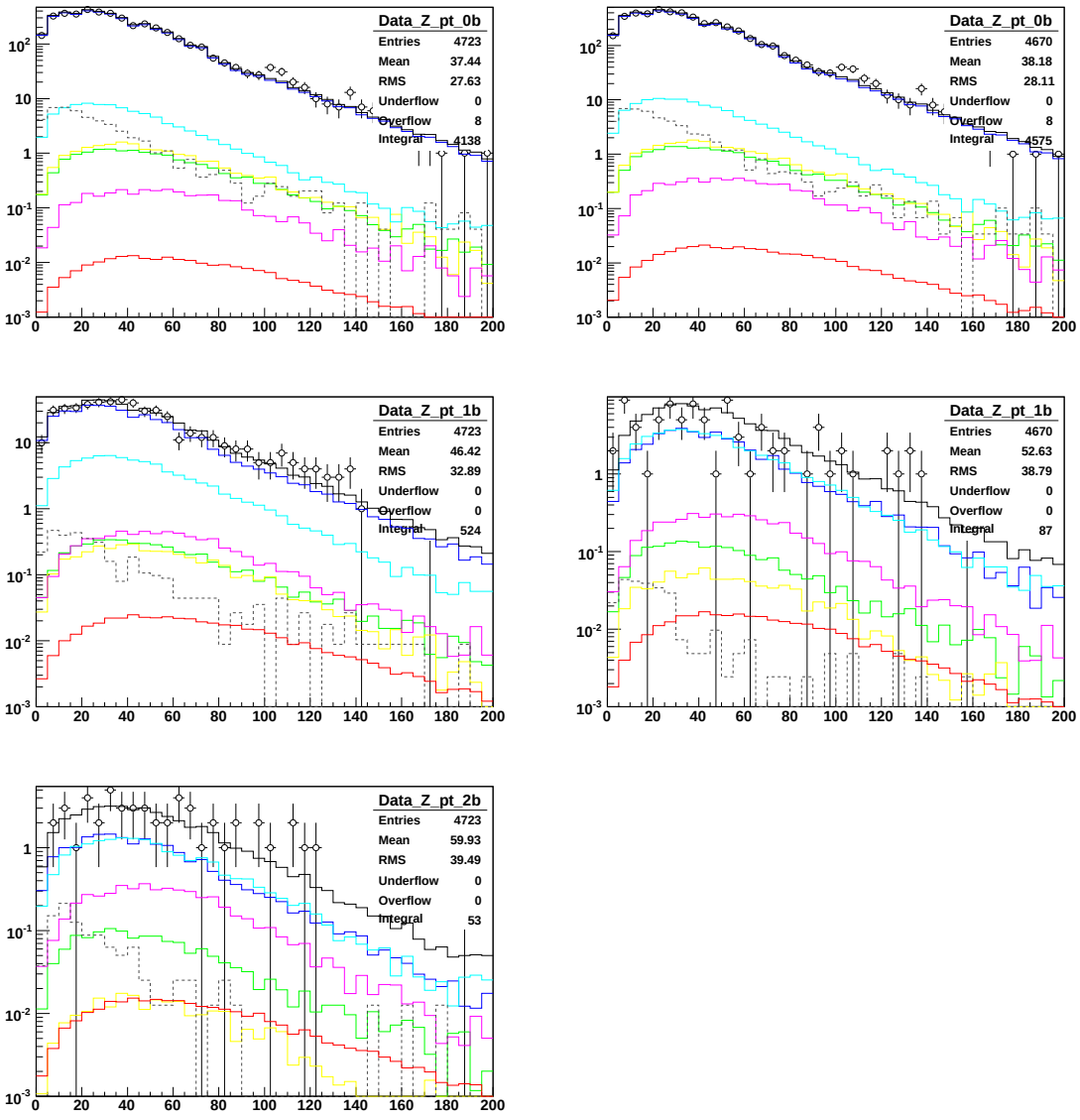

Figure 61: The Z-candidate p_T in events with 0, 1, and >=2 L4 b-tags (left) and 0, 1 VERYTIGHT b-tags but not 2 or more L4 b-tags (right).

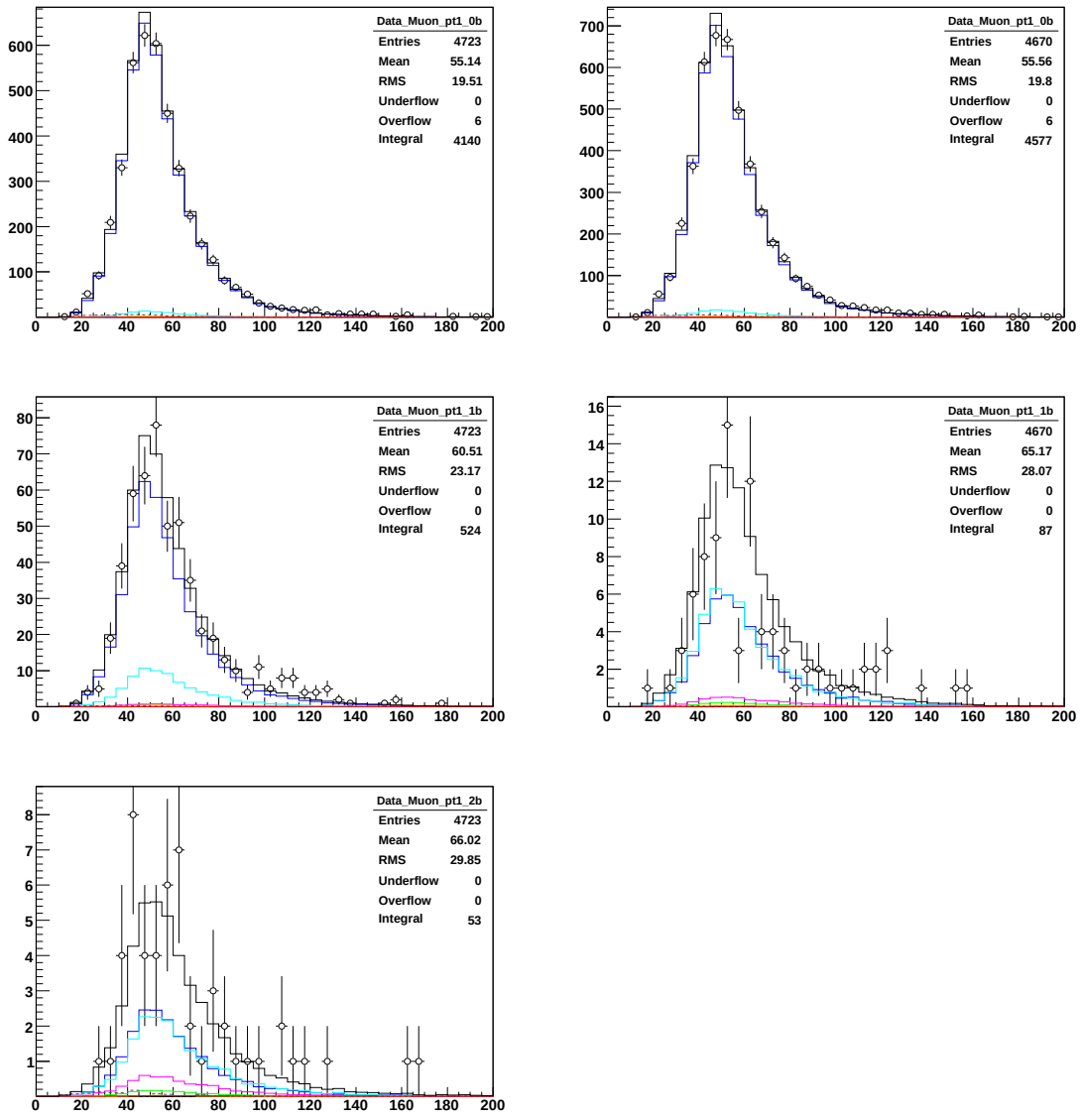

Figure 62: The leading muon p_T in events with 0, 1, and >=2 L4 b-tags (left) and 0, 1 VERYTIGHT b-tags but not 2 or more L4 b-tags (right), with no log scale.

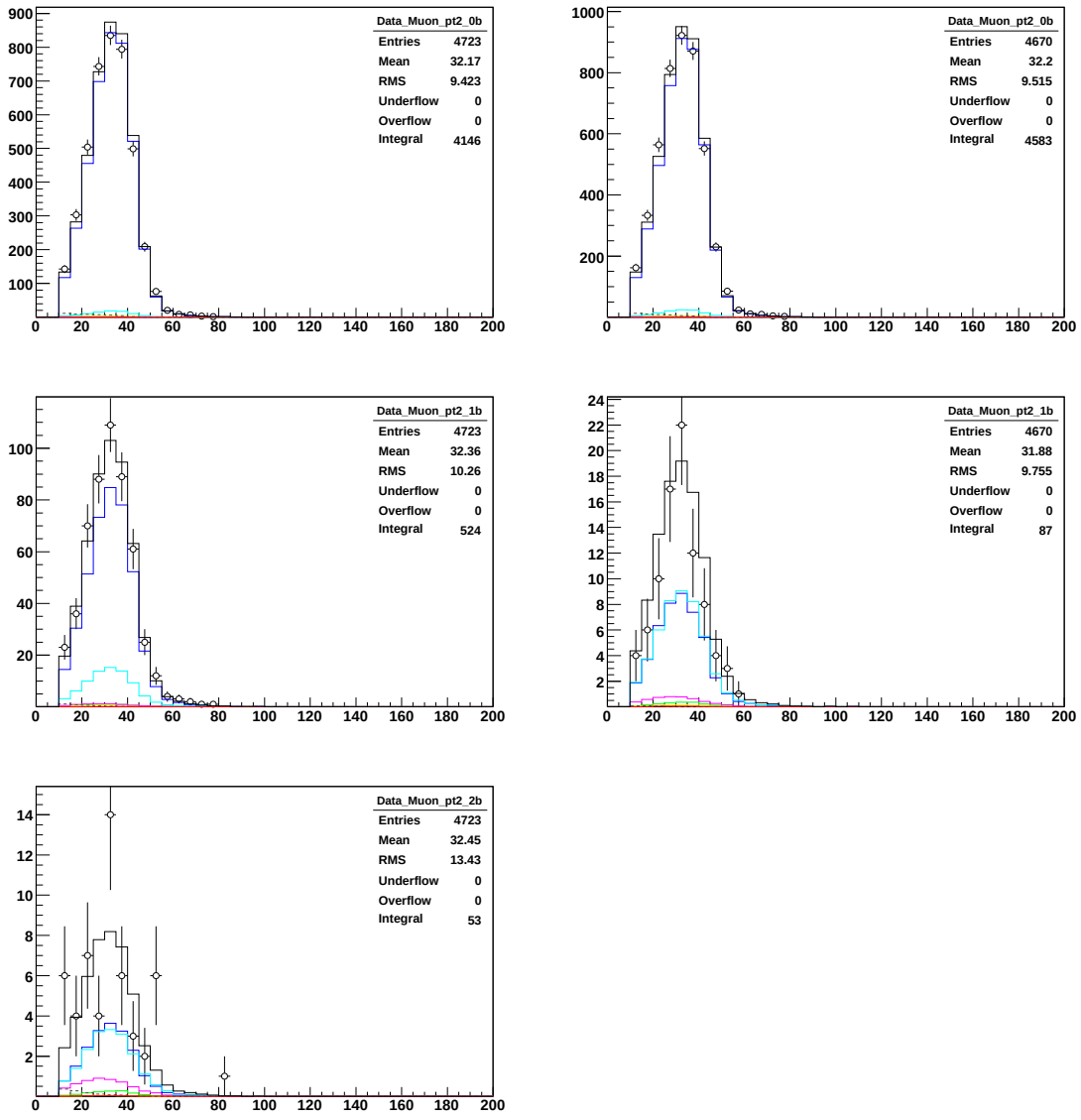

Figure 63: The second-leading muon p_T in events with 0, 1, and >=2 L4 b-tags (left) and 0, 1 VERYTIGHT b-tags but not 2 or more L4 b-tags (right), with no log scale.

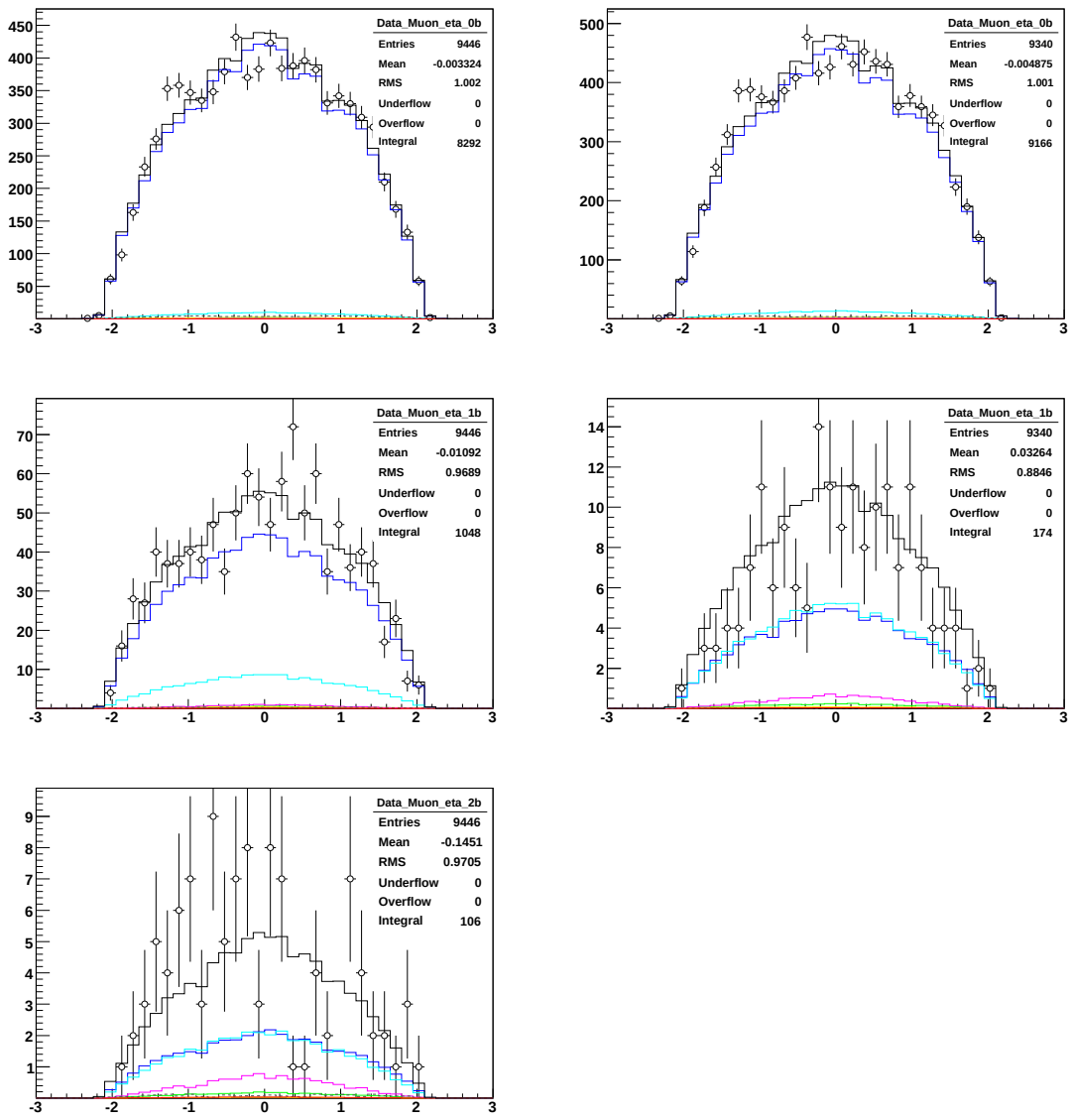

Figure 64: The η of the leading two p_T muons in events with 0, 1, and >=2 L4 b-tags (left) and 0, 1 VERYTIGHT b-tags but not 2 or more L4 b-tags (right), with no log scale.

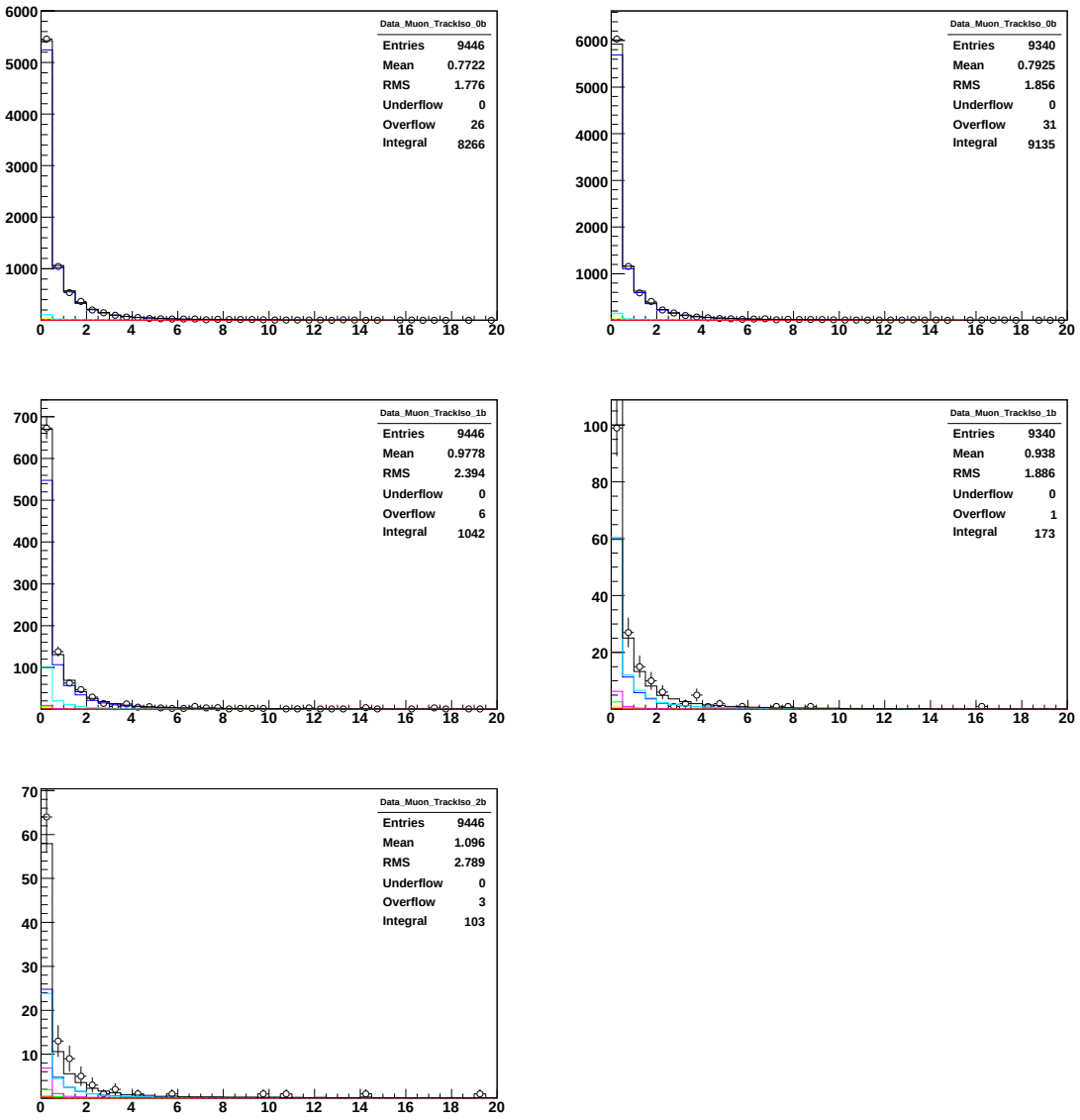

Figure 65: The Track isolation variable of the leading two p_T muons in events with 0, 1, and >=2 L4 b-tags (left) and 0, 1 VERYTIGHT b-tags but not 2 or more L4 b-tags (right), with no log scale.

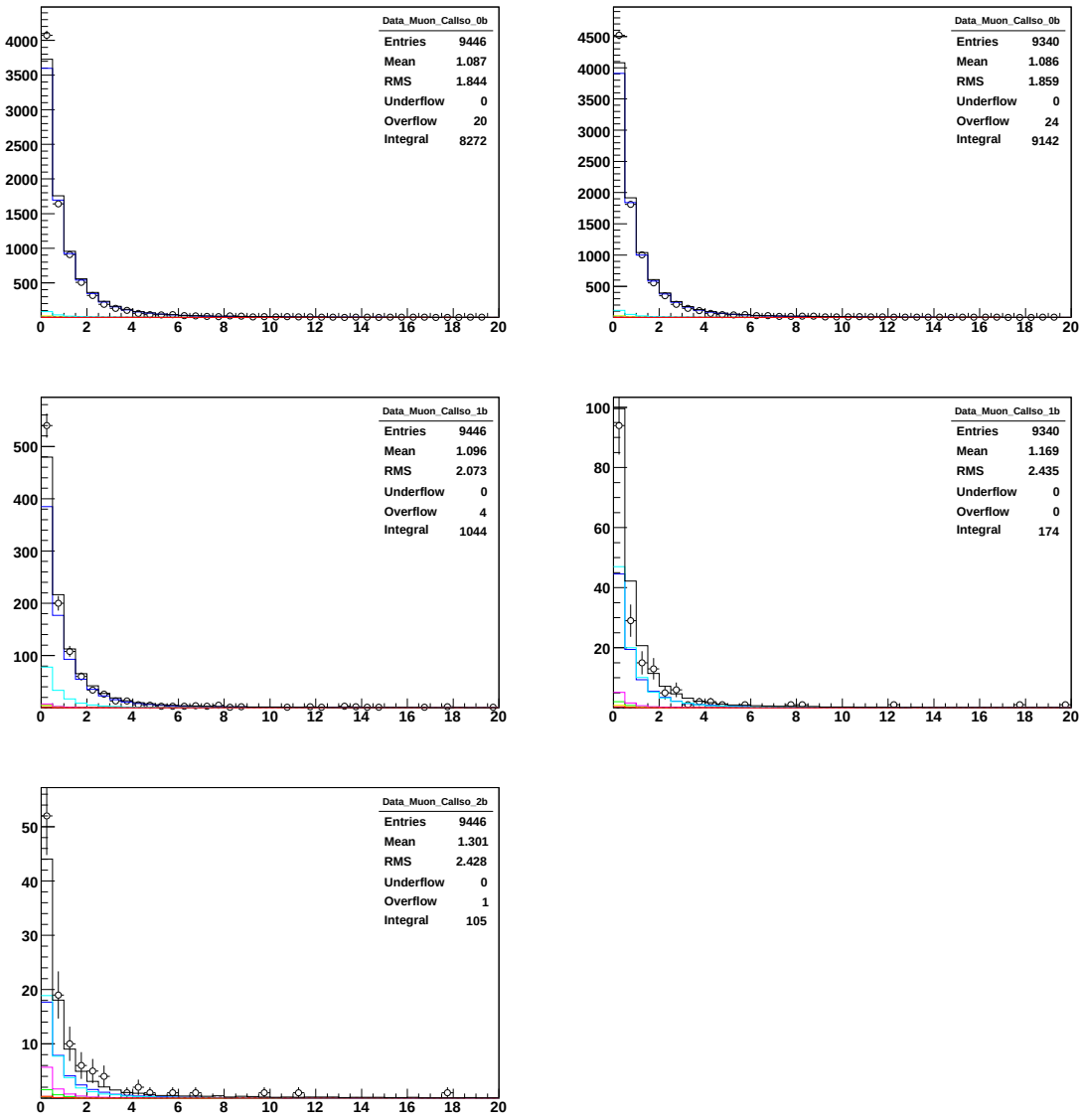

Figure 66: The calorimeter isolation variable of the leading two p_T muons in events with 0, 1, and >=2 L4 b-tags (left) and 0, 1 VERYTIGHT b-tags but not 2 or more L4 b-tags (right), with no log scale.

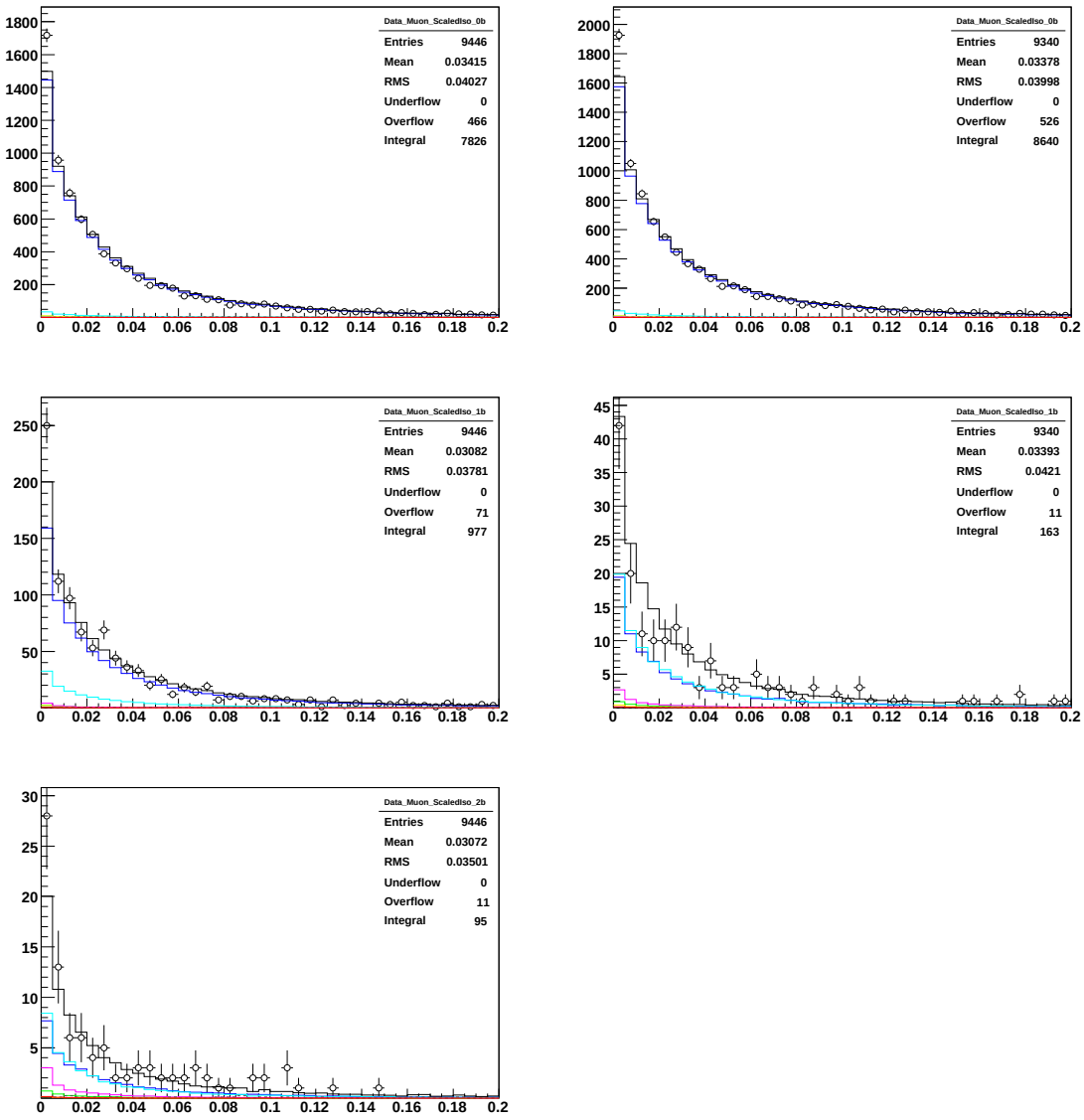

Figure 67: The Scaled isolation variable of the leading two p_T muons in events with 0, 1, and >=2 L4 b-tags (left) and 0, 1 VERYTIGHT b-tags but not 2 or more L4 b-tags (right), with no log scale.

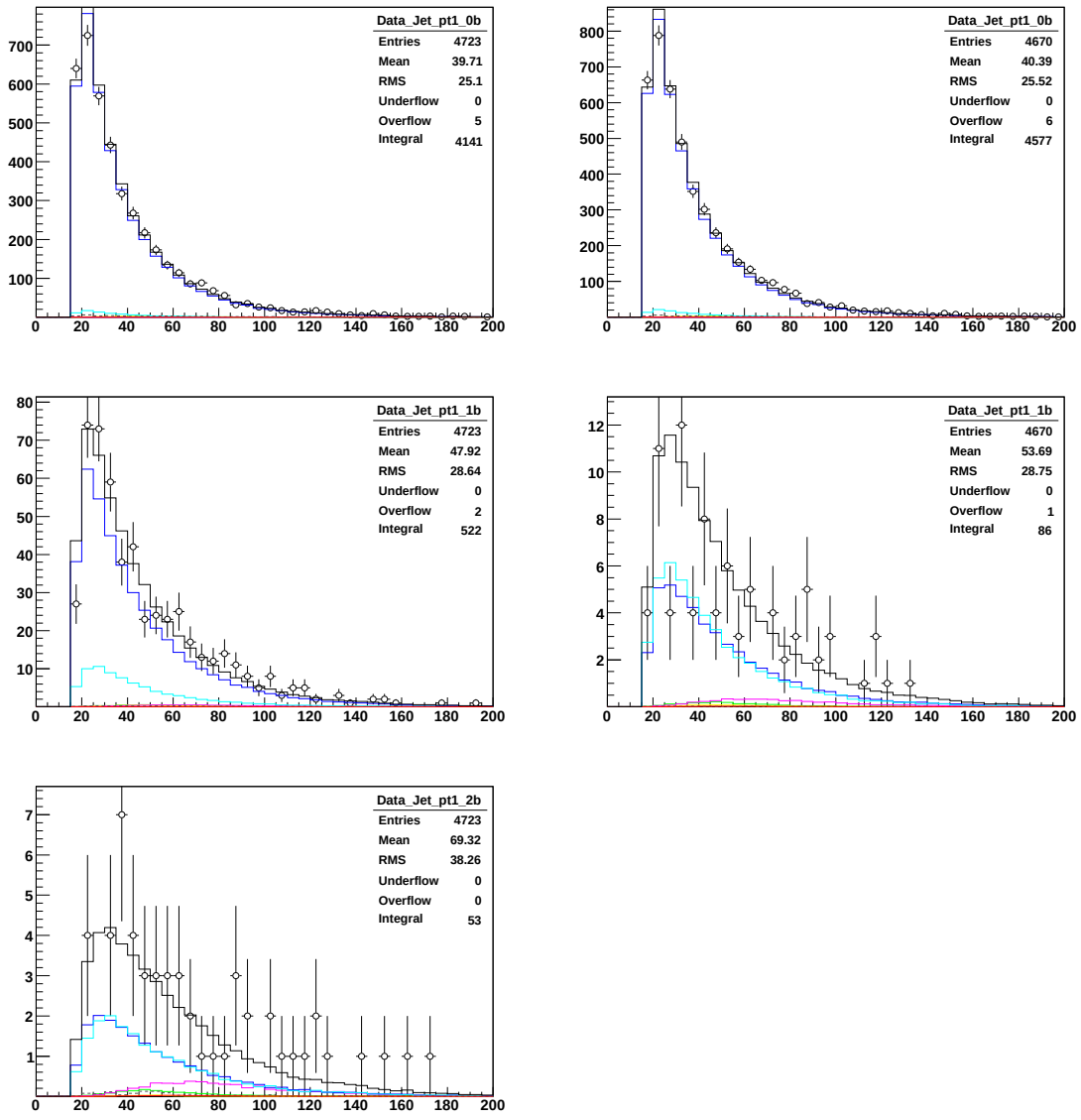

Figure 68: The leading jet p_T in events with 0, 1, and >=2 L4 b-tags (left) and 0, 1 VERYTIGHT b-tags but not 2 or more L4 b-tags (right), with no log scale.

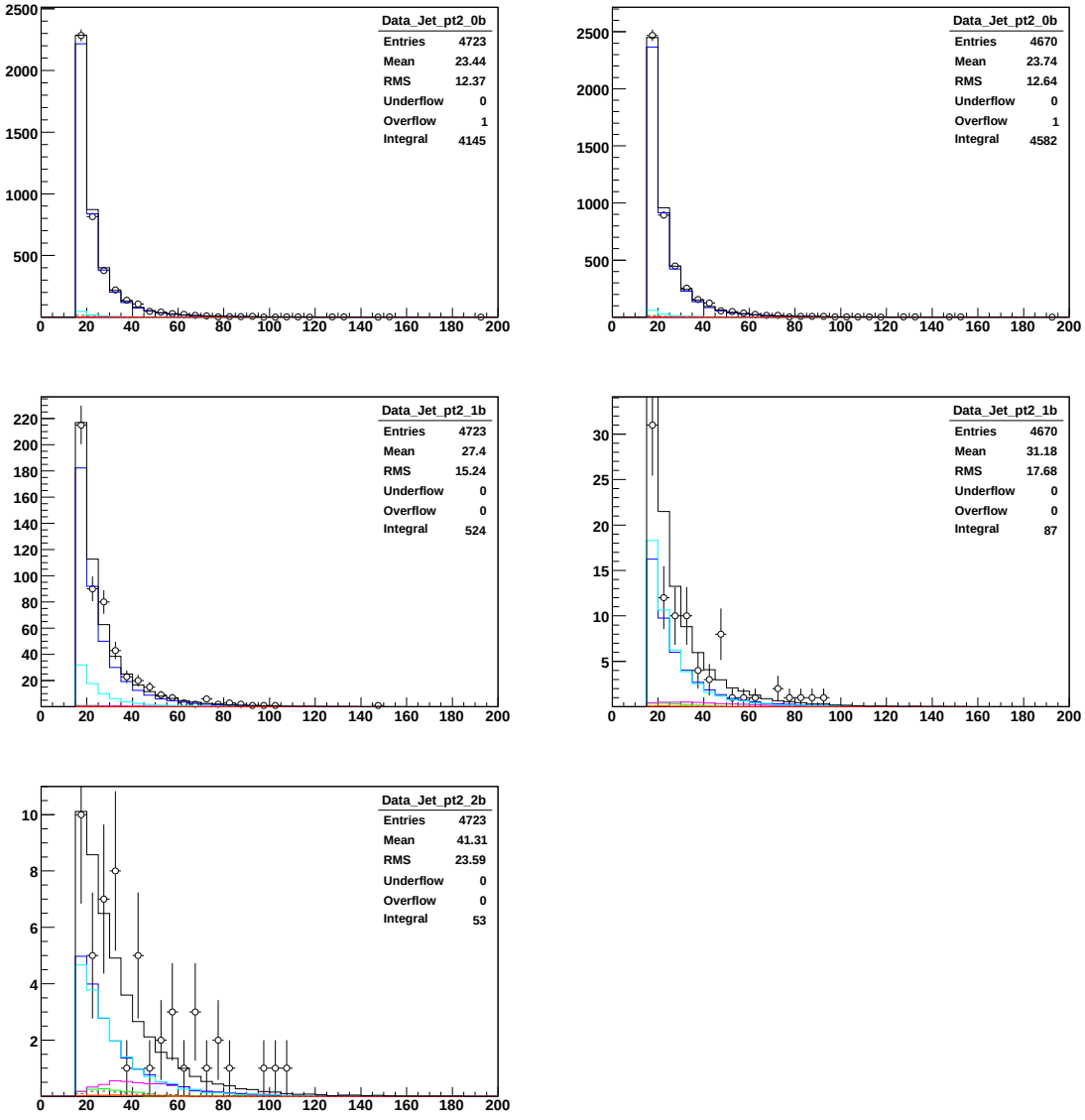

Figure 69: The second-leading jet p_T in events with 0, 1, and >=2 L4 b-tags (left) and 0, 1 VERYTIGHT b-tags but not 2 or more L4 b-tags (right), with no log scale.

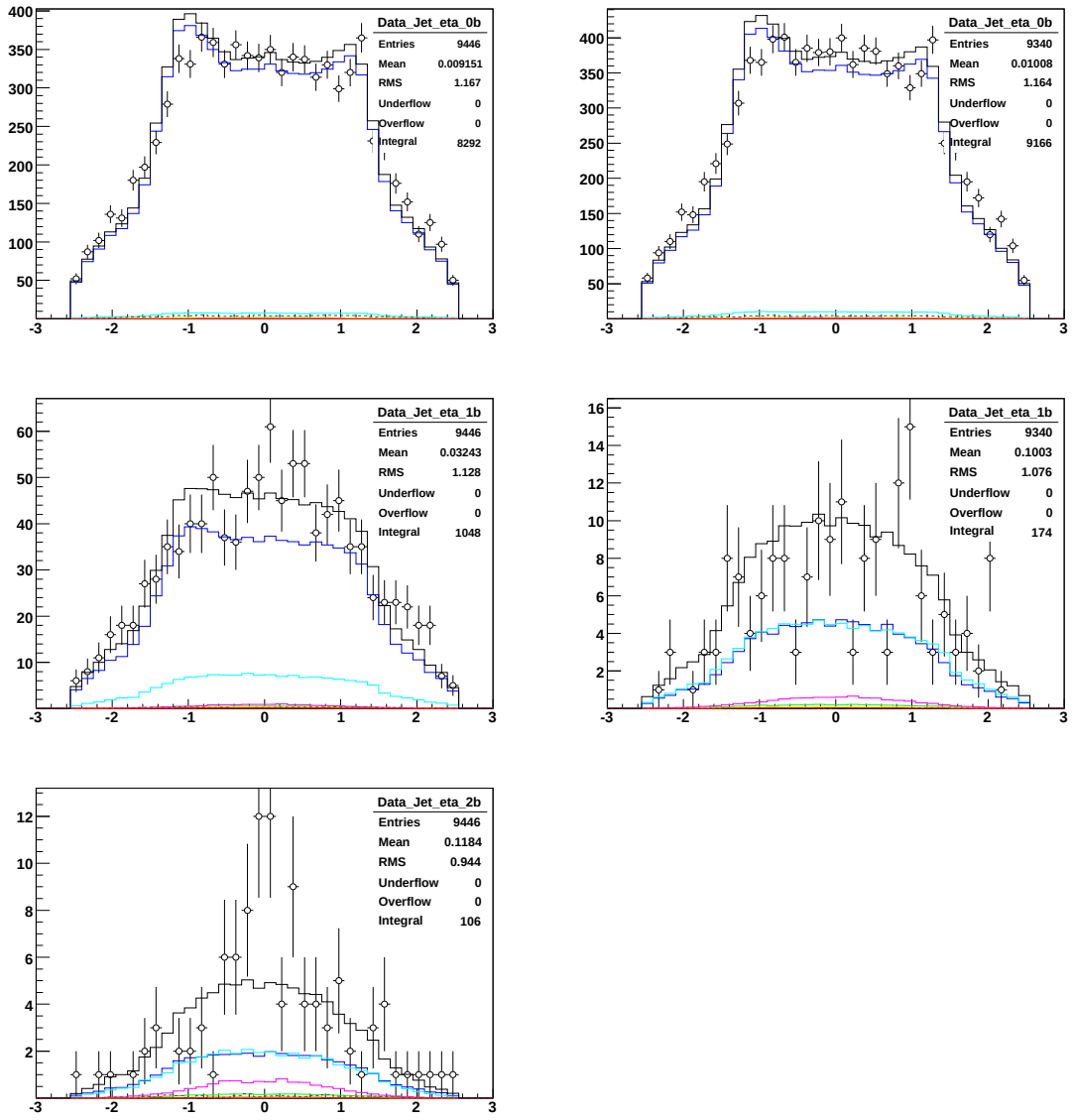

Figure 70: The η of the leading two p_T jets in events with 0, 1, and >=2 L4 b-tags (left) and 0, 1 VERYTIGHT b-tags but not 2 or more L4 b-tags (right), with no log scale.

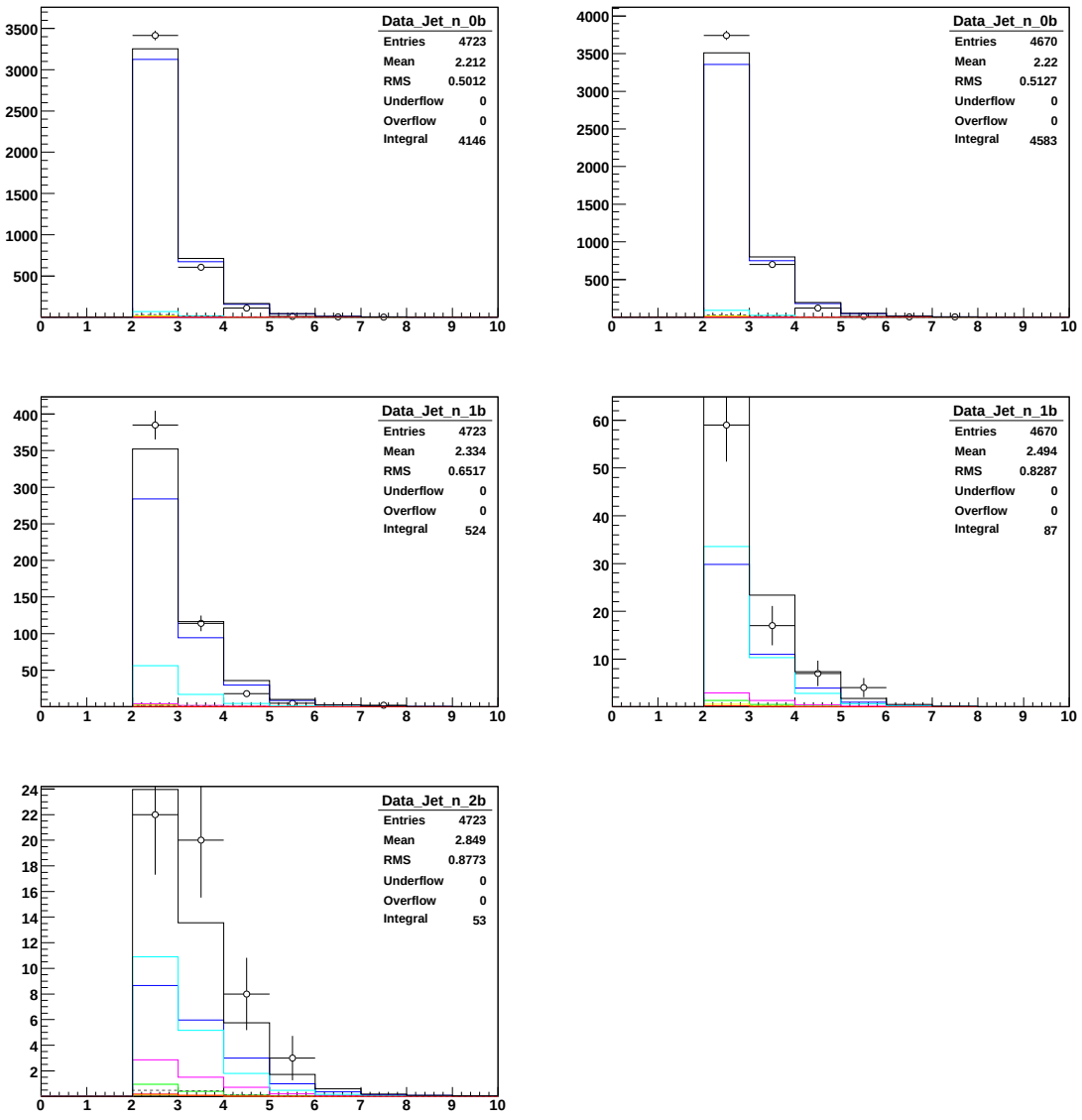

Figure 71: The jet multiplicity in events with 0, 1, and >=2 L4 b-tags (left) and 0, 1 VERYTIGHT b-tags but not 2 or more L4 b-tags (right), with no log scale.

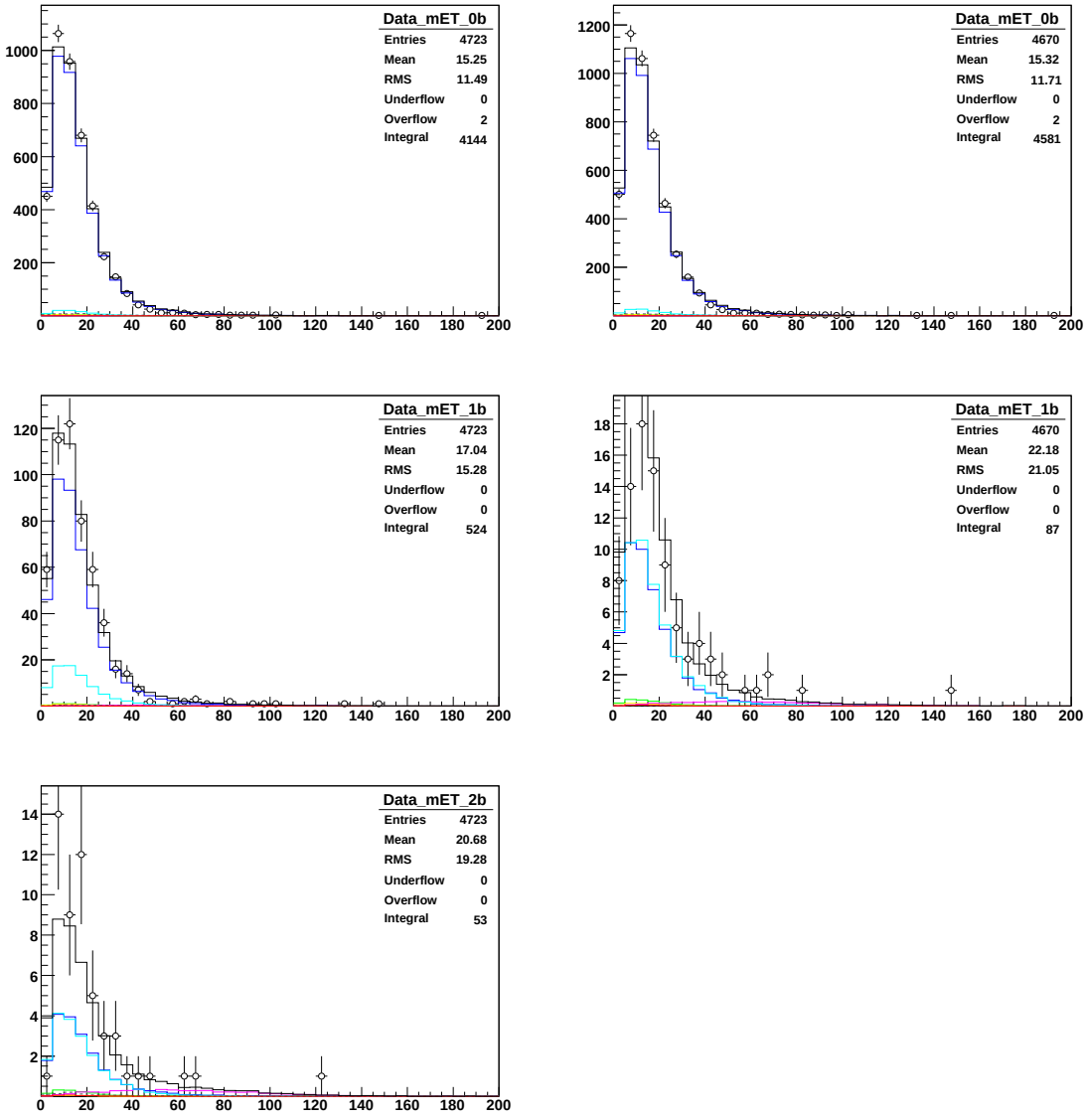

Figure 72: The missing E_T in events with 0, 1, and >=2 L4 b-tags (left) and 0, 1 VERYTIGHT b-tags but not 2 or more L4 b-tags (right), with no log scale.

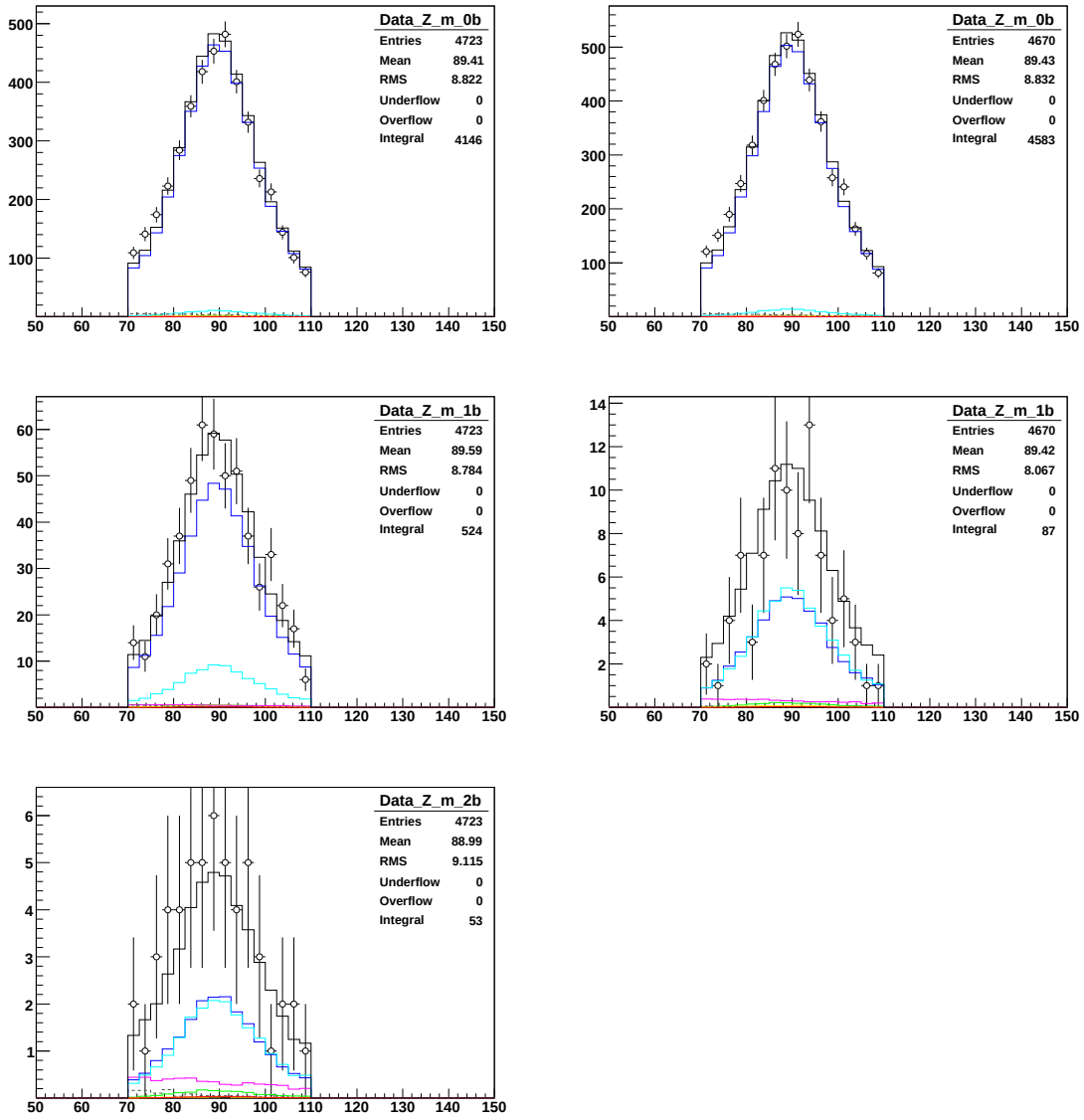

Figure 73: The Z-candidate invariant mass in events with 0, 1, and >=2 L4 b-tags (left) and 0, 1 VERYTIGHT b-tags but not 2 or more L4 b-tags (right), with no log scale.

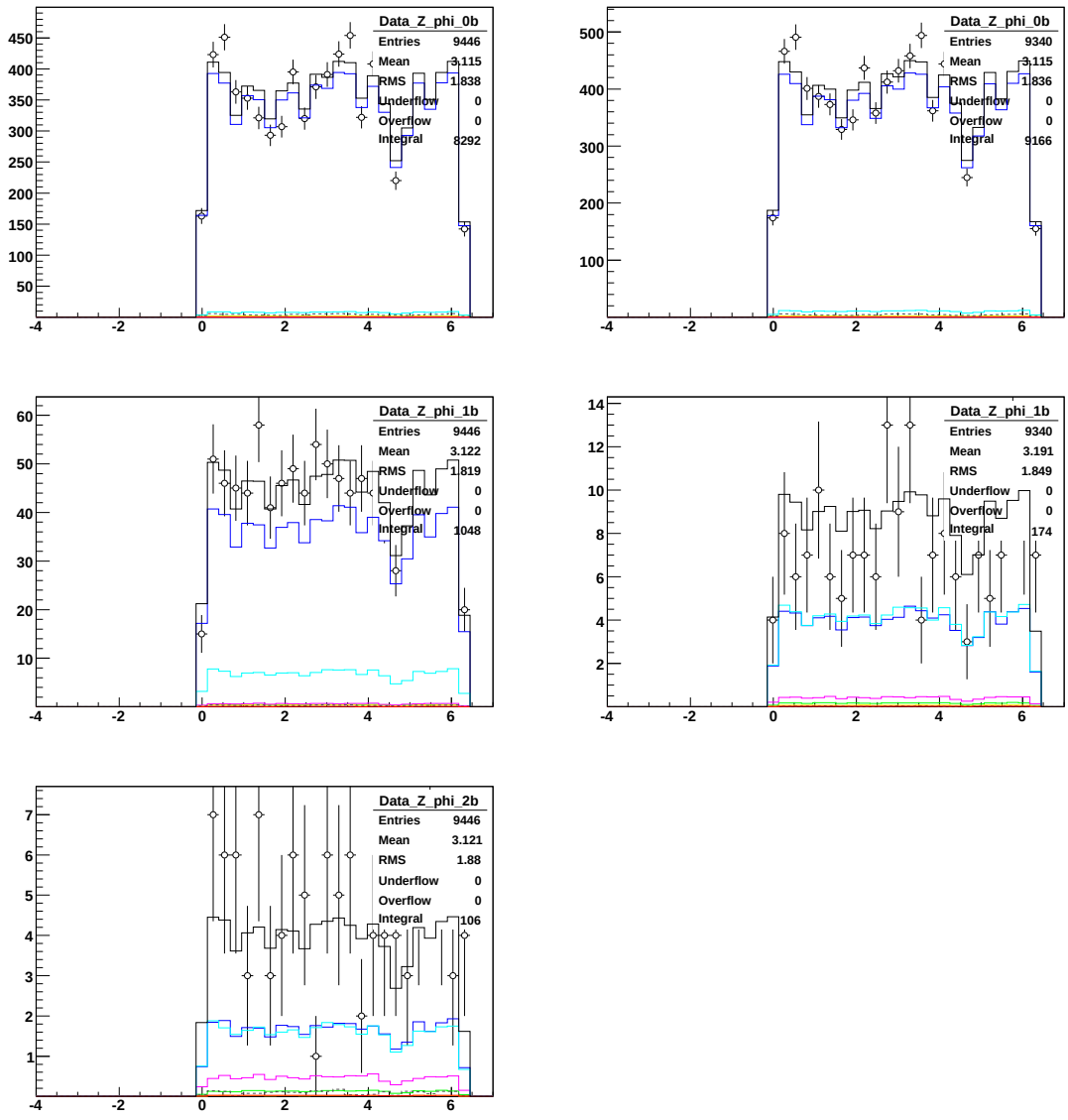

Figure 74: The Z-candidate ϕ in events with 0, 1, and >=2 L4 b-tags (left) and 0, 1 VERYTIGHT b-tags but not 2 or more L4 b-tags (right), with no log scale.

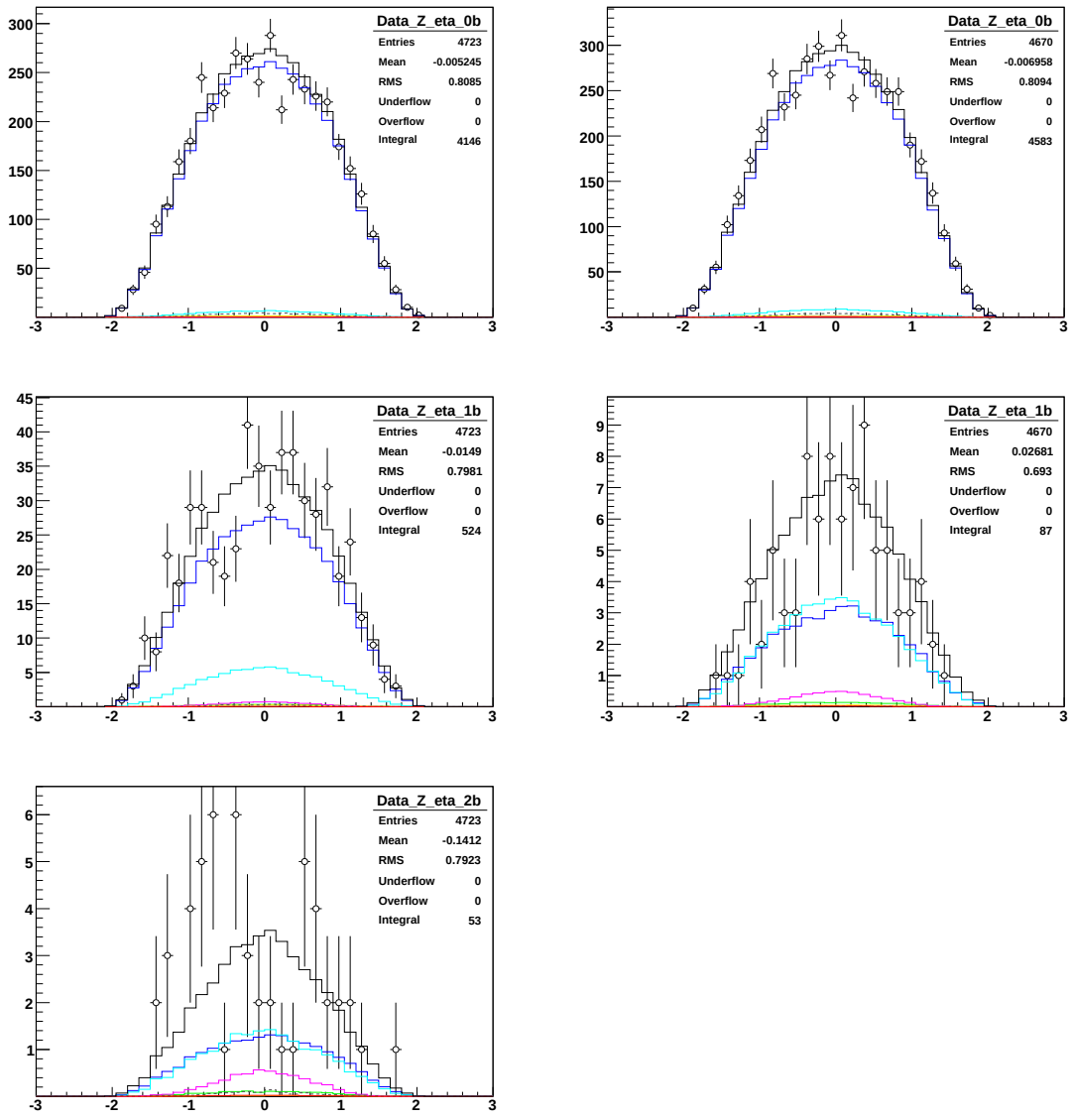

Figure 75: The Z-candidate η in events with 0, 1, and >=2 L4 b-tags (left) and 0, 1 VERYTIGHT b-tags but not 2 or more L4 b-tags (right), with no log scale.

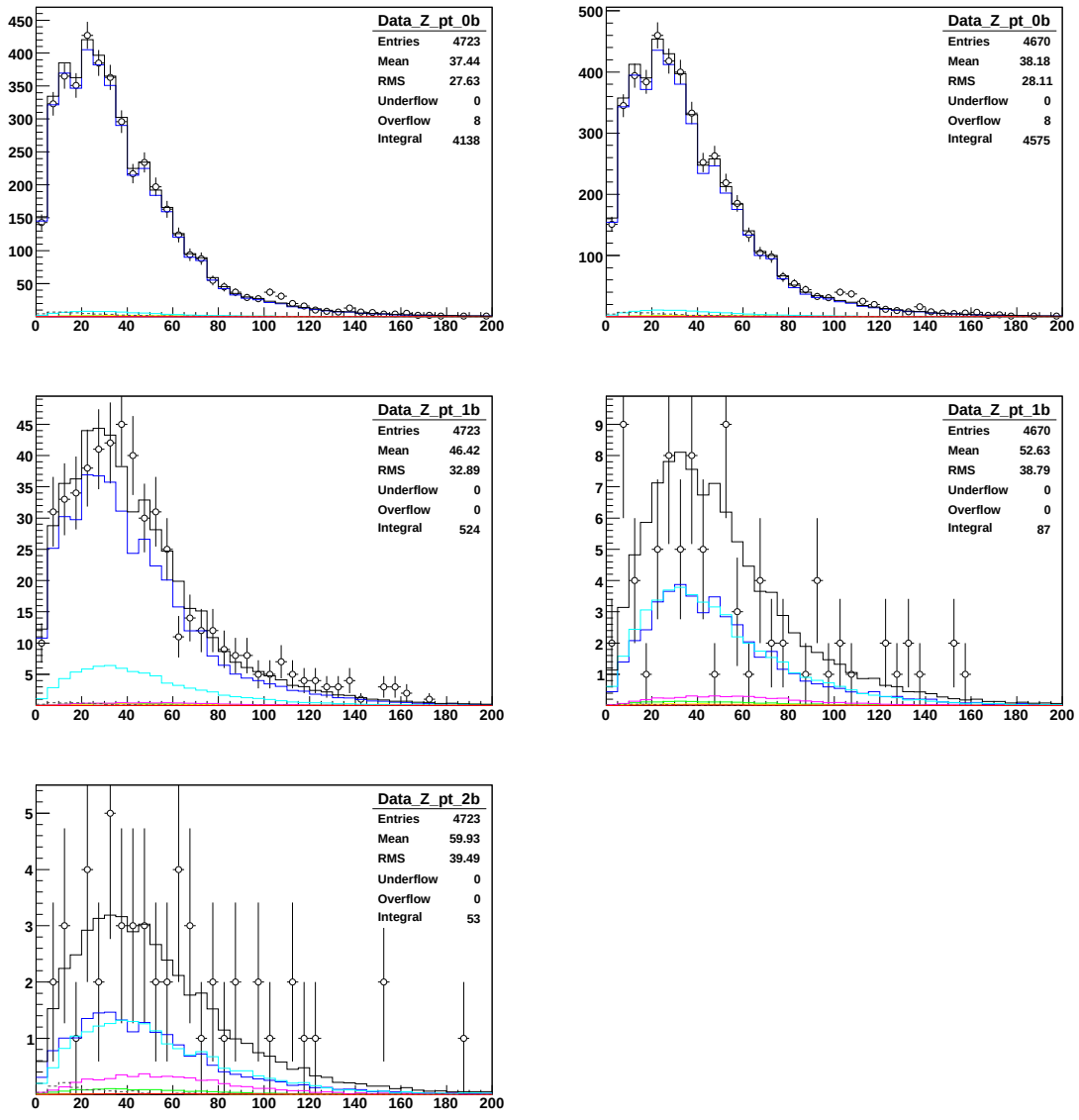

Figure 76: The Z-candidate p_T in events with 0, 1, and >=2 L4 b-tags (left) and 0, 1 VERYTIGHT b-tags but not 2 or more L4 b-tags (right), with no log scale.

References

[1] J. R. Ellis, D. Nanopoulos, K. A. Olive and Y. Santoso, Phys. Lett. B **633**, 583 (2006) [arXiv:hep-ph/0509331].

[2] LEP Electroweak Working Group, http://lepewwg.web.cern.ch/LEPEWWG/ (2006).

[3] T. Hahn, S. Heinemeyer, F. Maltoni, G. Weiglein and S. Willenbrock, "SM and MSSM Higgs boson production cross sections at the Tevatron and the arXiv:hep-ph/0607308.

[4] D0 Data Quality Coordination,
http://www-d0.fnal.gov/computing/data_quality/d0_private/forusers.html.

[5] MCFM Cross-sections for CAPS production,
http://www-clued0.fnal.gov/ nunne/cross-sections/caps_xsect.html,
http://mcfm.fnal.gov/.

[6] MLM matching procedure,
http://www-d0.fnal.gov/computing/MonteCarlo/generators/common_alpgen.html.

[7] Thomas Nunnemann, "Alpgen and MCFM studies on Wbb",
http://www-d0.hef.kun.nl//askArchive.php?
base=agenda&categ=a061709&id=a061709s1t3/transparencies,
Sept. 28, 2006.

[8] Angela Bellavance, Kristian Harder, Carsten Hensel, Gavin Hesketh, Norik Khalatyan, Alexandre Lobodenko, Dmitry Onoprienko, and Heidi Schellman, "Measurement of the ppbar→mumu yield in the Z mass region for D0 Run 2A data", D0Note XXXX.

[9] Thomas Gadfort, Gavin Hesketh, Vincent Lesne, Mark Owen, Raimund Strohmer, Boris Tuchming, "Muon Identification Certification for p17 data", D0Note 5157, Sept., 2006.

[10] Gavin Hesketh, https://plone4.fnal.gov/P1/D0Wiki/caf/wz_cafreco/.

[11] G. C. Blazey *et al.*, in *Proceedings of the Workshop: "QCD and Weak Boson Physics in Run II,"* edited by U. Baur, R. K. Ellis, and D. Zeppenfeld, (Fermilab, Batavia, IL, 2000) p. 47; see Sec. 3.5 for details.

[12] "Certified preliminary JES for p17 data", JetCorr v07-01-02, http://www-d0.fnal.gov/phys_id/jes/public/plots_v7.1/, Feb., 2006.

[13] Nikola Makovec and J.F. Grivaz, "Shifting, Smearing, and Removing Simulated Jets", D0Note 4914, Nov., 2005.

[14] Miruna Anastasoaie, Stephen Robinson, and Tim Scanlon, "Performance of the NN b-tagging Tool on p17 Data", D0Note 5213, http://www-d0.fnal.gov/phys_id/bid/d0_private/certification/cert_p17/, Sept., 2006.

[15] Shaohua Fu, "D0 Search for ZH→ee $b\bar{b}$ using p17 data", http://www-d0.fnal.gov/Run2Physics/d0_private/eb/Run2EB_004/Run2EB_004_09a.html, Oct., 2006.

[16] "Simple Limit Calculator", D0Note 3476, CVS package: limit_calculators, http://www-clued0.fnal.gov/ hobbs/limit_calc/limit_calc.html.

[17] Wade Fisher, "Systematics and Limit Calculations", D0Note 5309.

[18] W.-M.Yao et al. (Particle Data Group), J. Phys. G 33, 1 (2006).

[19] Huishi Dong, John Hobbs, "Search for SM Higgs Boson in ZH→$\mu\mu$+$b\bar{b}$ Channel in $p\overline{p}$ Collisions at $\sqrt{s} = 1960$ GeV ", D0Note XXXX, July 26, 2006.

10 Thanks

I thank Kazu, Fu, and the members of EB004 for help with this analysis.